REVIEWS OF
MODERN PHYSICS

VOLUME 44, NUMBER 2 APRIL 1972

The Vibrational Properties of Disordered Systems: Numerical Studies

P. DEAN
Division of Quantum Metrology, National Physical Laboratory, Teddington, Middlesex, England

A review is presented of the direct numerical approach to the study of the atomic vibrational properties of disordered systems. The basis and details of the numerical methods employed are first described. This is followed by a review of applications of the approach to two-component disordered lattices, glasses, mixed-crystal systems, orientationally disordered crystals, and random polymers.

CONTENTS

1. INTRODUCTION

Lattice dynamics has a history extending to the early years of this century, to the classic papers of Debye (1912) and Born and von Karman (1912). These studies of the normal modes and thermodynamic properties of simple models of solids initiated what was to be the main stream of research in lattice dynamics, that on crystalline solids within the harmonic approximation, up to perhaps 15 years ago. Since then, other areas of interest and activity have emerged, not all related to the dynamics of atoms in perfectly periodic structures. In this review we shall be concerned with one of these relatively new fields, that of the vibrational properties of disordered atomic structures of various kinds.

It is a measure of the complexity of the mathematical problems which arise in the study of atomic vibrations in disordered systems that although much effort has been put into the field over the past years, progress has been relatively slow. The primary difficulty stems directly from the absence of any real simplifying feature in the geometry of disordered systems. There is no periodicity in the structures and so we cannot invoke the elegant theorems implicit in the theory of crystalline solids, nor are disordered systems sufficiently closely related to any basically simpler structures that some form of perturbative approach is likely to be really profitable. There is, in fact, such a difference in character between the problems of atomic vibrations in disordered and periodic systems that one finds that methods of lattice dynamics which have proved quite adequate for crystals or dilute impurity systems generally yield relatively little information on disordered systems. As a consequence of this, a variety of new methods have been devised and used. The main object of this paper is to review in detail one such approach, an approach that has proved to be quite successful in leading to an understanding of the nature of atomic vibrations in disordered systems, the direct numerical approach. In order to assess this approach and evaluate the results that have come from it, we must necessarily touch upon and make comparisons with the results of other methods. To this extent, but only to this extent, this review encompasses the whole area of theoretical work to date on the atomic vibrations of disordered structures.

One of the major difficulties associated with the study of atomic vibrations in disordered structures is that we cannot use some of the quite familiar concepts associated with phonons in regular lattices. In a lattice, a phonon is a wavelike excitation which extends spatially throughout the whole structure; this is not generally true for a disordered system in which an excitation of

atomic vibrations may be highly localized spatially and thus have no well-defined momentum, or **k** value. Thus, we see at the outset that the familiar description of atomic vibrations in a solid, in terms of dispersion relations, no longer holds for disordered crystals. The information that can be obtained is of a somewhat different kind, and an adequate description of this information depends upon the introduction of new ideas and concepts totally inapplicable to crystals.

The present state of our understanding of atomic vibrations in disordered systems is appreciably less advanced than is the case for crystals, with theoretical approaches to date having been aimed largely at studying and understanding basically simple disordered models. Effort has been confined almost entirely to the study of models with harmonic forces and, within this approximation, the force fields have usually been short range in character. In stating this we are excluding reference to the molecular dynamics approach, in which the equations of motion of a system of particles are integrated forward in time; in that approach the use of a complicated potential function presents no difficulty of principle. Our interest, in this review, is on the effects of disorder on vibrational atomic motion as determined by numerical and related studies; attention in this area has been confined almost exclusively to harmonic systems.

We start this review, in Sec. 2, with a formulation of the harmonic lattice dynamical problem in the coordinate representation. In Sec. 3 we describe the basic methods of the numerical approach to the study of disordered systems. Section 4 is devoted to a discussion and review of work on two-component disordered lattices, the class of disordered system which has attracted most attention in the past. In Secs. 5–8 we review work by the numerical approach which has been carried out on glasses, mixed-crystal systems, orientationally disordered crystals, and random polymers.

2. FORMULATION OF THE PROBLEM

The basic model used in lattice dynamical studies—whether of periodic or disordered structures—is one in which the atoms of a system are free to vibrate with small amplitude about certain equilibrium positions $\mathbf{R}_i$ $(i=1, 2, \cdots, N)$. The Hamiltonian operator for this vibrational motion is the sum of two parts, related to the kinetic and potential energies, respectively, of the nuclei. In the harmonic approximation the potential energy term is quadratic in atomic displacement, and the Hamiltonian takes the form

$$H=-\hbar^2\sum_{i=1}^{N}\nabla_i^2+\sum_{i,j;\,i\neq j}^{N}\sum_{\alpha=1,\beta=1}^{3}a_{i\alpha,j\beta}q_{i\alpha}q_{j\beta}, \quad (2.1)$$

where $q_{i\alpha}$ is a mass-dependent component of displacement from equilibrium of the ith atom in the Cartesian direction α.

It is possible to find a unitary transformation

$$q_{i\alpha}=\sum_{l=1}^{3N}U_{i\alpha,l}Q_l,$$

$$Q_l=\sum_{i=1}^{N}\sum_{\alpha=1}^{3}U_l^{\dagger}{}_{,i\alpha}q_{i\alpha}, \quad (2.2)$$

which diagonalizes the Hamiltonian (2.1), so that the wave equation

$$\left(-\hbar^2\sum_{l=1}^{3N}\frac{\partial^2}{\partial Q_l^2}+\sum_{l=1}^{3N}\omega_l^2Q_l^2\right)\phi(Q_1, Q_2, \cdots, Q_N)$$
$$=E\phi(Q_1, Q_2, \cdots, Q_N) \quad (2.3)$$

is separable into $3N$ independent one-dimensional systems of the form

$$[-\hbar^2(d^2/dQ^2)+\omega_l^2Q_l^2]\phi_l(Q_l)=E_l\phi_l(Q_l), \quad (2.4)$$

where

$$\phi=\prod_{l=1}^{N}\phi_l(Q_l),$$

$$E=\sum_{j=1}^{N}E_j. \quad (2.5)$$

Equation (2.4) is the well-known equation for the harmonic oscillator, with eigenvalues

$$E_l(n)=(n+\tfrac{1}{2})\hbar\omega_l, \qquad (n=0, 1, 2, \cdots). \quad (2.6)$$

It is clear that the quantities ω_l are of prime importance in characterizing the energy levels and thus the vibrational properties of the model. In the case of systems such as molecules having a small number of degrees of freedom, the individual ω_l's are fully meaningful and may usefully be determined. On the other hand, for systems such as solids, containing large numbers of atoms, interest is normally confined to the statistical distribution of ω_l, i.e., the ω_l spectrum, rather than particular individual values.

The classical Hamiltonian corresponding to (2.1) is

$$H_c(p, q)=\sum_{i=1}^{N}\sum_{\alpha=1}^{3}p_{i\alpha}{}^2+\sum_{i,j;\,i\neq j}^{N}\sum_{\alpha=1,\beta=1}^{3}a_{i\alpha,j\beta}q_{i\alpha}q_{j\beta}, \quad (2.7)$$

with $p_{i\alpha}$ the component of momentum of atom i in the α direction. The transformation (2.2) reduces this to the diagonal form

$$H_c'(P, Q)=\sum_{l=1}^{3N}P_l^2+\sum_{l=1}^{3N}\omega_l^2Q_l^2 \quad (2.8)$$

leading to classical equations of motion for the system

$$\ddot{Q}_l=-\omega_l^2Q_l \qquad (l=1, 2, \cdots, 3N). \quad (2.9)$$

This equation indicates that it is possible to derive the quantities ω_l, upon which the energy levels of the system depend [as in (2.6)], purely by considering the classical problem. Because of this, and because of the simplicity of the classical formulation, it has become one of the accepted procedures in lattice dynamical calculations.

We start, then, with a classical formulation of the problem and write down the equations of motion of the system based on (2.7), viz.

$$\ddot{q}_{i\alpha} = -\sum_{j}^{N}\sum_{\beta=1}^{3} a_{i\alpha,j\beta} q_{j\beta}. \qquad (2.10)$$

In these equations the quantities $a_{i\alpha,j\beta}$ are simple functions of interatomic force constants and atomic masses. We take the $a_{i\alpha,j\beta}$ to form a symmetric coefficient matrix, i.e., one in which $a_{i\alpha,j\beta}=a_{j\beta,i\alpha}$; this can always be arranged if the variables $q_{i\alpha}$ in Eq. (2.1) are chosen to be mass dependent of the form $q_{i\alpha}=m_i^{1/2}\alpha_i$, where m_i is the mass of the ith atom, and α_i is the component of its displacement from equilibrium along the Cartesian α axis.

For a normal mode of circular frequency ω, we have $q_{i\alpha}=A_{i\alpha}e^{i\omega t}$, where $A_{i\alpha}$ is a mass-dependent amplitude component. Equations (2.10) thus reduce to the linear algebraic set

$$\sum_{j=1}^{N}\sum_{\beta=1}^{3} (a_{i\alpha,j\beta}-\omega^2\delta_{i\alpha,j\beta})A_{j\beta}=0$$

$$(i=1, 2, \cdots, N; \alpha=1, 2, 3), \qquad (2.11)$$

where

$$\delta_{i\alpha,j\beta}=1 \quad \text{if } i=j,\ \alpha=\beta$$
$$=0 \quad \text{otherwise.}$$

The determination of the frequencies and normal modes of the system thus reduces to a standard eigenvalue problem, one familiar in the fields of the lattice dynamics of crystalline materials and molecular spectroscopy. In both of these areas the problem is a tractable one in practice as well as principle, because of certain simplifying features in the dynamical matrix $\{a_{i\alpha,j\beta}\}$. For periodic structures, the matrix is of a simple recurrent pattern, and basic theorems of matrix algebra can be invoked to reduce the problem to one associated with a set of matrices of much lower order (Dean, 1967). For most problems of molecular vibrations, $\{a_{i\alpha,j\beta}\}$ is already of small order and thus quite amenable to conventional computational procedures.

The presence of atomic or spatial disorder injects a new feature into the problem. The dynamical matrix is now neither of a simple recurrent form as in problems of crystal dynamics, nor of small order as in molecular vibrations. The mathematical problems, in fact, become very substantial, and no fully satisfactory way of dealing with them has yet been devised. The essence of the approach described in this paper is the development and use of efficient methods of numerical analysis so that the general problem (2.11) presented by disordered structures can be made tractable.

There is one feature of the eigenvalue problem presented by disordered systems that should be mentioned at this stage. Equations (2.11) relate to just one *particular* disordered system of N atoms. For large N, one assumes that properties computed from this system relate not only to just this one particular system, but to a whole class or *ensemble* of disordered systems of which it is representative. A considerable quantity of evidence suggests that for N of the order of thousands, or even less, properties—such as frequency spectra—obtained for a single system represent meaningful ensemble averages; certainly they are closer to ensemble averages than results so far obtained by other approaches, excepting certain special exact results.

3. NUMERICAL METHODS

The numerical approach has as its basis highly efficient techniques for extracting information from general symmetric matrices of large order, matrices such as $\{a_{i\alpha,j\beta}\}$ [in (2.11)]. There are essentially two major numerical problems, somewhat distinct from each other, arising from the dynamical equations. The first is that of the determination of the distribution of eigenvalues of a general $(n\times n)$ symmetric matrix **M** (which we shall identify as $\{a_{i\alpha,j\beta}\}$), where n is large. This distribution could in principle be found by computing each of the n eigenvalues separately, but such a method would be impracticable for large order matrices. Moreover, it would provide appreciably more data than needed, for the quantity of physical interest is the frequency spectrum, a function simply related to the distribution of eigenvalues of the dynamical matrix. Individual eigenvalues have no particular physical significance for systems containing large numbers of atoms, except in rather special cases.

The second numerical problem is that of the direct determination of selected eigenvectors of **M**. Here again, we recognize that the determination of all the eigenvectors of a large-order matrix is quite impracticable. Indeed, as the computation of an eigenvector involves first the accurate determination of its eigenvalue, the process of calculating a complete set of vectors would involve an effort that we have dismissed, in the preceding paragraph, as being impracticable. Fortunately, a complete set of eigenvectors is by no means an essential requirement for an understanding of the atomic vibrations of systems of large order. One can normally derive quantities such as infrared absorption, Raman intensities, and degree of localization and gain a fairly full understanding of the form of atomic motion in the various regions of the spectrum by considering a relatively small sample of "typical" eigenvectors. This, in fact, has been the procedure adopted in all published work to date on large-order systems.

3.1 The Distribution of Eigenvalues

We describe here an efficient method of computing the distribution of eigenvalues of a real symmetric matrix by means of a theorem, introduced by Dean and Martin (1960a), known as the negative eigenvalue theorem. There are other ways (cf., Wilkinson, 1965) of showing

that the method described here leads correctly to the required eigenvalue distribution, but the negative eigenvalue theorem is itself of some wider significance in lattice dynamical applications, and so we shall use it here.

The theorem relates to a partitioned matrix of the form

$$\mathbf{M}=\begin{bmatrix} \mathbf{A}_1 & \mathbf{B}_2 & & & 0 \\ \mathbf{B}_2^T & \mathbf{A}_2 & \mathbf{B}_3 & & \\ & \cdot & \cdot & \cdot & \\ & & \cdot & \cdot & \cdot \\ & & & \cdot & \cdot & \cdot \\ 0 & & & & \mathbf{B}_m^T & \mathbf{A}_m \end{bmatrix}, \tag{3.1}$$

where $\mathbf{A}_i$ is a (symmetric) square matrix of order l_i (say), $\mathbf{B}_i$ is of order $(l_{i-1}\times l_i)$, $\mathbf{B}_j^T$ is the transpose of $\mathbf{B}_j$, and all of the elements of $\mathbf{M}$ other than those in the $\mathbf{A}$ and $\mathbf{B}$ submatrices are zero. The negative eigenvalue theorem states that, if $\eta\{\mathbf{X}\}$ denotes the number of real negative eigenvalues of a matrix $\mathbf{X}$, then

$$\eta\{\mathbf{M}-x\mathbf{I}\}=\sum_{i=1}^{m}\eta\{\mathbf{U}_i\}, \tag{3.2}$$

where

$$\mathbf{U}_i=\mathbf{A}_i-x\mathbf{I}_i-\mathbf{B}_i^T\mathbf{U}^{-1}{}_{i-1}\mathbf{B}_i \qquad (i=2, 3, \cdots, m),$$
$$\mathbf{U}_1=\mathbf{A}_1-x\mathbf{I}_1 \tag{3.3}$$

and, of course,

$$\sum_{i=1}^{m} l_i=n.$$

In our notation, $\mathbf{I}_i$ is the unit matrix of order l_i, and $\mathbf{I}$ is of order n. A concise proof of the theorem is given in the Appendix.

The particular form of the negative eigenvalue theorem that we wish to use rests upon a simple partition of $\mathbf{M}-x\mathbf{I}$ into only four submatrices, $\mathbf{A}_1$, $\mathbf{A}_2$, $\mathbf{B}_2$, and $\mathbf{B}_2^T$, with $\mathbf{A}_1$ of order unity (i.e., scalar), and $\mathbf{A}_2$ of order $n-1$. Thus we have

$$\mathbf{A}_1=m_{11}$$
$$\mathbf{B}_2=\{m_{12}, m_{13}, m_{14}, \cdots, m_{1n}\}$$
$$\mathbf{A}_2=\begin{bmatrix} m_{22} & m_{23} & \cdot & \cdot & \cdot & m_{2n} \\ m_{32} & & & & & \cdot \\ \cdot & & & & & \cdot \\ \cdot & & & & & \cdot \\ \cdot & & & & & \cdot \\ m_{n2} & & & & & m_{nn} \end{bmatrix}, \tag{3.4}$$

where m_{ij} $(i, j=1, 2, \cdots, n)$ is the (i, j)th element of $\mathbf{M}$. We then apply the negative eigenvalue theorem. However, before doing so we shall introduce at this point, for reasons which become obvious later, a new notation. We write

$$\mathbf{X}_1=\mathbf{A}_1-x\mathbf{I}_1,$$
$$\mathbf{Z}_1=\mathbf{A}_2-x\mathbf{I}_2,$$
$$\mathbf{Y}_1\equiv\mathbf{B}_2, \tag{3.5}$$

where $\mathbf{A}_1$, $\mathbf{A}_2$, and $\mathbf{B}_2$ are as defined in (3.4); we shall also write $\mathbf{M}_1(x)\equiv\mathbf{M}-x\mathbf{I}$.

In this new notation, the partitioning of the matrix $\mathbf{M}-x\mathbf{I}$ referred to above takes the form

$$\mathbf{M}_1(x)=\left[\begin{array}{c|c} \mathbf{X}_1 & \mathbf{Y}_1 \\ \hline \mathbf{Y}_1^T & \mathbf{Z}_1 \end{array}\right] \tag{3.6}$$

and the negative eigenvalue theorem gives the result

$$\eta\{\mathbf{M}_1(x)\}=\eta\{\mathbf{X}_1\}+\eta\{\mathbf{Z}_1-\mathbf{Y}_1^T\mathbf{X}_1^{-1}\mathbf{Y}_1\}. \tag{3.7}$$

Thus, $\eta\{\mathbf{M}_1(x)\}$ can be determined from the sign of the scalar quantity $\mathbf{X}_1$ (in this case simply the element $m_{11}-x$ of the matrix $\mathbf{M}-x\mathbf{I}$) and the number of negative eigenvalues of a matrix $\mathbf{Z}_1-\mathbf{Y}_1^T\mathbf{X}_1^{-1}\mathbf{Y}_1$ of order $n-1$.

We now write

$$\mathbf{M}_2(x)=\mathbf{Z}_1-\mathbf{Y}_1^T\mathbf{X}_1^{-1}\mathbf{Y}_1 \tag{3.8}$$

and partition $\mathbf{M}_2(x)$ as follows:

$$\mathbf{M}_2(x)=\left[\begin{array}{c|c} \mathbf{X}_2 & \mathbf{Y}_2 \\ \hline \mathbf{Y}_2^T & \mathbf{Z}_2 \end{array}\right], \tag{3.9}$$

where $\mathbf{X}_2$ is a scalar, and $\mathbf{Z}_2$ is a square matrix of order $n-2$. The negative eigenvalue theorem, applied to (3.8), gives

$$\eta\{\mathbf{M}_2(x)\}=\eta\{\mathbf{X}_2\}+\eta\{\mathbf{Z}_2-\mathbf{Y}_2^T\mathbf{X}_2^{-1}\mathbf{Y}_2\}. \tag{3.10}$$

The reasons for the notation change introduced in (3.5) should now be clear. The new notation at once suggests that we can continue the procedure indicated by the Eqs. (3.5)–(3.10) for a total of $n-1$ stages, the ith stage being summarized by the equations

$$\mathbf{M}_i(x)=\mathbf{Z}_{i-1}-\mathbf{Y}_{i-1}^T\mathbf{X}_{i-1}^{-1}\mathbf{Y}_{i-1} \qquad (i>1),$$
$$[\mathbf{M}_1(x)=\mathbf{M}-x\mathbf{I}], \tag{3.11}$$

$$\mathbf{M}_i(x)=\left[\begin{array}{c|c} \mathbf{X}_i & \mathbf{Y}_i \\ \hline \mathbf{Y}_i^T & \mathbf{Z}_i \end{array}\right] \tag{3.12}$$

and

$$\eta\{\mathbf{M}_i(x)\}=\eta\{\mathbf{X}_i\}+\eta\{\mathbf{Z}_i-\mathbf{Y}_i^T\mathbf{X}_i^{-1}\mathbf{Y}_i\}, \tag{3.13}$$

where $\mathbf{X}_i$ is a scalar, and $\mathbf{Z}_i$ is a square matrix of order $n-i$. The set of Eqs. (3.13), with i running from 1 to

$n-1$, together yield the result

$$\eta\{\mathbf{M}-x\mathbf{I}\}\equiv\eta\{\mathbf{M}_1(x)\}=\sum_{i=1}^{n}\eta\{\mathbf{X}_i\}, \qquad (3.14)$$

where, for notational convenience and consistency, we have written the scalar $\mathbf{Z}_{n-1}-\mathbf{Y}_{n-1}{}^T\mathbf{X}_{n-1}{}^{-1}\mathbf{Y}_{n-1}$ as $\mathbf{X}_n$.

Equation (3.14) is the central result needed for the efficient determination of eigenvalue spectra. It shows that the number of eigenvalues of a real symmetric matrix $\mathbf{M}$ which are smaller than a real parameter x can be found from the signs of n scalar quantities $\mathbf{X}_i(x)$; these quantities are the (1, 1) elements of a set of matrices $\mathbf{M}_i(x)$, calculable from a recurrence relation (3.11).

The amount of computation in determining a value of $\eta\{\mathbf{M}-x\mathbf{I}\}$ may be estimated as follows. The calculation at the ith stage involves a determination of the matrix $\mathbf{Z}_i-\mathbf{Y}_i{}^T\mathbf{X}_i{}^{-1}\mathbf{Y}_i$, given $\mathbf{Z}_i$ as a symmetric $(n-i\times n-i)$ matrix, $\mathbf{Y}_i$ as a $(1\times n-i)$ vector, and a scalar $\mathbf{X}_i$. Let us take $\mathbf{M}$ to be a band matrix of half-bandwidth $s\leq n$ [so that all elements (i,j) such that $|j-i|\geq s$ are zero]. It is easy to see, by induction, that $\mathbf{Z}_i$ (for all i) is then also of band form with a half-bandwidth s, and $\mathbf{Y}_i$ has zero elements beyond its $(s-1)$th place. The determination of $\mathbf{Z}_i-\mathbf{Y}_i{}^T\mathbf{X}_i{}^{-1}\mathbf{Y}_i$ involves $s-1$ scalar divisions (in calculating $\mathbf{X}_i{}^{-1}\mathbf{Y}_i$) and, within unity, $\frac{1}{2}s(s-1)$ scalar multiplications, taking account of symmetry—and there are also $\frac{1}{2}s(s+1)$ subtractions. The total calculation over $n-1$ stages involves no more than $(n-1)(s-1)$ scalar divisions and $\frac{1}{2}(n-1)s(s-1)$ scalar multiplications (with a similar number of subtractions). We use the term "no more than" here for, in the final $s-1$ stages the matrices $\mathbf{Z}_i$ and $\mathbf{Y}_i$ are reduced to sizes within the half-bandwidth s; in some cases it may be more convenient, however, to program the algorithm to add zeros to these matrices in the final stages so that one is dealing with similarly sized matrices throughout.

This procedure, then, involving essentially $(n-1)\times(s-1)$ scalar divisions and $\frac{1}{2}(n-1)s(s-1)$ scalar multiplications gives the number of eigenvalues of $\mathbf{M}$ less than x. By giving x (say) n' values throughout the range of the spectrum and then differencing, one can determine to any desired accuracy the distribution of eigenvalues of $\mathbf{M}$. The total calculation involves $n'(n-1)(s-1)$ divisions and $\frac{1}{2}n'(n-1)s(s-1)$ multiplications; i.e., of the order of $\frac{1}{2}n'(n-1)s^2$ scalar multiplicative operations when s is not small.

A considerable body of practical experience in the procedure described here indicates that it is numerically stable, and leads to accurate results. There is, however, a danger in the process that the programmer or user of a computer program must be aware of. In rare cases, the top left-hand element ($\mathbf{X}_i$) of the matrix $\mathbf{M}_i(x)$ will be of very small magnitude or, possibly, zero. If this element is zero the numerical process breaks down, for the formation of $\mathbf{M}_{i+1}$ involves a division by $\mathbf{X}_i$. The program must therefore test for zero $\mathbf{X}_i$ and discard results for values of x which lead to such zeros. This represents no limitation in practice, for by adding a small number (say 10^{-6}) to x one can always obtain the information one requires.

The problem of the effects of a very small $\mathbf{X}_i$, rather than a zero $\mathbf{X}_i$, is more serious. The process defined by Eqs. (3.11) and (3.12) indicates that if $\mathbf{X}_i$ is small then the $s\times s$ top left-hand block of $\mathbf{M}_{i+1}(x)$ may become completely dominated by the elements $\mathbf{Y}_i{}^T\mathbf{X}_i{}^{-1}\mathbf{Y}_i$. As an example, if $\mathbf{X}_i$ is of order 10^{-6} but all the other elements of $\mathbf{M}_i$ are of order unity then, clearly, the contribution to $\mathbf{M}_{i+1}(x)$ of $\mathbf{Y}_i{}^T\mathbf{X}_i{}^{-1}\mathbf{Y}_i$ is six orders of magnitude greater than that of $\mathbf{Z}_i$. If only six decimal places are retained in the computation, all information on the $s\times s$ top left-hand block of $\mathbf{Z}_i$ will be lost. Fortunately it appears that the probability of $\mathbf{X}_i$ becoming really small (except in the special case we mention in the next paragraph) is negligible. It is, though, important that the danger is known, and that tests to anticipate a potentially unstable situation are written into the program.

One meets, in practice, only a rather special situation in which $\mathbf{X}_i$ is zero (or, because of rounding errors, close to zero). This occurs at small values of i and, in particular, at the first stage, $i=1$. At these early stages, for certain systems, it is not uncommon to find that the elements of $\mathbf{M}_i(x)$ will be integers or simple ratios of integers, thus leading occasionally, for simple selected values of x, to zero $\mathbf{X}_i$'s. As indicated earlier, the solution here is to increase the values of x by some small increment such as 10^{-6}.

The difficulties of the effects of small $\mathbf{X}_i$ can in general be almost completely met by the methods of pivoting, described by Wilkinson (1965) in his description of Gaussian elimination. The disadvantage of pivotal procedures is that they increase the bandwidth of the matrices, and therefore substantially increase the amount of computation involved in the problem. Fortunately, a considerable body of experience on lattice dynamical systems indicates that the procedure described here, with tests for small $\mathbf{X}_i$ written into the program, is quite satisfactory both in determining distributions of eigenvalues and also in calculating particular eigenvalues accurately, as needed for eigenvector determinations.

3.2 Computation of Eigenvectors

We mentioned earlier that the accurate determination of an eigenvector involves, first, a precise calculation of its eigenvalue. An excellent method of locating the eigenvalue is to use an extension of the procedure outlined in the last section for finding an eigenvalue distribution. There we showed how to compute the number of eigenvalues of a symmetric matrix $\mathbf{M}$ less than a real number x. We may extend the method as follows. If, for example, the pth eigenvalue of $\mathbf{M}$ is required accurately, then by using a few trial values of x (normally with the help of the already-determined eigen-

value distribution), one finds real numbers $x_{p-1}^{(1)}$ and $x_p^{(1)}$ such that

$$\eta\{\mathbf{M}(x_{p-1}^{(1)})\}=p-1,$$
$$\eta\{\mathbf{M}(x_p^{(1)})\}=p. \tag{3.15}$$

The quantity $\eta\{\mathbf{M}(x^{(2)})\}$ is then calculated, again by the methods of Sec. 3.1, where

$$x^{(2)}=\tfrac{1}{2}(x_{p-1}^{(1)}+x_p^{(1)}). \tag{3.16}$$

If $\eta\{\mathbf{M}(x^{(2)})\}=p-1$ then, clearly, the pth eigenvalue lies between $x^{(2)}$ (which we now refer to as $x_{p-1}^{(2)}$) and $x_p^{(1)}$; on the other hand, if $\eta\{\mathbf{M}(x^{(2)})\}=p$ then the eigenvalue lies between $x_{p-1}^{(1)}$ and $x^{(2)}$ (now written as $x_p^{(2)}$). By successively bisecting the appropriate interval $x_{p-1}^{(i)}$ to $x_p^{(j)}$, where the notation has been extended in an obvious way, we can ultimately locate the required eigenvalue to any desired accuracy. Even closely separated eigenvalues can be satisfactorily evaluated by this method. Degenerate eigenvalues present a new feature. One can locate degenerate or near degenerate eigenvalues by the procedure mentioned above without trouble. The difficulty arises in specifying and converging to an appropriate eigenvector, as those associated with the degenerate eigenvalue are not unique. In lattice dynamical applications this difficulty can normally be evaded without penalty, for interest is usually confined to the determination of particular unique eigenvectors. Thus there is no need to invoke the special methods. Moreover, one finds in practice that disordered systems provide degenerate eigenvalues very rarely indeed, possibly because of the absence of any form of symmetry in the structure. The one common exception is the triply degenerate zero frequency motion associated with pure translations in a system under the free-end boundary condition.

Given, then, a well or reasonably well separated approximate eigenvalue the next problem is the accurate determination of its eigenvector. Here we recommend the technique of inverse iteration (cf. Wilkinson, 1965). In essence, the method is that of successively multiplying a trial vector by the matrix $(\mathbf{M}-h\mathbf{I})^{-1}$, where h is a computed approximation to λ_k, the eigenvalue whose vector we wish to determine.

More precisely, one can define the process of inverse iteration by the equations

$$\mathbf{v}_{s+1}=(\mathbf{M}-h\mathbf{I})^{-1}\mathbf{u}_s,$$
$$\mathbf{u}_{s+1}=\mathbf{v}_{s+1}/\max(\mathbf{v}_{s+1}), \tag{3.17}$$

where $\max(\mathbf{v}_{s+1})$ denotes the element of largest modulus in $\mathbf{v}_{s+1}$. If we write $\mathbf{u}_0$, the initial trial eigenvector, as

$$\mathbf{u}_0=\sum\alpha_i\mathbf{x}_i, \tag{3.18}$$

where $\mathbf{x}_i$ $(i=1, 2, \cdots, n)$ are the true eigenvectors of $\mathbf{M}$, and α_i are scalars, then, apart from a normalizing factor, the sth iterate is

$$\mathbf{u}_s=\sum\alpha_i(\lambda_i-h)^{-s}\mathbf{x}_i. \tag{3.19}$$

Hence, if $|\lambda_k-h|\ll|\lambda_i-h|$ (for all i other than k) the component of $\mathbf{x}_i(i\neq k)$ in $\mathbf{u}_s$ decreases rapidly with increasing s. It follows that the number of iterations needed to compute an accurate eigenvector x_k will be quite small if h is a good approximation to λ_k.

The iterative process described by (3.17) can be carried out in a straightforward manner. The sth step consists merely of solving the set of equations

$$(\mathbf{M}-h\mathbf{I})\mathbf{v}_{s+1}=\mathbf{u}_s \tag{3.20}$$

for the unknown $\mathbf{v}_{s+1}$. One method is based upon a decomposition such as

$$\mathbf{M}-h\mathbf{I}=\mathbf{LU}, \tag{3.21}$$

where $\mathbf{L}$ is a lower triangular matrix the elements L_{ij} of which are zero if $i<j$, and $\mathbf{U}$ is an upper triangular matrix with $U_{ij}=0$ if $j<i$. The decomposition into $\mathbf{L}$ and $\mathbf{U}$ is not unique and one needs to define, for example, the diagonal elements of $\mathbf{L}$ or $\mathbf{U}$. An $\mathbf{LU}$ decomposition is easily carried out in practice—it is, in fact, implicit in the eigenvalue determination—and enables one to solve the simultaneous equations (3.20) in two simple stages, by solving the triangular sets of equations

$$\mathbf{L}\mathbf{y}_s=\mathbf{u}_s$$

and

$$\mathbf{U}\mathbf{v}_{s+1}=\mathbf{y}_s. \tag{3.22}$$

Bell, Bird, and Dean (1968) have found it convenient, in practice, to use the decomposition (3.21) in the form

$$\mathbf{M}-h\mathbf{I}=\mathbf{U}^T\mathbf{D}\mathbf{U}, \tag{3.23}$$

where $\mathbf{U}^T$ is the transpose of $\mathbf{U}$, and the diagonal matrix $\mathbf{D}$ is such that the diagonal elements of $\mathbf{U}$ are all unity. In each iteration one solves the equations

$$\mathbf{U}^T\mathbf{y}_s=\mathbf{u}_s,$$
$$\mathbf{D}\mathbf{z}=\mathbf{y}_s,$$
$$\mathbf{U}\mathbf{v}_{s+1}=\mathbf{z}_s, \tag{3.24}$$

each of which represents a straightforward computational procedure on a high speed computer. This particular decomposition was used primarily because it enables the data to be processed speedily: the matrix $\mathbf{U}$ was stored on magnetic tape and the first and last of the Eqs. (3.24) could conveniently be carried out with the same storage data processed alternately in opposite directions. The initial trial vector was usually taken to be the vector of unit elements and, in practice, it was found that convergence was quickest if this was regarded as a $\mathbf{z}$ vector and used to yield a first $\mathbf{v}$ vector by the third equation (3.24). The computational process thus described has been found quite satisfactory in all cases, convergence to several decimal places (and this is more than adequate for lattice dynamical applications) being normally attained in two or three iterations for an h known to one part in 10^6, and with n of the order of 10^3. In practice there is no need to always compare

successive iterate vectors in order to be sure of convergence. Increasing convergence to the two eigenvectors is indicated by the growth in magnitude of successive iterates, and one can always arrange to terminate the iteration process when the element of maximum absolute magnitude of any iterate exceeds a certain prestated value (such as, say, 10^{16} times the maximum element of the initial trial eigenvector).

Wilkinson (1965) states that it is tempting, but unwise, to omit interchanges in the inverse iteration of band matrices. We cannot therefore unreservedly recommend the process described above and must refer the reader to the pivotal interchange schemes recommended by Wilkinson to give greater assurance of numerical stability. However, the penalty for using interchanges is that the amount of computational work increases considerably—to an extent which in many cases would have made projects successfully completed quite impracticable to carry through. In defense of the methods outlined here, it is important to state that in numerous cases computed eigenvectors have been compared with exactly known mathematical results showing, in all cases, excellent agreement. In addition, one often has some foreknowledge of the physical characteristics of computed eigenvectors and, again, in no case that we are aware of has any untoward result occurred. It would appear, then, that although the method outlined is capable, in principle, of producing errors induced by the particular computational procedure, the practical probability (at least, for matrices of the kind one encounters in atomic vibrational work) of such an occurrence is extremely small.

The calculation of eigenvalues or eigenvalue distributions and eigenvectors is, as we have already indicated, the central problem of atomic dynamical systems described by potential functions in the harmonic approximation. The calculation of macroscopically observed properties such as infrared absorption and Raman intensities at various frequencies depends upon the further application of particular physical ideas—often simple ones such as ascribing unit positive and negative charges to alternate masses on a vibrating lattice—although sometimes of a sophisticated character. Given the solution to the basic eigenvalue problem, the computation of these quantities and others, such as the extent of phonon localization, and lattice thermal properties (with the exception of thermal conductivity) presents no difficulty of principle and is normally substantially easier to carry out than the matrix procedures already outlined.

4. TWO-COMPONENT DISORDERED LATTICES

4.1 One-Dimensional Work

Since the paper by Dyson (1953), on the dynamics of disordered linear chains, there has been much interest in the subject of the atomic vibrations of two-component disordered structures. The mathematical problems which arise in this area are quite substantial, and progress by analytical methods has been correspondingly slow. The case of the two-component disordered chain illustrates well the kind of detailed and precise information that can be obtained using the direct numerical approach. We shall therefore consider this system in some detail in this section, indicating various approaches and results in order to attain a proper perspective of this much studied disordered dynamical system.

Dyson's paper, and also later work by Schmidt (1957) and others, was concerned with setting up a functional equation for the two-component disordered chain, the solution of which in principle enabled the distribution of frequencies to be found. In a linear chain of N atoms with nearest neighbor harmonic interactions, the equations of motion are of the form

$$\beta_i u_{i-1}+(\alpha_i-\omega^2)u_i+\beta_{i+1}u_{i+1}=0$$
$$\beta_0=\beta_N=0; \qquad i=1, 2, \cdots, N, \tag{4.1}$$

where the u_i are mass-dependent amplitudes (cf. Sec. 2), and the α_i and β_i are simple functions of the force constants and atomic masses of the system. Thus $\alpha_i=(\gamma_i+\gamma_{i-1})m_i^{-1}$, $\beta_i=-\gamma_{i-1}m_{i-1}^{-1/2}m_i^{-1/2}$, where m_i is the mass of the atom at the ith site, and γ_i is the force constant of the interaction between atoms i and $i+1$. Equations (4.1) indicate clearly that the dynamical matrix is tridiagonal in form, and it is just this simple structure of $\mathbf{M}$ upon which Dyson's and Schmidt's methods depend.

The negative eigenvalue theorem is particularly simple to apply to the tridiagonal matrix based upon equations such as (4.1). In (3.1) we simply replace $\mathbf{A}_i$ by α_i, and $\mathbf{B}_i$ by β_i. Equations (3.3) then take the form

$$h_i=\alpha_i-x-\beta_i^2/h_{i-1}, \qquad (i=2, 3, \cdots, N),$$
$$h_1=\alpha_1-x, \tag{4.2}$$

where we have substituted h_i for $\mathbf{U}_i$, and written x for ω^2, and the negative eigenvalue theorem states that

$$\eta\{\mathbf{M}-x\mathbf{I}\}=\sum_{i=1}^{N}\eta(h_i)$$
$$=\text{number of negative } h_i\text{'s.} \tag{4.3}$$

The essence of Dyson's and Schmidt's methods is the setting up of an equation for the probability distribution of h_i in terms of probabilities of uncorrelative parameters in the system. One considers an ensemble of chains, and a large value of i, i.e., one well removed from the end $i=1$, and then equates the probability distributions of h_{i-1} and h_i. If, for example, h_{i-1} and the pair of parameters (α_i, β_i) on the right-hand side of Eq. (4.2) are uncorrelated, then such a procedure gives

$$P(h_i)=\sum A(\alpha_i, \beta_i)P[\beta_i^2/(\alpha_i-x-h)]$$
$$\times\beta_i^2(\alpha_i-\omega^2-h_i)^{-2}, \tag{4.4}$$

where $A(\alpha_i, \beta_i)$ represents the probability of (α_i, β_i)

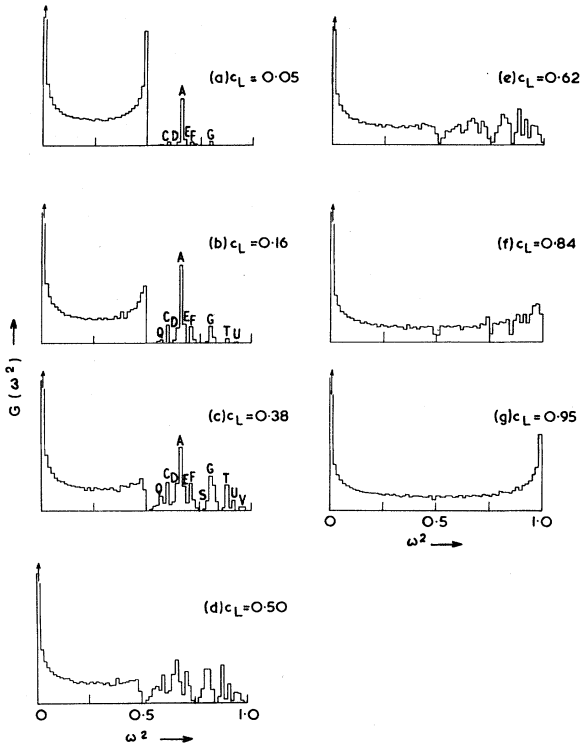

FIG. 1. Computed squared frequency spectra for two-component disordered chains containing 8000 atoms. The mass ratio is 2:1 and forces are restricted to nearest-neighbor pairs with force constants all equal. The parameter c_L refers to the fraction of light atoms in the chain. The abscissa is in terms of the maximum squared frequency of the monatomic light chain as a unit; thus 1.0 corresponds to the squared frequency $\omega_M^2(L)$, and 0.5 to $\omega_M^2(H)$.

taking on a particular pair of values, and the summation extends over all possible pairs of (α_i, β_i). It is clear, from the negative eigenvalue theorem, that

$$\int_0^{\omega^2} D(x)\,dx = \int_{-\infty}^{0} P[h(x)]\,d[h(x)], \qquad (4.5)$$

where $D(x)$ is the eigenvalue distribution function.

Dyson's formulation was complicated by the introduction of additional transformations which somewhat obscured the essential points of his argument, and which certainly made the practical realization of his method for finding $D(\omega^2)$ most difficult to attain. Schmidt's formulation was almost identical to that outlined here, and was later used by Agacy (1964) to compute an accurate spectrum.

In some cases of practical interest it is not possible to derive a simple functional equation such as (4.4) for $P(h)$ in view of correlations which exist between h_{i-1} and α_i and β_i. It is normally still possible to formulate exact expressions from which $P(h)$ may, in principle, be derived—but the system of equations may be very complex indeed. Dean and Martin (1960b), for example, have derived a set of four coupled functional equations whose solutions yield the distribution function $P(h)$ for the case of a two-component chain with nearest-neighbor forces which depend on the types of atoms to which they relate. It is unfortunate that such equations, because of their complexity, give little hope of accurate solutions in the foreseeable future.

Other early studies of two-component disorder in linear chains by the transfer-matrix method (Hori and Asahi, 1957; cf., Hori, 1968a)—again a method based originally upon the specific properties of tridiagonal dynamical matrices—provided techniques which, in principle, could lead to eigenvalue distribution functions. However, no specific calculations were carried out because of the difficult computing problems that were foreseen. The transfer-matrix method of Hori and Asahi (1957) was later to be of much value in clarifying and predicting many special properties of disordered systems, not only the two-component disordered chain, but also (in a generalized form of the theory) more complex systems (cf., Hori, 1968a). However, the method was not used for the precise calculation of frequency spectra.

The first attempt at a numerical evaluation of a frequency distribution function for the disordered two-component chain was that of Domb *et al.* (1959), using the moment trace method. This method depends upon the theorem that

$$\mu_i = \mathrm{trace}(\mathbf{M}^i), \qquad (4.6)$$

where μ_i is the ith moment of the eigenvalue distribution of the matrix $\mathbf{M}$. Thus we have

$$\mu_i = \int G(\omega^2)\omega^{2i}d(\omega^2). \qquad (4.7)$$

Spectra were computed by determining μ_i, for low i, by combinatorial means from the dynamical matrix $\mathbf{M}$, and then by inverting the transformation (4.7). The results obtained by this method, for a wide range of parameters of the system, showed fairly smooth featureless spectra with, over certain restricted ranges of frequency, one or sometimes two fairly distinct high frequency bands. Although these results were accepted at the time, it was later shown by the more precise numerical approach based on the negative eigenvalue theorem that they are incorrect. The difficulty was that the true frequency spectra are (as we shall see) most complicated in structure, and simply cannot be represented by low-order polynomials.

The negative eigenvalue theorem, in its specialized form for tridiagonal matrices was first used for the accurate computation of vibrational frequency spectra by Dean (1960, 1961). The basic equations of the technique are (4.2) and (4.3) which may be derived either as already indicated or, alternatively, from the sequence of Eqs. (3.6)–(3.14). The technique employed was to set up, by means of computer programs employing random number generators, typical long two-component chains of some thousands of atoms, having prespecified statistical properties. The sequence of numbers $\{h_i\}$ $(i=1, 2, \cdots, N)$ was then computed for

various values of ω^2, and the spectral points plotted merely by noting the proportion of negative h_i's. This method for tridiagonal matrices is known by numerical analysis as the Sturm sequence method; it has the virtue of being exceptionally stable numerically, as shown by Wilkinson (1965).

Figures 1 and 2 summarize the kind of information obtained for two-component chains by the numerical approach. The histograms are computed eigenvalue (i.e., squared frequency) spectra for randomly generated chains of length 8000 atoms, with an atomic mass ratio of 2:1, and with all force constants equal. The percentage of light atoms varies from 5% in Fig. 1(a), to 95% in Fig. 1(f), as indicated on the diagrams. In Fig. 2(a) we have plotted, again, the spectra for mass ratio 2:1, equal force constants, and 50% light atoms, but for a chain of length 32 000 atoms and with a somewhat smaller histogram interval than in Fig. 1; on this diagram we depict, for comparison, the spectra of two-component alternating chain $\cdots$ABABAB$\cdots$, and the result (Domb *et al.*, 1959) of a calculation for the disordered chain using the moment trace method as described earlier. Figure 2(b) depicts a histogram computed for a statistically identical system to that in Fig. 2(a), but composed of 250 000 atoms. This comparison is shown in order to indicate just how little is the change in the spectrum in increasing the chain length from 32 000 atoms to a quarter of a million; chains of several thousand atoms give as much information as is normally required.

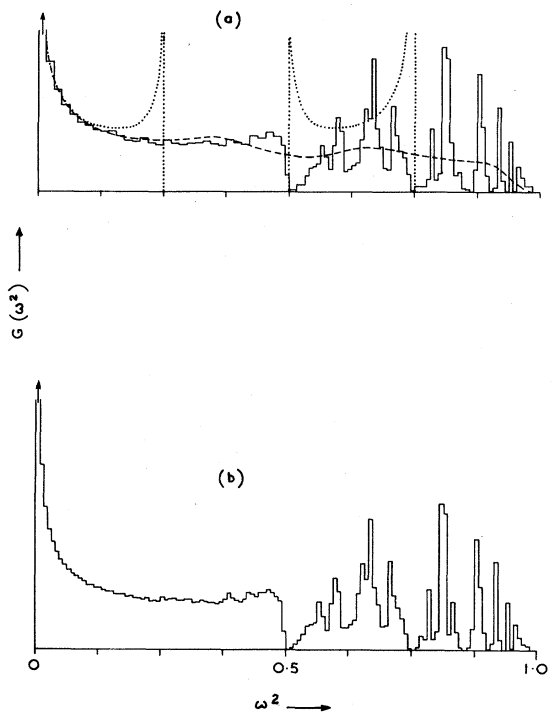

FIG. 2. Computed squared frequency spectra for disordered two-component chains ($c_L=0.5$) of length 32 000 in (a), and 250 000 in (b). The mass ratio is 2:1 as in Fig. 1, and the nearest-neighbor force constants are equal. In Fig. 2(a) we have depicted also (broken curve) the results of a moment-trace calculation using the first seven moments of the eigenvalue spectrum (after Domb *et al.*, 1959), as well as the well-known spectrum for the ordered chain $\cdots$ABAB$\cdots$ of the same mass ratio and force field.

The histograms depicted in Figs. 1 and 2 are complicated in form. The detailed structure in the spectra—induced by the disordered arrangement of the two atomic species—came as a considerable surprise when first published and, indeed, was at first greeted with a certain scepticism. However, a variety of later work, including some mathematically exact results, has amply confirmed the accuracy of the work and has also verified a suggested mechanism for the complex structure in the spectra. The basic idea proposed for the existence of the complicated system of peaks and valleys at the high-frequency end of the spectra was as follows. Each well-defined peak is regarded as associated with vibrational modes localized at particular types of local structure. Consider, for example, peak A in Fig. 1. This peak is composed of frequencies of modes which are highly localized about single light atoms surrounded in a local environment of heavy atoms. Thus, at each point in the chain where the local structure $\cdots$HHLHH$\cdots$ occurs (where L and H denote, respectively, light and heavy atoms), a strongly localized mode can be excited; such modes each contribute a frequency towards the peak A.

The other peaks in the high-frequency region of the spectrum are similarly associated with particular types of local structure. Thus peak G, for example, corresponds to the local structure $\cdots$HHLLHH$\cdots$, and F to the local structure $\cdots$HHLHLHH$\cdots$. Table I contains a list of such assignments.

The reason that each such local structure indicated in Table I can be regarded in essence as an independent unit when discussing normal modes of the complete chain is due to the effect of the two (or more) heavy atoms at each end of the unit. Provided the mass ratio is about 2:1 or greater, these heavy atoms act as almost impenetrable barriers to high and middle frequency modes; thus the nature and frequency of the localized mode of a light atom vibrating, for example, in a structure having the local geometry $\cdots$HHLHH$\cdots$ in a disordered chain are very little different from those of a light atom in an otherwise monatomic chain of H atoms. One can compare frequencies easily enough. The localized mode frequency of a light atom in a heavy monatomic chain (assuming all the force constants are equal) is given by

$$\omega_{\mathrm{loc}}^2=\omega_M^2(H)\,(1-\epsilon^2)^{-1}, \tag{4.8}$$

where $\omega_M^2(H)$ is the maximum squared frequency of the monatomic chain of heavy atoms and $\epsilon=1-m_L/m_H$, m_H and m_L being the respective masses of the heavy and light atoms. For the mass ratio 2:1 we obtain $\omega_{\mathrm{loc}}^2=\frac{4}{3}\omega_M^2(H)$, while the limits of peak A, simply

TABLE I. Correspondence between spectral lines (Figs. 1 and 3) and local chain structures.

Line(s)	Local chain structure
A	-HHLHH-
B, G	-HHLLHH- [a,b]
C	{-HHLLLHH-} [c] {-HHLHLHH-}
D, E	-HHLHHLHH- [b]
F	-HHLHLHH-
P, R, U	-HHLLLLHH- [a,b,d]
Q	{-HHLLLHLHH-} [c] {-HHLLLLLHH-}
S, V	-HHLLLLLHH- [b]
T	-HHLLLHH-

[a] The lines B and P occur only at mass ratios greater than 2.
[b] Two or more letters associated with a chain structure indicate that more than one distinct type of localized mode is associated with the local structure.
[c] Lines C and Q each contain frequencies associated with modes localized at two types of local structure, as indicated.
[d] For mass ratio 2, the line R occurs roughly at the frequency of line F.

reading abscissa values from Fig. 1, are $(21/16)\omega_M^2(H)$ and $(43/32)\omega_M^2(H)$ which clearly encompass the value ω_{loc}^2; a study of computed results using finer intervals (cf. Fig. 2) indicates that, in fact, peak A lies between $(85/64)\omega_M^2(H)$ and $(86/64)\omega_M^2(H)$, an interval which again includes the value ω_{loc}^2. We see therefore that the frequency of the localized mode of a light atom surrounded locally by at least two heavy atoms on each side is remarkably little affected by the form of chain structure elsewhere. A similar situation holds for other clusters containing light atoms surrounded locally by heavy atoms.

This simple picture of associations between peaks of the spectrum and local chain structure accounts fully for the changes which occur in the high-frequency region of the spectrum as the proportion of light and heavy atoms is changed. Thus, for the case of mass ratio 2:1, we notice that at low concentrations of light atoms the spectrum consists mainly of a band in the region $\omega^2=0$ to $\omega_M^2(H)$ reminiscent of the U-shaped function

$$G(\omega^2)=\pi^{-1}\omega^{-1}[\omega_M^2(H)-\omega^2]^{-1/2} \qquad (4.9)$$

for the spectrum of the monatomic lattice of heavy atoms; there is just a little structure at high frequencies, dominated by the peak A due to isolated light atoms. As the proportion of light atoms increases, the peak A first increases in intensity, due to the greater number of single light atom clusters. Also, peaks such as C, D, E, and F, due to clusters containing two light atoms become more dominant. At a certain stage, with increasing numbers of light atoms, peak A reaches a maximum intensity and then starts to decline at the expense of secondary peaks. This occurs because of the increasing probability of single light atom clusters joining together to form two- or multi-light atom clusters. At the composition of 38 per cent light atoms [in Fig. 1(c)] one can see that peak A has already decreased in intensity from its maximum value, and that the secondary and even tertiary peaks (such as T which corresponds to three-atom clusters) are quite pronounced. At the 50 percent composition and beyond, the structure becomes very complicated indeed, although it is clear that the identity of the individual peaks holds for quite high concentrations of light atoms. Ultimately the spectrum tends to the form (4.9), with $\omega_M^2(L)$ replacing $\omega_M^2(H)$.

At higher mass ratios, changes of the same kind occur and they are somewhat easier to follow because the individual peaks are more widely separated. Figure 3 shows computed spectra for the chain of mass ratio 3:1, with equal force constants, for three compositions. One notices that one effect of increasing the mass ratio is the emergence of additional peaks from the low-frequency continuum: peak B, for example, which is the lower of the two frequencies associated with cluster ···HHLLHH··· has no counterpart in Figs. 1

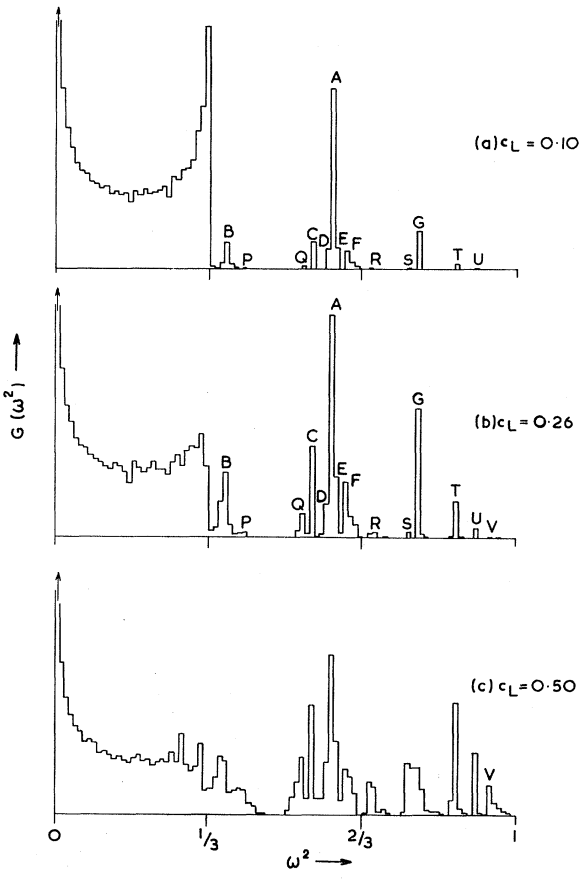

FIG. 3. Computed squared frequency spectra for disordered chains of length 8000 atoms, of mass ratio 3:1, with equal nearest-neighbor force constants. On the abscissa axis, we have $\omega_M^2(L)=1.0$ and $\omega_M^2(H)=\frac{1}{3}$.

and 2. It is also noticeable that the continuum exhibits structure, particularly towards its higher frequencies, a feature which is not evident in the spectrum for the mass ratio of 2:1.

As the mass ratio increases beyond 3:1, the spectrum becomes increasingly discontinuous in character. The limit of infinite mass ratio has been investigated by Domb *et al.* (1959), along with their moment trace investigation. They point out that the infinitely heavy atoms separate the light atom clusters into "islands" which vibrate quite independently of each other, so that the problem can be solved exactly. The spectrum consists of a δ function at the origin corresponding to the zero-frequency modes of the infinitely heavy atoms, together with an infinite number of δ functions in the range between 0 and ω_M^2 which occur at all the possible frequencies generated by light-atom clusters of all possible lengths. Since the frequencies generated by a chain of length n between rigid walls are given by

$$\omega^2=\omega_M^2(L)\sin^2[\pi t/2(n+1)], \quad t=1, 2, \cdots, n \quad (4.10)$$

it follows that the δ-function frequencies are given by formula (4.10), with n taking all possible integer values. The intensity of lines (i.e., of individual δ functions) is related simply to cluster probabilities which, in turn, are governed by the over-all proportion of light to heavy atoms. It is interesting to note that such a spectrum of δ functions is a most pathological mathematical function, having the property of being discontinuous at every point in the range of interest, 0 to $\omega_M^2(L)$. As Domb *et al.* (1959) point out, near any one δ function frequency of the spectrum there will be infinitely many other δ functions, but the closer any such frequency comes to the first the larger is the difference in their magnitudes. Payton and Visscher (1967a) have carried out the numerical computation of spectra for high-mass ratios, using the negative eigenvalue theorem, and have obtained results consistent with the remarks of Domb *et al.* (1959). One interesting feature of the squared frequency spectrum at high-mass ratios is its symmetry about a central point (neglecting the zero-frequency δ function); this property follows from (4.10) but is also a consequence of a more general symmetry theorem established by Bell and Dean (1968a).

The spectrum obtained by Domb *et al.* (1959) for infinite mass ratio is perhaps of some relevance in connection with the recently reopened question of localization in relation to the Anderson model (Anderson, 1958, 1970; Thouless, 1970; Economou, 1971; Economou and Cohen, 1971). It contributes a well-defined example of a system where the spectrum is dense in the sense of having no intervals of zero density in the range 0 to ω_M; the eigenstates are localized and the spectrum discontinuous, as described.

At mass ratios below 2:1, the spectrum of the two-component linear chain becomes increasingly smooth, tending again to the monatomic form as the mass ratio approaches unity. In Fig. 4 we plot results obtained

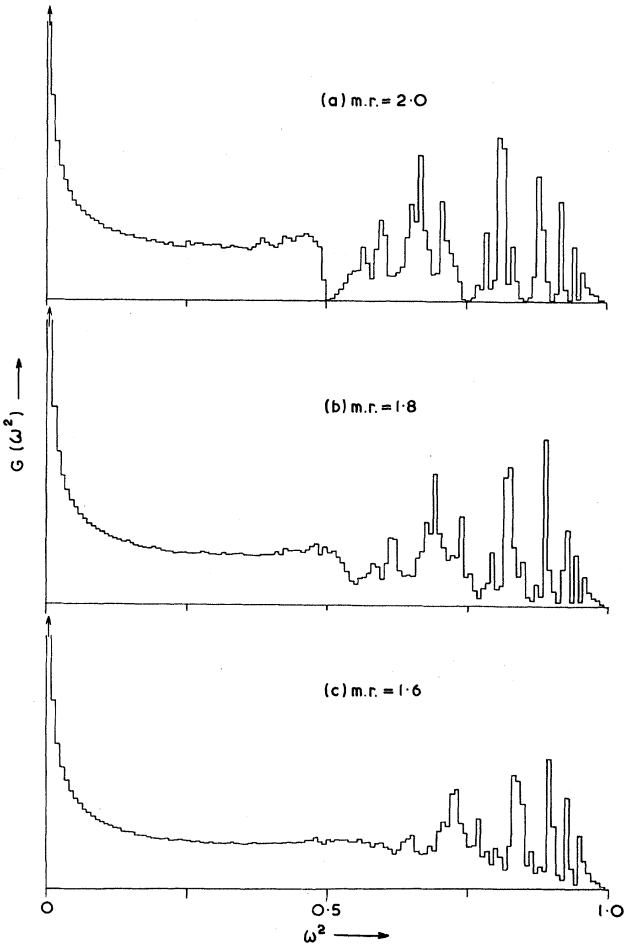

FIG. 4. Computed squared frequency spectra for disordered chains indicating changes which occur as the mass ratio decreases from 2:1 to lower values. For these three spectra $c_L=0.5$ and, as in previous figures, forces are confined to nearest-neighbor pairs with equal constants. In all three cases we have $\omega_M^2(L)=1.0$ on the abscissa axis, with $\omega_M^2(H)$ varying from 0.5 in (a) to 0.625 in (c).

for mass ratios 2:1, 1.8:1, and 1.6:1. It is clear that the form of the spectrum changes quite rapidly as the mass ratio moves below 2:1. The effect of having force constants which depend upon the types of nearest neighbor atoms to which they relate has been investigated by Payton (1966) and by Dean (unpublished). Again, one finds extremely complex spectra which can be explained in terms of the basic ideas already described.

We have mentioned that the study of the eigenvectors of the disordered nearest-neighbor two-component chain have fully verified the suggestions outlined for the existence of highly structured spectra. The first accurate vectors were obtained by Rosenstock and McGill (1962) using, in effect, the difference Eqs. (4.1) to compute successive vector components u_i. The method yielded accurate vectors for the short

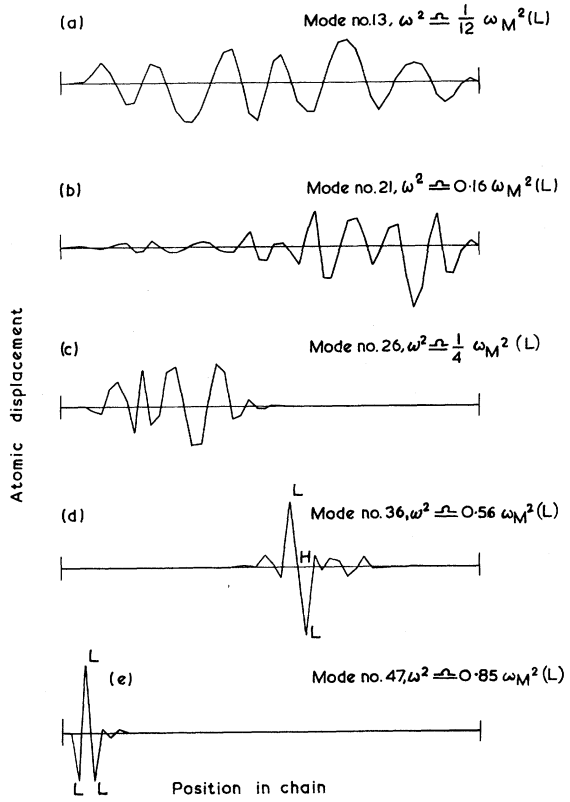

FIG. 5. Form of modes for the isotopic disordered chain of mass ratio 3:1 based on calculations (Dean and Bacon, 1963) for a chain of length 50 atoms (under the rigid wall boundary condition). Atomic displacements are plotted vertically, and atomic position in the chain horizontally. In the case of the two highest-frequency modes, the atomic types near the centre of localization are noted. Refer to Fig. 3(a) for the positions of the modes in the spectrum.

chain lengths involved, up to about sixteen atoms, but there is the danger that this approach could run into difficulties due to numerical instability if applied to very long chains. Dean and Bacon (1963) computed spectra for chains of length 50, using inverse iteration. Figure 5 indicates the form of vectors obtained for chains of mass ratio 3:1 at various frequencies: the association of the high-frequency modes with various types of local atomic arrangement, and the general intensification of localization with increasing frequency, are two features of the results. Eigenvector calculations for disordered two-component chains have also been carried out by Payton (1966) and Payton and Visscher (1967b), again by inverse iteration, and they confirm the features described above.

It was mentioned earlier that Agacy (1964) solved a functional equation—essentially one in the form derived by Schmidt (1957)—for the disordered two-component chain. He considered the case of mass ratio 2:1, with equal force constants, and solved the functional equation numerically using finite representation of the solution and standard linear algebra procedures. Agacy's spectrum agrees closely with that derived from the negative eigenvalue theorem. This agreement is most significant in that the functional equation relates to an ensemble-averaged system, unlike those calculated for particular chains.

A number of interesting and valuable exact results for the spectrum of the two-component disordered chain with nearest-neighbor and equal interactions has become known following the work of several authors (Borland, 1964; Hori, 1964a,b; Matsuda, 1964; Matsuda and Okada, 1965). These results apply to so-called "special" frequencies at which infinitesimal gaps occur for certain ranges of parameters in the frequency distribution function. Special frequencies occur at the points

$$\omega^2 \equiv \omega(s,t)^2 = \omega_M^2(L)\cos^2(\pi s/2t), \quad (4.11)$$

where s and t (with $s<t$) are integers prime to each other, provided only that the mass ratio m_H/m_L is greater than a certain critical value defined by

$$(m_H/m_L)_{\text{critical}} = 1 + \cot(\pi/2t)\tan(\pi s/2t). \quad (4.12)$$

Matsuda and Teramoto (1965) have proved that

$$\begin{aligned} N[\omega(s,t)^2] &= 1-[c(1-\alpha)\alpha^{t-2}/(1-\alpha^t)] \qquad (s=1), \\ &= 1-\frac{c(1-\alpha)}{\alpha(1-\alpha^t)}\sum_{j=1}^{s-1}\alpha^{[jt/s]} \qquad (s\geq 2) \end{aligned} \quad (4.13)$$

for the integrated frequency spectrum

$$N(\omega^2) = \int_0^{\omega^2} G(\omega^2)\,d\omega^2 \quad (4.14)$$

provided that $m_H/m_L \geq (m_H/m_L)_{\text{critical}}$. In Eq. (4.13), c is the concentration of light atoms, and α is the probability that a given site (say, the ith) is occupied by a light atom, given that its neighboring site (the $i-1$th) is also occupied by a light atom; also $[jt/s]$ denotes the largest integer not exceeding jt/s.

Equation (4.13), and the gap property of the special points, have provided most valuable checks on the validity of the numerical work. For example, for the case of 50% composition and a completely random structure ($c=\frac{1}{2}$, $\alpha=\frac{1}{2}$), we have

$$\begin{aligned} N[\omega(s,t)^2] &= 1-[1/(2^t-1)], \qquad (s=1) \\ &= 1-\frac{2^{t-1}}{2^t-1}\sum_{j=1}^{s-1}\alpha^{[jt/s]} \qquad (s\geq 2) \end{aligned} \quad (4.15)$$

giving, for $s=1$, $t=2$, and provided that $m_H/m_L \geq 2$, the result $N[\frac{1}{2}\omega_M^2(L)] = \frac{2}{3}$, and verifying the accuracy of figures given by Dean (1960, 1961). Moreover, at the point $\omega^2 = \frac{1}{2}\omega_M^2(L)$ one can actually observe the existence of a gap in the numerically calculated spectrum (as in Fig. 2, for example). Numerical results have similarly been confirmed at other points in the spectrum, and for numerous other cases.

Frequency spectra of disordered chains with second

as well as first neighbor atomic forces have been investigated by Martin (1961), again using the direct numerical approach. The dynamical matrix for Martin's model is of the five diagonal banded form

$$\mathbf{M}=\begin{bmatrix} \alpha_1 & \beta_2 & \gamma_3 & & & & 0 \\ \beta_2 & \alpha_2 & \beta_3 & \gamma_4 & & & \\ \gamma_3 & \beta_3 & \alpha_3 & \beta_4 & \gamma_5 & & \\ \cdot & \cdot & \cdot & \cdot & \cdot & & \\ & \cdot & \cdot & \cdot & \cdot & \cdot & \cdot \\ & & \cdot & \cdot & \cdot & \cdot & \cdot \\ 0 & & & & \gamma_N & \beta_N & \alpha_N \end{bmatrix}. \quad (4.16)$$

Martin computed the determinants of leading principal minors of the matrix $\mathbf{M}-\omega^2\mathbf{I}$, i.e., the sequence

$$\Delta_0\equiv 1, \Delta_1, \Delta_2, \cdots, \Delta_n, \quad (4.17)$$

where Δ_i is the determinant of the leading principal minor of order i. He used the recurrence formulas

$$\begin{aligned} \Delta_i &= (\alpha_i-\omega^2)\Delta_{i-1}-\beta_i^2\Delta_{i-2}-\gamma_i^2 A_{i-1}+2\beta_i\gamma_i B_{i-1}, \\ A_i &= (\alpha_i-\omega^2)\Delta_{i-2}-\gamma_i^2\Delta_{i-3}, \\ B_i &= \beta_i\Delta_{i-2}-\gamma_i B_{i-1}, \end{aligned} \quad (4.18)$$

where A_i and B_i are the determinants

$$A_i=\begin{bmatrix} & & 0 \\ & \Delta_{i-2} & \cdot \\ & & \cdot \\ & & 0 \\ & & \gamma_i \\ \hline 0 & \cdots\ 0\ \gamma_i & \alpha_i-\omega^2 \end{bmatrix}, \quad (4.19)$$

$$B_i=\begin{bmatrix} & & 0 \\ & \Delta_{i-2} & \cdot \\ & & \cdot \\ & & 0 \\ & & \gamma_{i-1} \\ \hline 0 & \cdots\ 0\ \gamma_i & \beta_i \end{bmatrix},$$

together with the initial conditions

$$\Delta_0=1, \quad \Delta_{-1}=\Delta_{-2}=A_0=B_0=0, \quad \Delta_1=\alpha_1-\omega^2. \quad (4.20)$$

He then invoked the theorem that the number of negative eigenvalues of $\mathbf{M}-\omega^2\mathbf{I}$ is the same as the number of changes in sign of adjacent determinants in the sequence (4.17). This theorem is the same basic mathematical property on which the negative eigenvalue theorem depends (cf. the Appendix), and Martin's computational method is, in fact, a particularization—for the five diagonal banded matrix—of the technique outlined in Sec. 3.1.

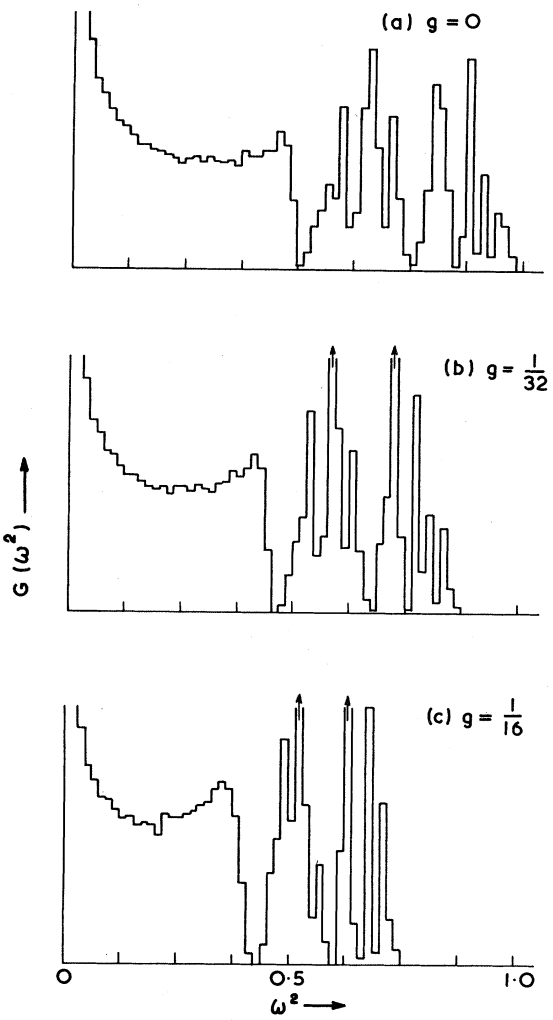

FIG. 6. Squared frequency spectra for the disordered isotopic chain of 50%–50% composition, length 8000 atoms, with first- and second-neighbor interactions. In each case $m_H=1$, $m_L=\frac{1}{2}$, and $f+4g=1$, f and g being the nearest-neighbor and second-neighbor force constants, respectively. The unit on the abscissa is in terms of $\omega_M^2(L)$, the maximum squared frequency for the light-atom chain with nearest-neighbor interactions only.

In applying his method, Martin generated by computer particular realizations of disordered two-component chains having various preset statistical properties. Figure 6 indicates the results he obtained for a completely disordered chain of mass ratio 2:1, 50%–50% composition and of length 8000 atoms. The top histogram is already familiar from earlier diagrams, and relates to the case of zero second-neighbor forces. The

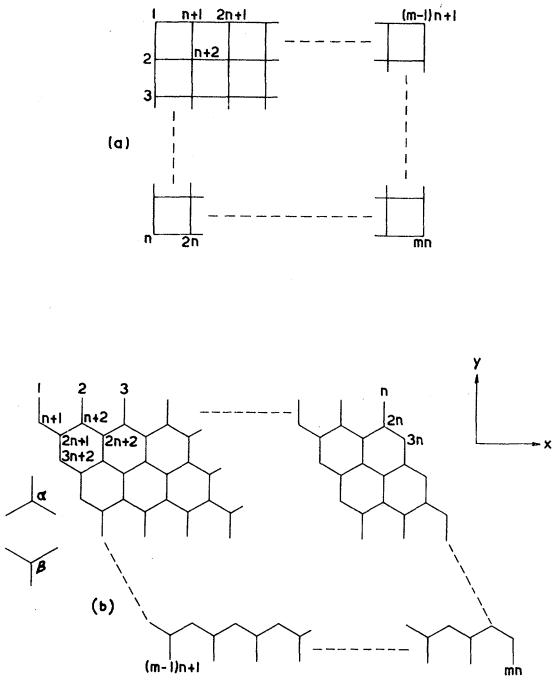

FIG. 7. Enumeration of lattice sites for (a) the simple quadratic lattice, and (b) the honeycomb lattice.

center histogram relates to the same chain but with the second neighbor to first neighbor force constant taking the ratio 1:28, and the lowest histogram to this ratio being 1:12. Martin's results show that the introduction of a relatively small amount of second-neighbor force has little effect on the major characteristics of the spectrum of the nearest-neighbor chain; there are some general drifts in the frequencies and features of the spectrum, and changes in the relative positions of peaks in the high frequency region, but the identity of peaks remains unchanged. Martin particularly noted this last point, that the identity of each peak in terms of a type of short-range structure about which certain modes are highly localized, remains unchanged. Sah and Srivasta (1970) have recently investigated the extent to which this holds good for higher relative values of the second-neighbor force, using the same method.

A considerable number of other studies of the disordered two-component chain have been carried out, using a variety of methods. We mention in passing the Green function approach first applied to this problem by Langer (1961) and Davies and Langer (1963), and since developed by other authors. This approach depends essentially upon the technique of expanding elements of the inverse dynamical matrix, averaging over all chains of the ensemble, and evaluating terms in the ensemble averaged series using diagrammatic methods. It has not been successful in showing the fine structure indicated by the numerical approach. A real shortcoming of the method is its inability to provide an assessment of the accuracy of the results it predicts.

Another method for the study of the disordered two-component chain is that of Flinn, Maradudin, and Weiss (1961) which is based on a modification of the transfer matrix method of Hori and Asahi (1957) as described by Faulkner and Korringa (1961). However, the method of ensemble averaging employed by Flinn *et al.* is now accepted to be erroneous. Yet another published method is that of Domb (1963): power series expansions were derived for the very long wave region of the spectrum, and a method was proposed which was stated to offer reasonable prospects for practical evaluation of the spectrum over the whole frequency range.

Apart from the Monte Carlo approach of studying the spectra of a small sample of particular long chains, one other particularly simple numerical approach has achieved some success. This is the technique of computing either the exact eigenvalues or the eigenvalue spectrum (using a convenient histogram interval) of chains of short length, say 10 or 12 atoms, and averaging over all possible structural configurations (2^{10} or 2^{12}). One finds that the high-frequency region of the resulting average spectrum reproduces almost exactly the correct spectrum for a very long chain. The reason lies in the high localization of the higher frequency modes; the localization is such that, at least for mass ratios of 2:1 or greater, the modes are relatively little affected by the proximity of the boundaries and thus vibrate very much as they would in an infinite system. Both Rosenstock and McGill (1968) and Borland (unpublished) have computed spectra for short chains in this way and observed their use in reproducing the high-frequency spectrum of the disordered chain. At low frequencies, where the modes interact appreciably with the boundaries, and for mass ratios much less than about 2:1, the method is of little value.

The effects of chain length and related questions in the numerical approach have been discussed in some detail by Matsuda (1966a). Perhaps the most complete catalogue, to date, of results for the disordered two-component chain are contained in the reports and papers by Payton (1966), and Payton and Visscher (1967a, b, 1968). This work carried out at Los Alamos discusses in detail the effects of variation of all the main parameters such as mass ratio, composition, chain lengths, order–disorder parameters, and force constants.

The two-component disordered chain does not represent accurately any physical system, and so one cannot make direct comparisons with experiment. This system is, rather, a testing ground for theory and numerical techniques and, in this sense, has proved most valuable. We already know, having introduced quite general equations in Sec. 3, that the numerical methods used for the linear chain are applicable to two- and three-dimensional systems. It is interesting, and emphasizes the value of studying the linear chain, that the general nature of the results discovered for this system extend to the higher dimensional structures.

4.2 Two- and Three-Dimensional Work

The numerical methods described in Sec. 3 have been applied to various two- and three-dimensional lattices and have clearly shown that the properties discussed for the one-dimensional system extend, in an obvious way, to these more realistic systems. It is perhaps not generally realized that one of the advantages of the numerical approach is that it is independent of dimension. Some other approaches used in one dimension—such as, for example, the method of setting up functional equations from which the spectrum can be derived—fail in two- and three-dimensional problems because of the lack of a sequential ordering in the atomic positions. The Green's function approach has been more successful in three, rather than in one, dimensions. However, as we indicate in Sec. 9, it shows no real promise as a predictive technique.

Dean and Bacon (1965) applied the direct numerical method to the problems of the two-component simple quadratic and honeycomb lattices. In both cases a nearest-neighbor force field was used and, for stability, noncentral as well as central forces for the simple quadratic lattice. With the lattice points enumerated as in Fig. 7(a), the equations of motion for displacement in the x direction of the atom i (not a boundary atom) can be written as

$$m_i\ddot{x}_i=\gamma_{ii+1}'(x_{i+1}-x_i)+\gamma_{ii-1}'(x_{i-1}-x_i)+\gamma_{ii+n}(x_{i+n}-x_i)+\gamma_{ii-n}(x_{i-n}-x_i), \quad (4.21)$$

m_i being the mass of the ith atom, and γ_{ij} and γ_{ij}' being the central and noncentral force constants, respectively, between the atoms i and j. After substituting $\ddot{x}_i=-\omega^2x_i$ (for a normal mode of circular frequency ω), dividing the ith equation by $m_i^{1/2}$, and changing to new displacement variables $u_i=m_i^{1/2}x_i$ ($i=1, 2, \cdots, mn$), the equations (4.21) can be cast in the form

$$(\mathbf{M}_{SQ}-\omega^2\mathbf{I})\,\mathbf{u}=0, \quad (4.22)$$

with $\mathbf{M}_{SQ}$ a symmetric matrix of block tridiagonal form of order $(mn\times mn)$, and $\mathbf{u}$ a vector of mn elements. A toroidal boundary condition was imposed in the y direction (thus, giving the atom $2n$ a noncentral force interaction with the atom $2n+1$), and a rigid wall boundary condition in the x direction.

The feature of this model of simple quadratic lattice with nearest-neighbor interactions is that the atomic vibrations in the x and y directions are independent. Dean and Bacon (1965) considered explicitly motion in the x direction; vibrations in the y direction can be treated in an exactly analogous manner.

The equations of motion for the honeycomb lattice are rather more complicated than those for the simple quadratic lattice, there being no question of separating atomic motions in two perpendicular directions in this case. A section of lattice as in Fig. 7(b) was considered. Notice that there are two kinds of lattice site, denoted by α and β in the diagram. The equations of motion for an atom i, on an α lattice site may be written as follows:

$$m_i\begin{pmatrix}\ddot{x}_i\\ \ddot{y}_i\end{pmatrix}=\gamma_{ii-n}\begin{pmatrix}0&0\\0&1\end{pmatrix}\begin{pmatrix}x_{i-n}\\ y_{i-n}\end{pmatrix}+\begin{pmatrix}-\frac{3}{4}\gamma_{ii+n-1}-\frac{3}{4}\gamma_{ii+n} & -\frac{1}{4}\sqrt{3}\gamma_{ii+n-1}+\frac{1}{4}\sqrt{3}\gamma_{ii+n}\\ -\frac{1}{4}\sqrt{3}\gamma_{ii+n-1}+\frac{1}{4}\sqrt{3}\gamma_{ii+n} & -\frac{1}{4}\gamma_{ii+n-1}-\frac{1}{4}\gamma_{ii+n}-\gamma_{ii-n}\end{pmatrix}\begin{pmatrix}x_i\\ y_i\end{pmatrix}$$
$$+\gamma_{ii+n-1}\begin{pmatrix}\frac{3}{4}&\frac{1}{4}\sqrt{3}\\ \frac{1}{4}\sqrt{3}&\frac{1}{4}\end{pmatrix}\begin{pmatrix}x_{i+n-1}\\ y_{i+n-1}\end{pmatrix}+\gamma_{ii+n}\begin{pmatrix}\frac{3}{4}&-\frac{1}{4}\sqrt{3}\\ -\frac{1}{4}\sqrt{3}&\frac{1}{4}\end{pmatrix}\begin{pmatrix}x_{i+n}\\ y_{i+n}\end{pmatrix} \quad (4.23)$$

provided that the atom is not at a boundary. Here x_i and y_i represent the x and y components of the displacement from equilibrium of the ith atom, m_i is the mass of the atom, and γ_{ij} is the central harmonic force constant acting between the atoms i and j. If i refers to an atom at a β lattice site then, again, provided the atom is not at a boundary, the equations of motion may be written as

$$m_i\begin{pmatrix}\ddot{x}_i\\ \ddot{y}_i\end{pmatrix}=\gamma_{ii-n}\begin{pmatrix}\frac{3}{4}&-\frac{1}{4}\sqrt{3}\\ -\frac{1}{4}\sqrt{3}&\frac{1}{4}\end{pmatrix}\begin{pmatrix}x_{i-n}\\ y_{i-n}\end{pmatrix}+\gamma_{ii-n+1}\begin{pmatrix}\frac{3}{4}&\frac{1}{4}\sqrt{3}\\ \frac{1}{4}\sqrt{3}&\frac{1}{4}\end{pmatrix}\begin{pmatrix}x_{i-n+1}\\ y_{i-n+1}\end{pmatrix}$$
$$+\begin{pmatrix}-\frac{3}{4}\gamma_{ii-n}-\frac{3}{4}\gamma_{ii-n+1} & \frac{1}{4}\sqrt{3}\gamma_{ii-n}-\frac{1}{4}\sqrt{3}\gamma_{ii-n+1}\\ \frac{1}{4}\sqrt{3}\gamma_{ii-n}-\frac{1}{4}\sqrt{3}\gamma_{ii-n+1} & -\frac{1}{4}\gamma_{ii-n}-\frac{1}{4}\gamma_{ii-n+1}-\gamma_{ii+n}\end{pmatrix}\begin{pmatrix}x_i\\ y_i\end{pmatrix}+\gamma_{ii+n}\begin{pmatrix}0&0\\0&1\end{pmatrix}\begin{pmatrix}x_{i+n}\\ y_{i+n}\end{pmatrix}. \quad (4.24)$$

Equations (4.23) and (4.24) become modified in obvious ways for boundary atoms according to the precise nature of the boundary conditions imposed.

Writing now $\ddot{x}_i=-\omega^2x_i$, $\ddot{y}_i=-\omega^2y_i$ for a normal mode of frequency ω, dividing each of the equations (4.23) and (4.24) by $m_i^{1/2}$, and changing to new displacement coordinates $u_i=m_i^{1/2}x_i$, $v_i=m_i^{1/2}y_i$, we find that the equation can be written in the matrix form

$$(\mathbf{M}_H-\omega^2\mathbf{I})\,\mathbf{w}=0. \quad (4.25)$$

The matrix $\mathbf{M}_H$ is of the block tridiagonal symmetric form

$$\mathbf{M}_H=\begin{bmatrix} \mathbf{P}_1 & \mathbf{R}_2 & & & & & 0 \\ \mathbf{R}_2^T & \mathbf{Q}_2 & \mathbf{S}_3 & & & & \\ & \mathbf{S}_3^T & \mathbf{P}_3 & \mathbf{R}_4 & & & \\ & & \mathbf{R}_4^T & \mathbf{Q}_4 & \mathbf{S}_5 & & \\ & & & \cdot & \cdot & \cdot & \\ & & & & \cdot & \cdot & \cdot \\ & & & & & \cdot & \cdot & \cdot \\ 0 & & & & & \mathbf{R}_m^T & \mathbf{Q}_m \end{bmatrix}, \tag{4.26}$$

with the submatrices $\mathbf{P}_i$, $\mathbf{Q}_i$, and $\mathbf{R}_i$ block diagonal as follows:

$$\mathbf{P}_i=\begin{bmatrix} \mathbf{C}_{(i-1)n+1} & & & & \\ & \mathbf{C}_{(i-1)n+2} & & & \\ & & \cdot & & \\ & & & \cdot & \\ & & & & \mathbf{C}_{in} \end{bmatrix}, \tag{4.27}$$

$$\mathbf{Q}_i=\begin{bmatrix} \mathbf{D}_{(i-1)n+1} & & & & \\ & \mathbf{D}_{(i-1)n+2} & & & \\ & & \cdot & & \\ & & & \cdot & \\ & & & & \mathbf{D}_{in} \end{bmatrix}, \tag{4.28}$$

$$\mathbf{R}_i=\begin{bmatrix} \mathbf{F}_{(i-1)n+1} & & & & \\ & \mathbf{F}_{(i-1)n+2} & & & \\ & & \cdot & & \\ & & & \cdot & \\ & & & & \mathbf{F}_{in} \end{bmatrix}. \tag{4.29}$$

The matrix $\mathbf{S}_i$ contains a subdiagonal of blocks, in addition to the main diagonal:

$$\mathbf{S}_i=\begin{bmatrix} \mathbf{G}_{(i-1)n+1} & & & & & \\ \mathbf{H}_{(i-1)n+1} & \mathbf{G}_{(i-1)n+2} & & & & \\ & \mathbf{H}_{(i-1)n+2} & \mathbf{G}_{(i-1)n+3} & & & \\ & & \cdot & \cdot & & \\ & & & \cdot & \cdot & \\ & & & & \cdot & \cdot \\ & & & & \mathbf{H}_{in} & \mathbf{G}_{in} \end{bmatrix}. \tag{4.30}$$

The matrices $\mathbf{C}_j$, $\mathbf{D}_j$, $\mathbf{F}_j$, $\mathbf{G}_j$, and $\mathbf{H}_j$ are functions of the masses and force constants of the lattice, and are all of order (2×2), as follows:

$$\mathbf{C}_j=(4m_j)^{-1}\begin{bmatrix}3(\gamma_{jj-n}+\gamma_{jj-n+1}) & \sqrt{3}(\gamma_{jj-n+1}-\gamma_{jj-n})\\ \sqrt{3}(\gamma_{jj-n+1}-\gamma_{jj-n}) & \gamma_{jj-n}+\gamma_{jj-n+1}+4\gamma_{jj+n}\end{bmatrix},$$

$$\mathbf{D}_j=(4m_j)^{-1}\begin{bmatrix}3(\gamma_{jj+n-1}+\gamma_{jj+n}) & \sqrt{3}(\gamma_{jj+n-1}-\gamma_{jj+n})\\ \sqrt{3}(\gamma_{jj+n-1}-\gamma_{jj+n}) & \gamma_{jj+n-1}+\gamma_{jj+n}-4\gamma_{jj-n}\end{bmatrix},$$

$$\mathbf{F}_j=\frac{\gamma_{jj-n}}{(m_{j-n}m_j)^{1/2}}\begin{bmatrix}0 & 0\\ 0 & 1\end{bmatrix},$$

$$\mathbf{G}_j=\frac{\gamma_{jj-n}}{4(m_{j-n}m_j)^{1/2}}\begin{bmatrix}-3 & \sqrt{3}\\ \sqrt{3} & -1\end{bmatrix},$$

$$\mathbf{H}_j=\frac{\gamma_{jj-n+1}}{4(m_{j-n+1}m_j)^{1/2}}\begin{bmatrix}-3 & -\sqrt{3}\\ -\sqrt{3} & -1\end{bmatrix},\qquad(\gamma_{ij}\equiv\gamma_{ji}).\tag{4.31}$$

The vector $\mathbf{w}$ in Eq. (4.25) is the column vector of elements $u_1, v_1, u_2, v_2, \cdots, u_{mn}, v_{mn}$.

The eigenvalue distributions of the matrices $\mathbf{M}_{SQ}$ and $\mathbf{M}_H$ were calculated for a range of parameters corresponding to various values of the mass ratio, the ratio of central to noncentral force in the case of the simple quadratic lattice, and the concentration of the light atom species. Typical results for the simple quadratic lattice are shown in Fig. 8, and for the honeycomb lattice in Fig. 9. One can see that the main features noted in the case of the two-component disordered chain carry over to these disordered two-dimensional systems. For example, one notices that at low concentrations of the light atomic species the spectrum consists largely of a band in the low-frequency region similar to the band of the heavy monatomic lattice; in the high-frequency region one notices the emergence of a small number of peaks of low intensity. As the concentration of the light atomic species increases, the peaks in the high-frequency region become progressively more dominant and the low-frequency band loses the form associated with the heavy monatomic lattice. As the light atom concentration approaches 0.5, the spectrum becomes quite complex with a number of peaks and valleys throughout its entire range, and it remains complex until the proportion of light atoms comes very close to unity.

TABLE II. Correspondence between spectral lines and local structure.

Simple quadratic lattice (Fig. 8) $m_H/m_L=3:1$, $\gamma/\gamma'=1$		Hexagonal lattice (Fig. 9) $m_H/m_L=3:1$	
Line	Cluster of L atoms (any orientation)	Line	Cluster of L atoms (any orientation)
A[a]	•	A	•
B	•—•	B	•—•
C	•—•—•	C	
D			

[a] Most of the frequencies in the shoulder of the peak at A and at $\omega^2=4.2\gamma/m_L$ are probably associated with localized modes extended over two (or possibly more) light-atom clusters, at least one of which is the single light-atom cluster.

As in one dimension the peaks in the high-frequency region of the spectrum are associated with modes of vibration localized in the vicinity of particular types of local atomic configuration. Thus the peaks marked A, for example, in Figs. 8 and 9 are associated with modes of vibration localized at single light atom clusters embedded in a local environment of heavy atoms. As the concentration of light atoms increases from very small values towards $c_L=0.5$, this peak becomes relatively less dominant in relation to other peaks (B, C, and D, etc.) in the high-frequency portion of the spectrum which are associated with clusters containing two and more light atoms embedded in a local environment of heavy atoms. The sequence of changes in the spectrum is therefore very similar to the sequence we noted in Sec. 4.1 for the one-dimensional lattice, but of course there are quantitative distinctions. The information in Table II, relating to the assignments of peaks in the high-frequency spectrum of Figs. 8 and 9, was obtained by the simple device of calculating spectra for various lattice samples containing just a small concentration of particular types of light-atom impurity cluster.

Payton and Visscher (1966, 1967a, b) have carried

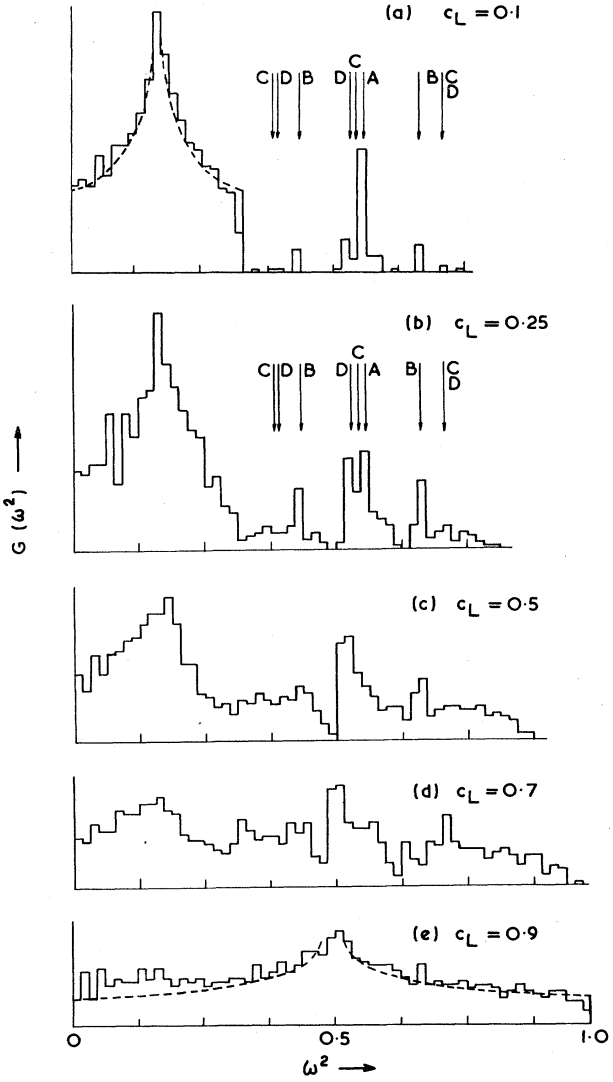

FIG. 8. Squared frequency spectra for the disordered two-component simple quadratic lattice of size 56×16 for which $M_H/M_L = 3:1$ and $\gamma = \gamma'$. The letters A, B, C, and D refer to Table II. The broken line in (a) is the spectrum of the monatomic heavy lattice, and that in (e) is the spectrum of the monatomic light lattice.

through a substantially more ambitious program of work on the vibrations of two- and also three-dimensional lattices. They computed not only the vibrational frequency spectrum of a whole range of lattice types and samples by the method outlined in Sec. 3.1, but also evaluated normal modes for these various lattices by an inverse iteration technique, accurate eigenvalues being first found by a diagonalization procedure devised by Ortega (1964). Ortega's method is a combination of the Householder method (Householder and Bauer, 1959) of matrix reduction and the diagonalization procedure of Givens (1953, 1954). The dynamical matrix is first reduced to tridiagonal form by a series of simple orthogonal similarity transformations, and the Sturm sequence technique of Givens is then used to find the accurate eigenvalues.

The lattices considered by Payton and Visscher are the square, triangular, simple cubic, body-centered cubic, and face-centered cubic structures. Figure 10 indicates a typical sequence of spectra obtained for the

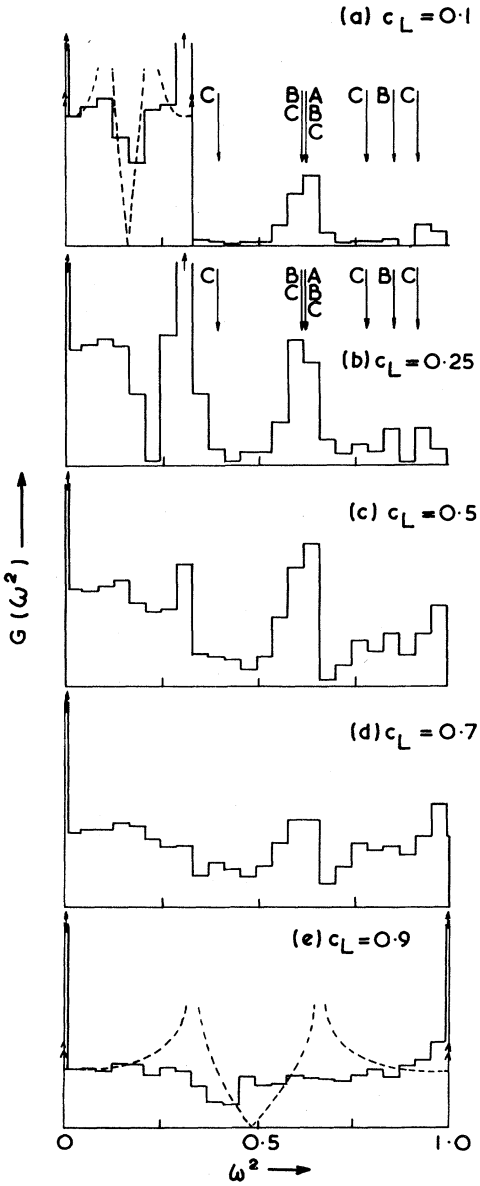

FIG. 9. Squared frequency spectra for the disordered two-component honeycomb lattice of size 50×18 for which $M_H/M_L = 3:1$. The letters A, B, and C refer to Table II. In (a) and (e), the broken curve represents part of the spectrum for the infinite monatomic lattice of heavy and light atoms, respectively. One-quarter of the frequencies of the theoretical spectra for the monatomic lattices also occur in a δ function at $\omega = 0$, and another quarter in a δ function at the maximum frequency of the continuous spectrum. These δ functions are represented in the diagrams by lines with double arrows.

simple quadratic lattice as the concentration is varied. These spectra correspond to a 30×30 atom section of lattice with a mass ratio of 3:1 and with equal central and noncentral forces. The agreement with the histogram of Fig. 8 is good in spite of the different lattice sizes chosen and the fact that Dean and Bacon used a coarser histogram interval in their work. Figure 11 indicates the effect of varying the mass ratio of the square lattice, as found by Payton and Visscher, for a given concentration of light to heavy atoms (25% light atoms; 75% heavy atoms). The spectrum becomes

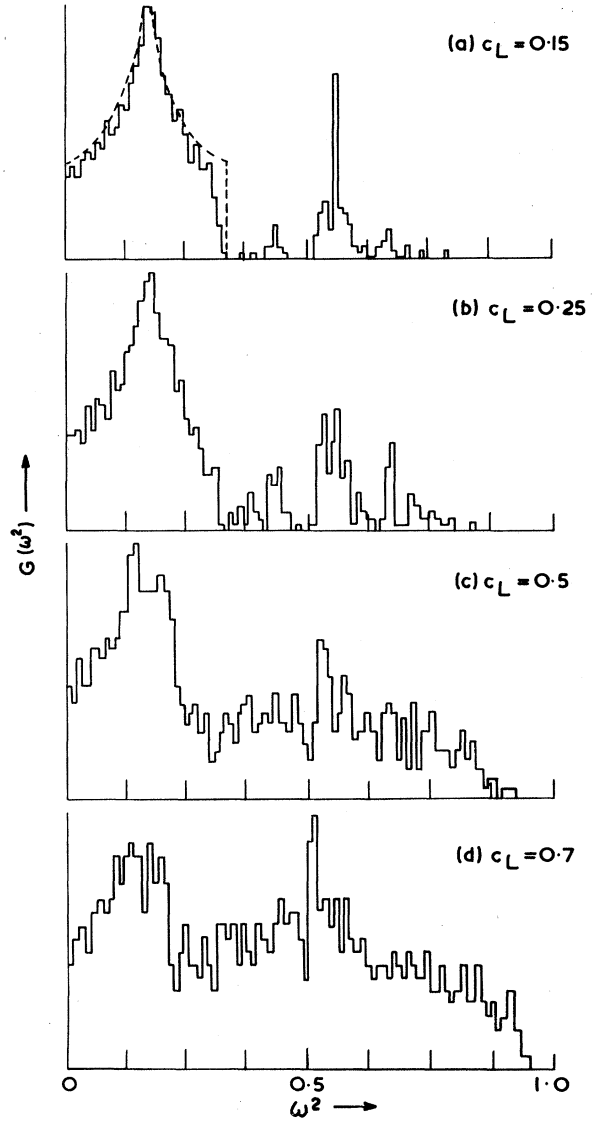

FIG. 10. Squared frequency spectra for disordered two-component simple quadratic lattices of size 30×30 with mass ratio 3:1, and equal central and noncentral force constants (after Payton and Visscher, 1967a). A good general agreement with the spectra of Fig. 8 is an indication of the reproducibility of results—even for quite small lattice sections—using the numerical approach.

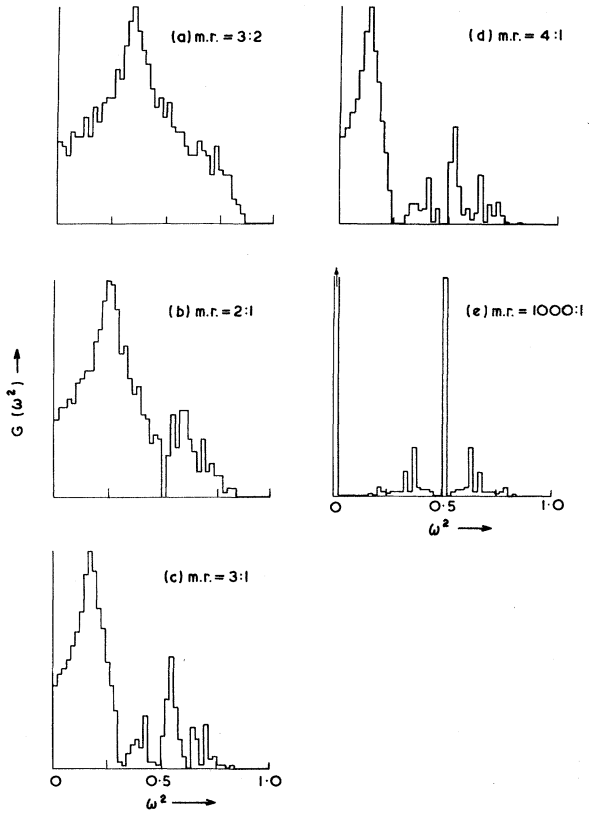

FIG. 11. Effect of varying the mass ratio on the squared frequency spectrum of the simple quadratic disordered lattice, given c_L=0.25 and γ/γ'=1. Special frequencies (see Sec. 4.1) begin to appear at the mass ratio 2:1; the low-frequency behavior of the spectra is determined largely by the harmonic mean mass up to the frequency of the big peak, whose position is inversely proportional to the harmonic mean mass, (after Payton and Visscher, 1967a).

progressively more peaky as the mass ratio increases, as in one dimension. At very high mass ratios, the squared frequency spectrum becomes symmetric about its center point, except for the existence of a low-frequency delta function; the explanation for this symmetry is given by Bell and Dean (1968a).

Calculated spectra for 10×50 sections of the triangular two-component disordered lattice are given in the report by Payton (1966). Again, these spectra show the existence of high-frequency peaks, corresponding to local modes, at low concentrations of light atoms.

The three-dimensional results of Payton and Visscher (1966, 1967a, b) are very much an extension of the findings for the linear chain and the two-dimensional lattices. The simple cubic lattice was mainly considered; this system has the advantage that one can again, as for the simple quadratic lattice, separate out motion in mutually perpendicular directions—provided forces are restricted to nearest neighbors. Payton and Visscher's results are based upon lattice sections of sizes 6×6×25 and thus are most limited in two of the three directions. Yet they all show features consistent with the changes

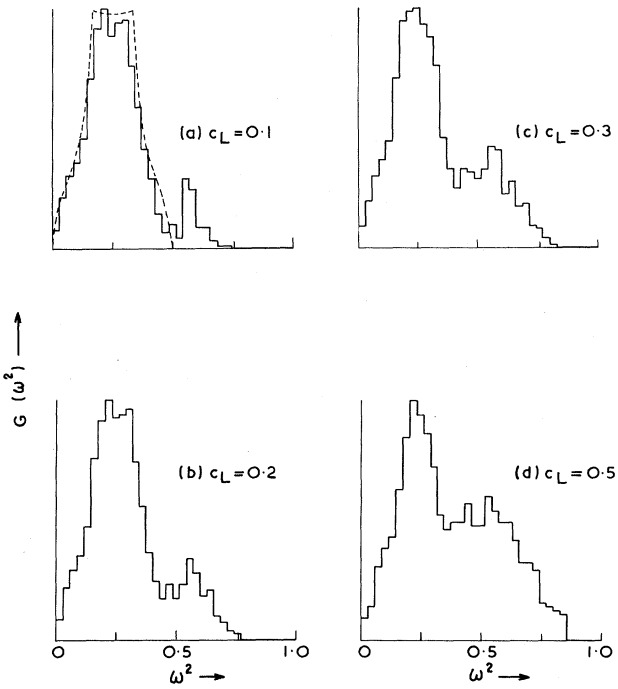

FIG. 12. Squared frequency spectra for disordered two-component simple cubic lattices of size 6×6×25 with mass ratio 2:1. The force field is one with equal nearest-neighbor central and non-central forces, and the broken line in (a) is the exact spectrum for the infinite monatomic lattice of heavy atoms (Payton and Visscher, 1967a).

mentioned for one- and two-dimensional lattices as parameters such as concentration of light atoms and the mass ratio of two atomic species are changed. These results are also supported by calculations of a similar type on sections of sizes up to 12×12×12 by Dean and Kingsley (unpublished), and there is little doubt that they represent well the general features of the spectrum of large three-dimensional two-component disordered structures.

Figures 12 and 13 depict spectra obtained by Payton and Visscher for sample structures of the simple cubic lattice. In Fig. 12, for the case of mass ratio 2:1, the fraction of light atoms is varied from 10% to 50% of the total. One notices here the existence of some high-frequency structure which becomes more clearly attached to the main low-frequency region of the spectrum as the light atom concentration is increased. In Fig. 13, the effect of varying the mass ratio is depicted for the concentration of 50% light atoms. At this concentration most light atoms belong to a cluster of infinite size (for the infinite lattice) and the spectrum has a quasicontinuous background at high frequencies. In both Figs. 12 and 13 the central and noncentral force constants were taken to be equal.

The fact that the three-dimensional lattice sections used are fairly small necessitates the use of a rather coarse histogram interval. This, in turn, makes it difficult to establish with certainty the existence of narrow and well-defined high-frequency peaks in the spectrum. However, Payton and Visscher have shown that the prominent high-frequency features in their computed spectra do encompass the frequencies of light atom modes embedded in local heavy atom environments. Their eigenvector calculations, which we discuss below, support the view that the nature of the high-frequency spectrum for three-dimensional disordered two-component lattices is qualitatively similar to that of the analogous one-dimensional systems.

We mentioned earlier that Payton and Visscher computed sample eigenvectors for the two- and three-dimensional disordered two-component structures. Although the vectors evaluated were for lattice samples fairly small in size, the results obtained point quite conclusively to the dominance of the local modes introducing the observed structure in the wide range of frequency spectra obtained for two- and three-dimensional lattices.

The interpretation of spectra, by Payton and Visscher (1967b), is based upon the computation of specific eigenvectors for small sample lattices in two and three dimensions. Thus, Fig. 14 is a squared frequency spectrum computed for a 14×14 section of a simple quadratic lattice, of mass ratio 3:1, with equal central and noncentral forces, and 15% light atom concentration. The lettering on the diagram refers to modes, picked out as examples, having the following characteristics:

(A) This is a mode of frequency $\omega^2/\omega_M{}^2 \simeq 1.99$, and is the higher-frequency vibration associated with an isolated pair of light impurities embedded in a heavy

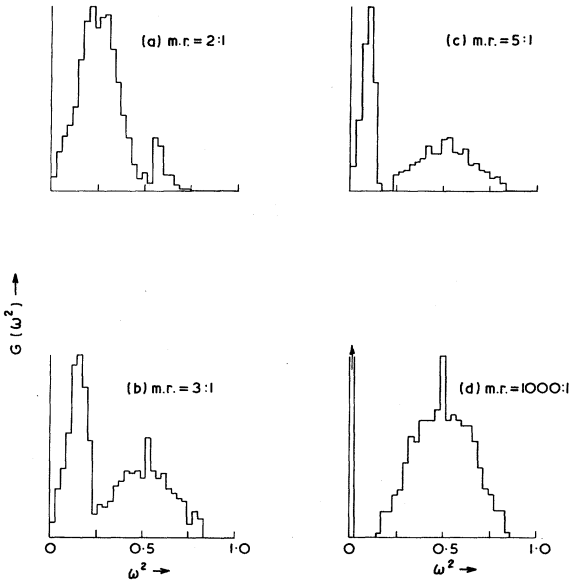

FIG. 13. Effect of varying the mass ratio on the squared frequency spectrum for the disordered simple cubic lattice of size 6×6×20 and 50%–50% concentration. The force field is one with equal nearest-neighbor central and noncentral forces (Payton, 1966).

atom local environment. It is an antisymmetric mode ($\leftarrow\rightarrow$), its symmetric counterpart ($\rightarrow\rightarrow$) having a frequency given by $\omega^2/\omega_M{}^2 \simeq 1.26$.

(B) This is the 13th highest frequency mode at $\omega^2/\omega_M{}^2 \simeq 1.7$, and it contributes to the high-frequency peak in the diagram. It is the localized mode associated with a single light atom embedded in a local environment of heavy atoms. The size of the peak in the figure reflects the facts that there are several isolated impurities of this kind in the lattice section and that many clusters of odd numbers of light atoms have modes which are almost degenerate with those of the isolated light atoms.

(C) This is the 26th highest mode and corresponds to the frequency $\omega^2/\omega_M{}^2 \simeq 1.1$. It is the first mode above the continuum, and is highly localized about a particular cluster of light atoms having the configuration

$$\begin{pmatrix} & L & L \\ L & & \end{pmatrix},$$

and embedded in a heavy atom local environment. The mode is a vibration of the form

$$\begin{pmatrix} & \rightarrow & \rightarrow \\ \rightarrow & & \end{pmatrix}.$$

Other modes for this particular light atom cluster are

$$\begin{pmatrix} & \rightarrow & \rightarrow \\ \leftarrow & \leftarrow & \end{pmatrix}, \quad \begin{pmatrix} & \leftarrow & \rightarrow \\ \rightarrow & \leftarrow & \end{pmatrix}, \quad \begin{pmatrix} & \leftarrow & \rightarrow \\ \leftarrow & \rightarrow & \end{pmatrix}$$

and correspond to the frequencies $\omega^2/\omega_M{}^2 \simeq 1.36$, $\omega^2/\omega_M \simeq 1.8$, and $\omega^2/\omega_M{}^2 \simeq 2.2$, respectively.

(D) This is the 27th highest mode and corresponds to the frequency $\omega^2/\omega_M{}^2 = 0.96$. This mode is the mode of highest frequency in the host lattice continuum and it is not nearly as localized as the higher frequency modes discussed above. Even so it is substantially more localized than the typical wavelike forms associated with monatomic or regular two-component lattices, only perhaps one quarter of the atoms of the lattice section contributing substantially to atomic motion in this particular mode.

Payton and Visscher were able to interpret the spectra of simple cubic lattices in an analogous manner. In Payton's original report (1966), their calculated modes for small two- and three-dimensional lattices are depicted as stereographic pairs, and it is recommended that the reader observe their diagrams and attempt (with or without the aid of a stereo viewer) to visualize the nature of the two- and three-dimensional vibrations. The diagrams of their published paper (1967b) consist only of single members of the stereo pairs. As mentioned earlier, these authors also carried out calculations of the spectra of two other three-dimensional lattices, the face-centered cubic and body-centered cubic lattices.

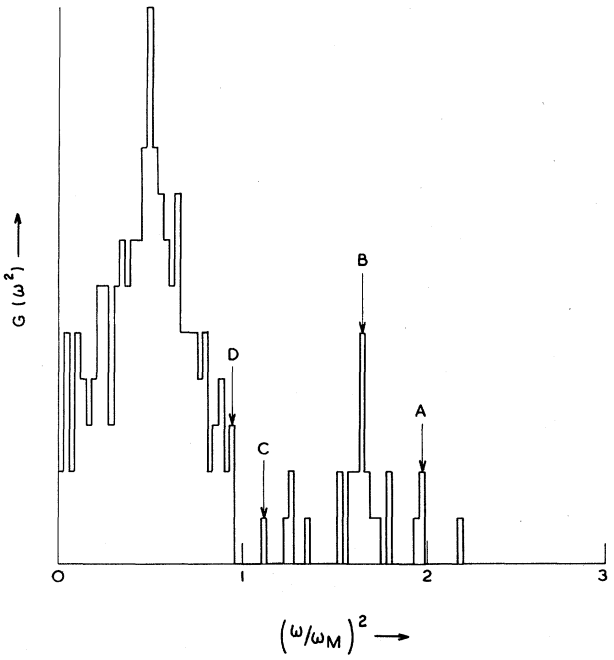

FIG. 14. Squared frequency spectrum of a 14×14 simple quadratic disordered lattice, some modes of which are described in the text. The mass ratio of the lattice is 3:1 and the noncentral and central nearest-neighbor forces are equal; the concentration of light atoms is 15%. The maximum frequency of the heavy monatomic lattice is denoted by ω_M. (After Payton and Visscher, 1967b.)

The results they obtained are qualitatively of the same kind as those found for all the other lattices considered. One notices, particularly at low light-atom concentrations, the existence of fairly well defined high-frequency peaks in the spectra, clearly associated with the localized vibrations of small light-atom clusters. As the concentration of light atoms increases away from small values, the spectra become very complex indeed, tending towards a more continuous form at high concentrations of the light-atom species.

All this shows that the picture obtained for the vibrations of atoms in disordered two-component chains carries over, with apparently few changes, to two- and three-dimensional disordered structures. As we have mentioned, however, certain qualitative differences do occur for the higher dimensional disordered structures. At any given concentration of the light atom species, it is clear that the high-frequency spectrum consists of many more peaks each of substantially less intensity than in the corresponding two-component linear chain. The reason is that there are, in three dimensions, many more types of small light atom clusters than in one dimension, and a correspondingly smaller probability of any particular type of cluster contributing a local mode frequency to the spectrum. At low concentrations of light atoms, the spectrum is basically quite similar to that of the one-dimensional chain. As the concentration of light atoms increases,

the spectrum becomes very complex indeed, with substantial numbers of peaks all of fairly low intensity appearing at the high-frequency end of the spectrum. Because of the relative small intensity of each of the peaks in the spectrum and the large number of such peaks the high frequency spectrum takes something of the appearance of a continuum. It is important to realize, though, that even at high light atom concentrations a sufficiently detailed analysis of the spectra of two- and three-dimensional lattices would show numerous peaks, possibly superimposed on a reasonably continuous background. Because the form of spectra is limited by the probability of occurrence of various light atom clusters, one expects rapid changes in the spectrum for two- and three-dimensional disordered lattices as the light atom concentration varies at values near the so-called "critical percolation concentrations" (Dean and Bird, 1967). This expectation is supported by the results of the various numerical studies.

Approaches other than the direct numerical method for two- and three-dimensional systems have not elucidated in any such detail the nature of atomic vibrations in the two-component disordered solids. The Green's function approach, as applied to the phonon problem, has however had some success. Maris (1966) calculated the spectrum of a disordered face-centered cubic system with a mass ratio close to unity. Taylor (1967), using a self-consistent approach based upon equations derived from multiple-scattering theory, produced results for frequency spectra in good agreement with the studies of Payton and Visscher (1967a) for the simple cubic lattice. He also used his result to reinterpret experimental data for Ge–Si alloys with some success. Leath and Goodman (1969) carried through a calculation based on an unperturbed reference lattice of mean-inverse mass and obtained results for the simple cubic structure again consistent with the numerical studies of Payton and Visscher (1967a); however, comparison of a calculation on a linear chain with one-dimensional numerical results showed a failure to reproduce spectral detail at high frequencies. Other work on the development of the approach includes papers by Yonezawa (1968), Takeno (1962, 1968) and Aiyer *et al.* (1969). As indicated earlier in the section on one-dimensional two-component systems, a major difficulty of the Green's function method is the lack of a means to provide an assessment of the accuracy of computed results.

The moment-trace method, outlined in Sec. 4.1, is independent of dimensionality, and Bradley (1961) has carried through a calculation for a simple cubic disordered structure. However, the substantial difficulties in obtaining large numbers of moments, as required for a detailed spectrum, provide a real barrier to any real progress by this method for three-dimensional systems.

The concept of "special" frequencies, discussed in Sec. 4.1 in connection with the two-component disordered chain, carries over in a somewhat restricted sense to higher dimensional lattices. Matsuda (1966b) showed that every cluster frequency, that is every frequency of a finite cluster of light atoms surrounded in its lattice environment by infinitely massive heavy atoms becomes what he terms a "generalized special frequency" or GSF. These frequencies are such that there appear at these points infinitesimal gaps in the spectrum provided that certain conditions in the atomic arrangements and mass ratio of the species hold good. No simple formula exists, as in one dimension, either for the values of the GSF's or the corresponding critical mass ratios. Hori (1968b) has shown how to calculate these quantities, and with Wada gives a readable and full account of the concept of GSF's in a recent review (Hori and Wada, 1970). There seems to be good agreement between the results of these calculations and spectral features obtained by the direct numerical method in cases where comparisons are appropriate.

5. GLASSES

Glasses represent a totally different class of disordered system from those considered hitherto, both in their properties as real materials and in the theoretical problems they present. A great deal of experimental work relating fairly directly to their atomic vibrations have been carried out. Simon (1960) documents most of the infrared and Raman work on simple glasses up to about 1959, and since that time numerous other studies have been carried out. Thus, on the experimental side, there is a wealth of data available from work extending back over many years.

The major difficulty associated with the theory of atomic vibrations in glasses lies not so much in attempting to solve equations of atomic motion, but rather in formulating the mathematical problem from a starting point of the usual insufficient and rather vague information on the structure of glasses. The significant characteristic of the atomic structure of glasses is that of spatial disorder, i.e., that the atoms do not lie on sites of a regular lattice but in random positions in space, subject to certain near-neighbor restrictive conditions. Such structures cannot easily be specified mathematically in the way one can specify—in a statistical sense—the disorder in, for example, a two-component lattice, and it is not possible to set up easily models on which to base theoretical investigations or computational work. This has, in fact, been the central difficulty for work on glasses, that of setting up a model as a starting point for investigations—and the problem of the equations of atomic motion seems relatively tractable in comparison with this.

In practice some progress has been made in theoretical studies. First, one-dimensional models exhibiting disorder in interatomic distances can be tackled without undue difficulty; one can order the atomic sites along the chain and use the techniques described in Sec. 3. However, it can be argued that such models neglect the problem of topological disorder. Bell (private com-

munication), though, has recently studied a one-dimensional system exhibiting topological disorder, as we indicate later. A second and important point of progress is that methods of building physical models of realistic atomic arrangements in glasses have proved most fruitful. In this work particular sample configurations of atoms representing the structure of a glass are built, and the coordinates of atoms in these models are used as a basis for calculating atomic vibrational properties. The Green's function and numerical approaches have both been used for the one-dimensional problem, but only the numerical method—used in connection with the physical models just mentioned—has so far been used for the three-dimensional problem.

5.1 One-Dimensional Models

In one dimension one cannot reproduce the kind of spatial disorder which characterizes the atomic geometry of real glasses. The most one can do is to introduce the concept of a continuous distribution of interatomic distances or (what amounts to the same thing) forces in the model. Thus, Dean (1964) studied the monatomic glass defined by the equations

$$-m\omega^2 x_i=\gamma_i(x_{i+1}-x_i)+\gamma_{i-1}(x_{i-1}-x_i) \qquad (i=1, 2, \cdots, N), \quad (5.1)$$

where the force constants γ_i are governed by an *a priori* continuous probability distribution function $P(\gamma_i)$ which is nonzero only in the region $0\leq\gamma_a\leq\gamma_i\leq\gamma_b$. Stated in this way, Eqs. (5.1) together with $P(\gamma_i)$ define an ensemble of chains. The work was concerned both with specific properties of the ensemble, and with the properties of individual representative chains as determined by the direct numerical method. A general result proved in the paper, one based upon an ergodic-type hypothesis, states that unless the chain is ordered (i.e., $\gamma_a=\gamma_b$), all nonzero frequency vibrational modes are localized. This result is supported by the numerical studies of particular chains from which, incidentally, one also sees a strong suggestion of a trend towards increasing spatial localization of modes with increasing frequency.

The numerical methods employed are essentially those described earlier. Chains of length 7900 atoms were realized using a random number computer routine which chose numbers γ_i in the range $\gamma_a\leq\gamma_i\leq\gamma_b$ with equal probability; this, in effect, gives harmonic force constants γ_i described by an *a priori* probability distribution

$$P(\gamma_i)=(\gamma_b-\gamma_a)^{-1} \quad \text{for } 0\leq\gamma_a\leq\gamma_i\leq\gamma_b$$
$$=0 \quad \text{otherwise.} \qquad (5.2)$$

The vibrational properties of the particular chains realized were investigated, using the Sturm sequence method for the distribution of frequencies, as outlined in Sec. 4, and the method of inverse iteration for a selection of atomic displacement eigenvectors (cf. Sec. 3). Typical spectra of squared frequencies are depicted in Fig. 15. The U-shaped form

$$G(\omega^2)=(2/\pi)[\omega_M^2-\omega^2]^{-1/2}, \qquad (0\leq\omega^2\leq\omega_M^2=4\gamma/m)$$

for the regular chain $\gamma_a=\gamma=\gamma_b$ is indicated by the continuous line in diagram (a). As the disorder of the structure increases, i.e., $P(\gamma)$ increases in width, the high-frequency end of the spectrum changes as indicated successively in Figs. 15(a), (b), and (c). In contrast to the cases of two-component disordered structures studied in Sec. 4, there is no structure in the spectrum. The small variations in the height of histogram intervals in the diagram are merely statistical fluctuations, as was verified by comparing results for chains of identical statistical properties but different realizations.

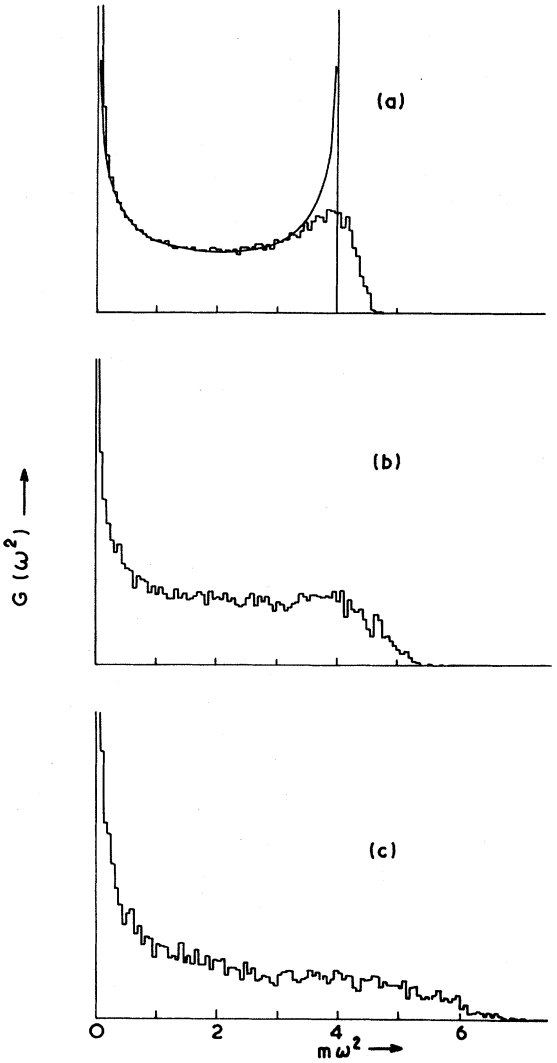

FIG. 15. Spectra of squared frequencies for monatomic chains in which the distribution of force constants is of the form (5.2). (a) $\gamma_a=\frac{3}{4}$, $\gamma_b=1\frac{1}{4}$; (b) $\gamma_a=\frac{1}{2}$, $\gamma_b=1\frac{1}{2}$; (c) $\gamma_a=0$, $\gamma_b=2$. The smooth curve in (a) is the spectrum for the ordered chain ($\gamma=1$).

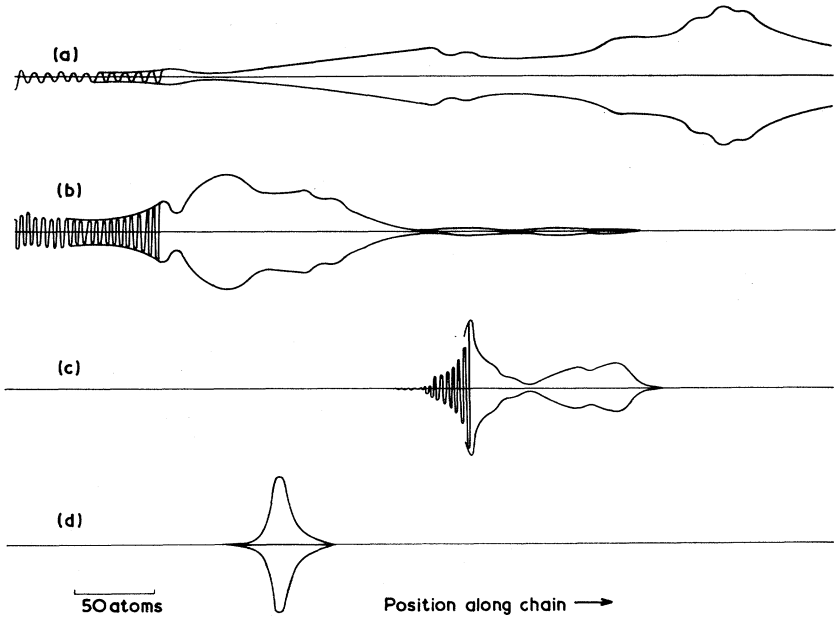

FIG. 16. Envelopes of atomic amplitudes for typical eigenvectors [(a) 128th, (b) 224th, (c) 288th, (d) 368th, corresponding approximately to $m\omega^2=1$, 7/4, 9/4, 3 on Fig. 15(a)] for a chain of 512 atoms in which the distribution of force constants is of the form (5.2), with $\gamma_a=\frac{3}{4}$, $\gamma_b=1\frac{1}{4}$. The fluctuations of individual atomic displacements are indicated to the left of the envelopes in (a), (b), and (c).

Atomic amplitude eigenvectors for the one-dimensional glass differ considerably from those typical of the periodic chain. In Fig. 16 we depict amplitude envelopes for four typical eigenvectors calculated for a chain of length 512 atoms with $\gamma_a=\frac{3}{4}$, $\gamma_b=1\frac{1}{4}$. The increase of localization with increasing frequency is most noticeable both here and in numerous other computed results obtained when the work was carried out. In the diagram, regions in which the amplitude appears to be zero indicate parts of the chain in which the atomic amplitudes of vibration for the mode depicted are extremely small, rather than identically zero. The equations of motion indicate that no two (or more) successive atoms can have zero amplitude in a (nontrivial) mode of vibration.

The smooth squared frequency spectra and the form of eigenvectors calculated for the monatomic glass models do not indicate any obvious dependence of vibrational modes on particular types of local atomic geometry, as is the case noted in Sec. 4 for two-component disordered structures. This difference may well be a consequence of the fact that, in the glasslike chain, the nature of changes in local environment due to disorder is not so discrete as that in two-component disordered systems, and moreover, in the case of the glasslike chains there exist (in the chains of infinite length) an infinity of local situations and not just a finite number (for, say, small atomic clusters surrounded locally by at least two heavy atoms on each side). It follows that even if highly localized modes are associated with particular types of local structure (as may be the case at high frequencies) there will be an infinity of such frequencies—not just a few preferred values as in Figs. 3–6—and these will average out to a continuum.

In addition to the monatomic chain, the alternating diatomic chain $\cdots$ABABAB$\cdots$ in which the force constants are governed by a continuous bounded probability distribution was considered (Dean, 1964). In a study of the effect of increasing disorder on the band gap, it was shown analytically that if $m\gamma_b<M\gamma_a$, no frequencies exist in the region

$$2\gamma_b/M<\omega^2<2\gamma_a/m. \tag{5.3}$$

Here M and m (with $M>m$) are the masses of the two types of atoms in the chains, and γ_a and γ_b (with $\gamma_b>\gamma_a>0$) are the limits of the bounded probability distribution function $P(\gamma)$ of the nearest-neighbor interatomic force constants. It was inferred that, as for monatomic chains, the atomic modes are localized if one assumes an ergodic-type hypothesis. As in the case of monatomic chains, a particular class of diatomic chains, with a $P(\gamma)$ distribution given by Eq. (5.2), was studied. Typical results for various degrees of order and the mass ratios 2:1 and 4:1 are depicted in Fig. 17. As the disorder is increased, the general trend of the results—away from the well-known diatomic form for the alternating chain towards a more continuous distribution—is clear from the histograms. Again, as in the monatomic case, there is no fine structure in the spectra—the small discontinuities arise merely from statistical fluctuations. The absence of frequencies in the range (5.3) was confirmed in all the cases of diatomic chains studied.

One particular (and unphysical) class of diatomic chains was studied exactly. These are disordered chains in which the mass ratio is infinity, i.e., in which single light atoms of mass m are separated by infinitely heavy walls (corresponding to the atoms of mass M) and with $P(\gamma)$ again given by, for example, (5.2). In this case the distribution of squared frequencies was shown to be of the form

$$G(\omega^2)=\delta(\omega^2)+\tfrac{1}{2}G_L(\omega^2), \tag{5.4}$$

with

$$G_L(\omega^2) = m(m\omega^2 - 2\gamma_a)(\gamma_b - \gamma_a)^{-2} \quad \text{for } 2\gamma_a \leq m\omega^2 \leq \gamma_a + \gamma_b$$
$$= m(2\gamma_b - m\omega^2)(\gamma_b - \gamma_a)^{-2} \quad \text{for } \gamma_a + \gamma_b \leq m\omega^2 \leq 2\gamma_b$$
$$= 0 \quad \text{elsewhere.} \qquad (5.5)$$

The δ function at the origin is associated with the zero vibrational frequency of the heavy atoms, whereas the "triangular" squared frequency spectrum, $G_L(\omega^2)$, is that due to the lighter atoms. A tendency towards the triangular form of spectrum is evident in chains of mass ratio 4:1 and is even more obvious in results for chains of mass ratio 8:1 not depicted in the original paper.

This work represents the only study by a direct numerical method of fully disordered "glasslike" chains with nearest-neighbor interactions. Studies using Green's function methods have been undertaken by Hindley (1967), and by Wu and Taylor (1969). In both cases agreement with the earlier numerical work, where tested, is good. In a sense Dyson (1953) was the first to consider glasslike disorder in a one-dimensional system for he studied analytically rather special models with continuous disorder similar in some respects to those described in this section. His results showed the frequency spectrum to be featureless and smooth, very much in agreement with the conclusions noted above from numerical studies. Anderson (1965) conjectured from general considerations that the frequency spectrum of a diatomic glasslike chain would be of the form similar to that eventually derived in the computer experiments.

As mentioned earlier, Bell (private communication) has studied the effect of topological disorder on the vibrational properties of one-dimensional disordered systems. He considered two classes of chains. In the first, each atom, in addition to interacting with its two nearest neighbors, was coordinated also to two other atoms of the chain randomly selected. In the second class of system, each atom of a chain was coordinated to four atoms, each of which was selected randomly. For both models, the interatomic forces were all taken to be equal and thus independent of the particular interacting atoms, and the chains were mainly of length 1600. For computational speed and convenience interactions were always confined to atomic pairs no further than 16 atoms apart. Bell's models clearly exhibit a type of topological disorder, from the manner of atomic linkages, rather than the usual random force (or mass) magnitude disorder (with topological order) normally associated with linear chains.

Bell, using numerical techniques similar to those outlined in this paper, found that for all classes of system the vibrational modes, except at very low frequencies, were spatially localized, and that the frequency spectra differed considerably from the spectra for periodic fourfold near-neighbor coordinated systems.

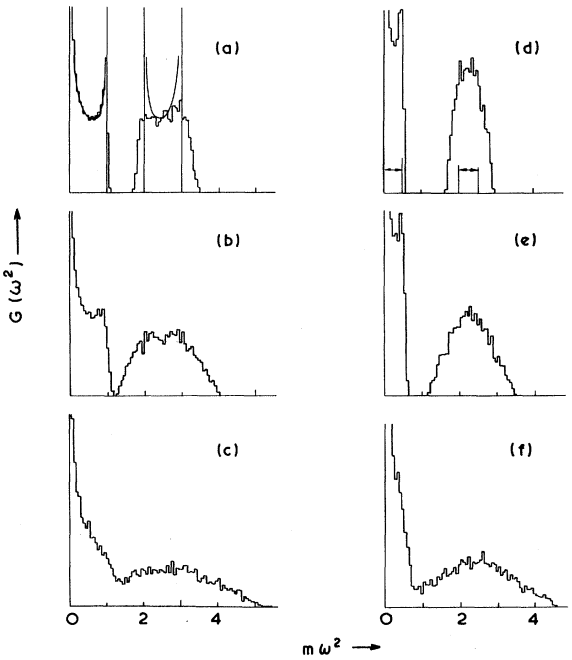

FIG. 17. Spectra of squared frequencies for diatomic alternating chains in which the distribution of force constants is of the form (5.2). Atomic masses are m and $2m$ in (a), (b), and (c), and m and $4m$ in (d), (e), and (f). The limits of the function $P(\gamma)$ are $\gamma_a = \frac{3}{4}$, $\gamma_b = 1\frac{1}{4}$ in (a) and (d); $\gamma_a = \frac{1}{2}$, $\gamma_b = 1\frac{1}{2}$ in (b) and (e), and $\gamma_a = 0$, $\gamma_b = 2$ in (c) and (f). In (a) the smooth curves depict the spectrum of the ordered chain ($\gamma = 1$), while in (d) the regions of the acoustic and optical bands of the spectrum of the ordered chain are indicated by the horizontal arrows.

Typically, for modes other than those having squared frequencies less than about one-tenth of the spectral maximum, perhaps only 100 to 200 atoms contributed effectively to the energy of vibration. The effect of the topological disorder of Bell's chains was thus very considerable. Bell's work was initiated specifically to meet the criticism that one-dimensional models provide results inapplicable to real glasses as linear chains lack the feature of topological disorder; it has succeeded in supplying useful new information.

5.2 Three-Dimensional Systems

The difficulties presented by the problem of atomic vibrations in a real glass have forced authors into a study of somewhat artificial three-dimensional systems having only some of the characteristics of a real glass. For example, molecular-like models containing just several atoms connected to rigid wall boundaries have been used in a number of cases; one way of attempting to impose glasslike disorder in a system of this kind is to calculate average properties over various configurations of the atoms. Work of this kind is closer in technique to that of conventional theoretical molecular spectroscopy than to studies of condensed disordered systems and will not be reviewed here. Other models of

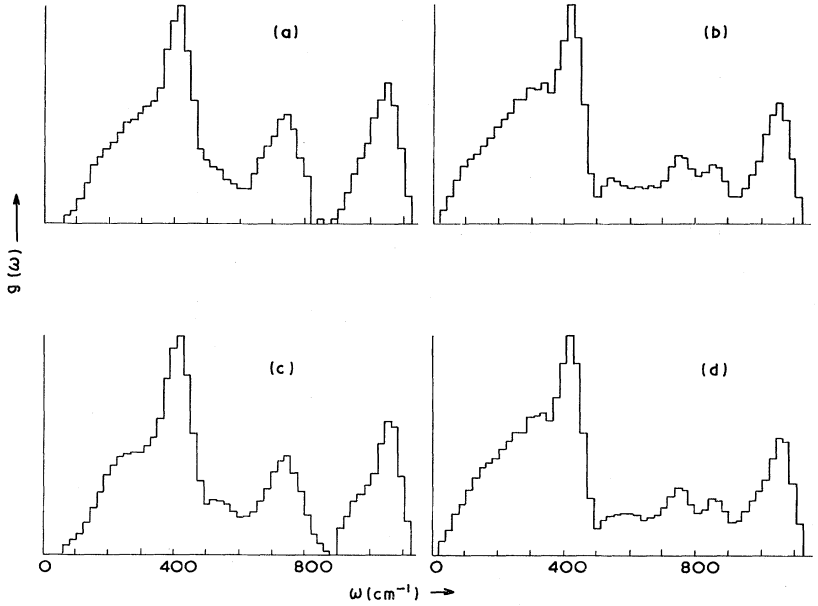

FIG. 18. Computed frequency spectra for vitreous silica for two sample atomic configurations (models I and II) each of about 500 atoms: (a) model I, fixed-end boundary condition; (b) model I, free-end boundary condition; (c) model II, fixed-end boundary condition; (d) model II, free-end boundary condition.

glasses considered in the past are quasilinear in form, having, for example, a regular zigzag chain as a basis structure. Although such models have also provided useful insights into certain aspects of atomic vibrations in a range of systems, this work, with its use of conventional techniques, does not really fall within the scope of this review (cf. Borrelli and Su, 1968).

To date there has been one investigation of atomic vibrations in realistic models of glasses—that is in models having the two essential features of size (and thus containing large numbers of atoms) and spatial disorder. This work has been based on sets of coordinates provided by the actual physical construction of models of glasses containing up to about 600 atoms each. Studies were undertaken of glasses of the vitreous silica type of structure—that is, of SiO_2, GeO_2, and BeF_2. The kind of physical model upon which the work is based has already been described in the literature (Bell and Dean, 1966, 1967). The aspect of model building and construction will not be dwelt upon in this review but rather we shall concern ourselves with the computation and results of the atomic vibrational properties.

The two ingredients upon which the vibrational work depends are (i) the atomic coordinates which specify a particular (and realistic) sample structure in the glass, and (ii) a reasonably accurate interatomic force field. We have already referred to the coordinates; these were obtained from various models, each containing some hundreds of atoms. The force field used was one involving nearest-neighbor interactions only, with both central and noncentral force components. Such a force field, with appropriately chosen parameters, is believed to simulate the true field in vitreous silica reasonably well, and is probably equally suitable for vitreous germania and beryllium fluoride.

The principle of the computational procedures for both the derivation of the frequency spectrum and atomic displacement eigenvectors is essentially that outlined in previous sections. The atomic coordinates and interatomic force fields are first processed to provide the elements of a symmetric dynamical matrix **M**, much as in Sec. 4, for example. In deriving **M**, it is important that the atomic coordinates are enumerated in a manner that provides a band form for **M** with the bandwidth at a minimum or near-minimum value. This is because of a point we noted in Sec. 3.1, that the amount of computation of the eigenvalue distribution of **M** varies approximately as the square of the bandwidth of the matrix.

The matrix **M** is of order three times the number of atoms in the model under consideration. The problem of attaining the minimum band form for a sparse matrix of this size (between 1000 and 2000 rows and columns) is, in general, extremely difficult. However, a reasonably economical bandwidth can easily be achieved by simply enumerating the atoms of the model upon which **M** is based in a systematic way, defining somewhat arbitrarily rows of atoms within successive vertical slabs within the model, and counting atoms in the successive "rows" as one would for atoms in a three-dimensional regular lattice. Alway and Martin (1965) have provided an algorithm whereby a minimum bandwidth can be achieved computationally; however implementation of this algorithm is very time consuming for a large matrix and therefore not desirable in view of the ease of attaining a near-minimum bandwidth as just stated.

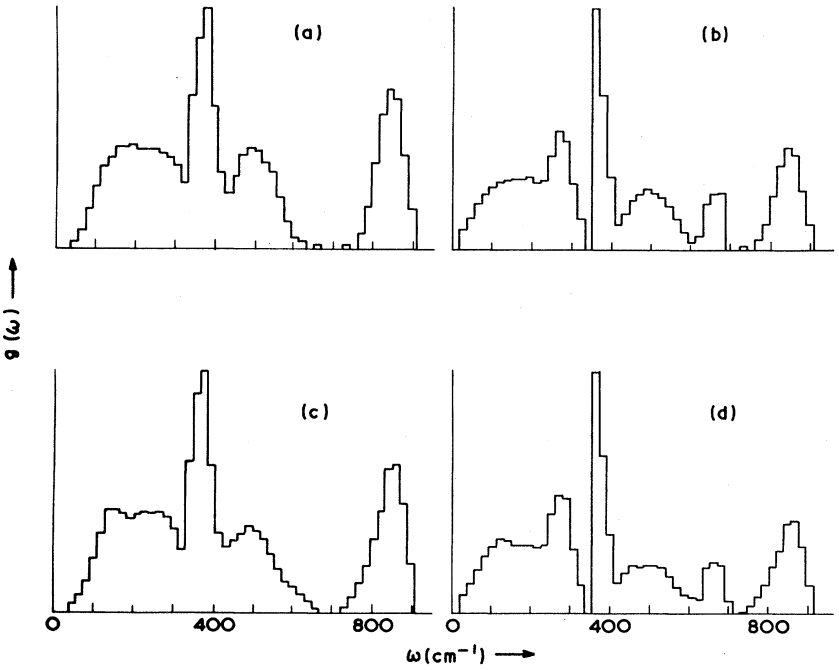

FIG. 19. Computed frequency spectra for vitreous germania. Designations of individual spectra are as for Fig. 18.

Computation of the eigenvalue distribution of **M** was achieved by the method described in Sec. 3. Starting at the top left-hand corner of the dynamical matrix, successive submatrices of size $s \times s$, where s is the maximum half-bandwidth of **M**, were operated upon as described, and the signs of successive top left-hand elements of the resulting matrix noted. Initially, the $s \times s$ block operated upon is sparse in form, containing mainly zero elements, but it soon fills with nonzero elements. Eigenvectors were calculated by inverse iteration, again as described in Sec. 3. Two types of boundary condition were used, the free-end condition—in which boundary atoms were allowed to vibrate freely under the influence of their neighboring atoms—and the fixed-end condition, in which the nonbridging boundary atoms were connected on one side to an

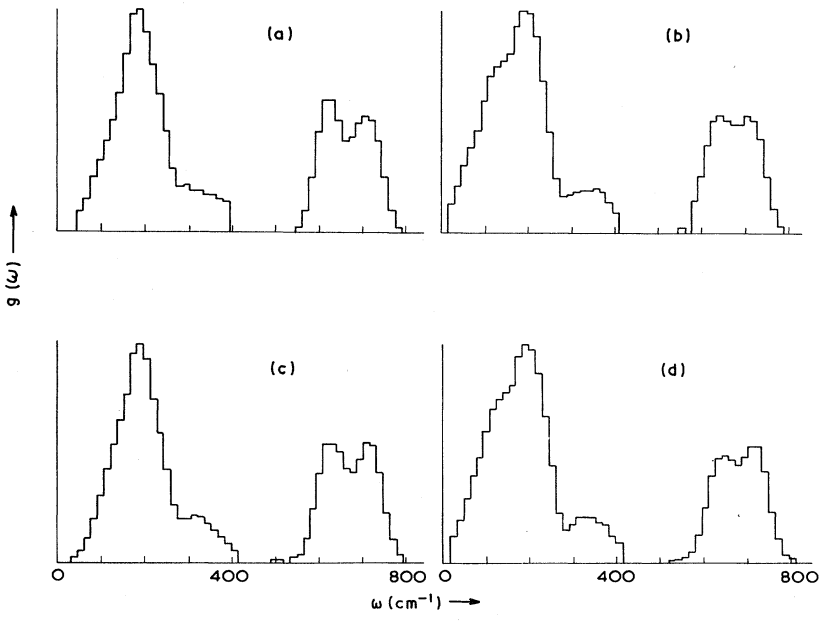

FIG. 20. Computed frequency spectra for vitreous beryllium fluoride. Designations of the individual spectra are as for Fig. 18.

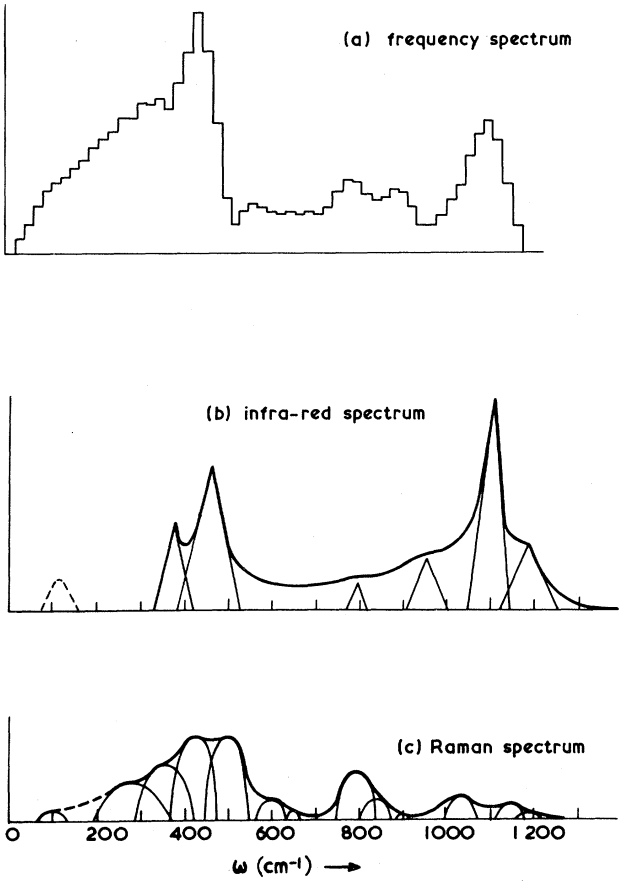

FIG. 21. Comparison of a computed vibrational frequency spectrum for vitreous silica [as in Fig. 18(b)] with composite infrared and Raman spectra of the glass from various experimental studies. Diagrams (b) and (c) are based upon composite spectra provided by Simon (1960). Abscissa values on the computed spectrum in (a) have been omitted, and the histogram scaled for the best fit with the spectra of (b) and (c); one can compare only the positions of bands between (a), (b), and (c), not the intensities.

atom of infinite mass, that is a rigid wall. In a three-dimensional structure containing several hundred atoms, the boundaries can in some circumstances exert a strong perturbing influence on the vibrational properties of the system, particularly at low frequencies. However, by using the two types of boundary condition, comparing results, and studying the nature of the calculated modes, the effect of the boundaries could be judged; the evidence suggested that their effect on the form of the frequency spectrum and on the general nature of the normal modes was not significant.

Figure 18 depicts computed frequency spectra (not squared frequency spectra as in some of the earlier diagrams) for two models of vitreous silica (Bell, Bird, and Dean, 1968). Diagrams (a) and (c) refer to spectra based on the fixed-end boundary condition, and (b) and (d) to spectra for the model with free-end boundary atoms. Thus (a) and (c) are directly comparable spectra for two models, and one notices the agreement in all the major features of these spectra. Again, (b) and (d) are directly comparable. In both cases statistical fluctuations due to differences in the models do not detract to any extent from the real and obvious features of the spectra. One interesting difference between the free-end and fixed-end spectra is the band (or rather peak) that occurs in the free-end case at about 900 cm^{-1}. As we show later, this band is associated with modes localized at nonbridging oxygen boundary atoms.

Similarly arranged spectra for vitreous germania and beryllium fluoride are depicted in Figs. 19 and 20. Again the excellent agreement of all the major features between spectra corresponding to different models under similar conditions is clear. In the case of vitreous germania, one notices two obvious additional spectral features induced by the presence of free-end oxygen atoms—a band between about 600 and 700 cm^{-1}, and a

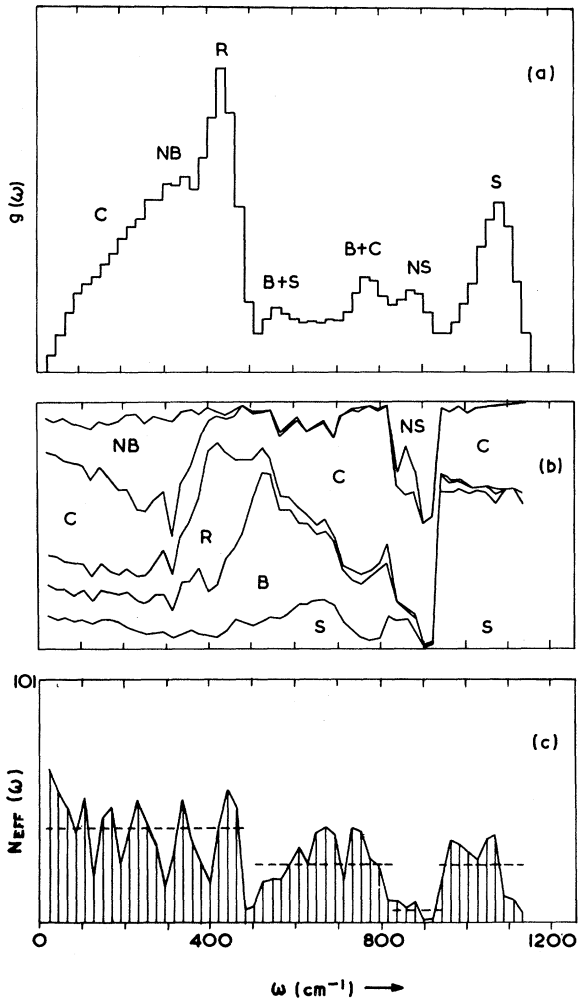

FIG. 22. Analysis of the vibrational modes for a free-end model of vitreous silica. Diagram (a) is the frequency spectrum, (b) an analysis of energy contributions to the normal modes throughout the spectrum, and (c) indicates the variation of spatial localization of the modes with frequency.

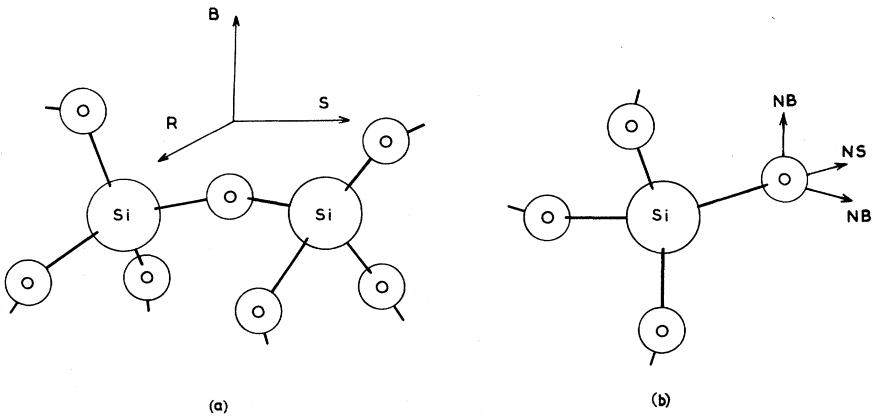

FIG. 23. Indication of the local coordinate systems for (a) bridging, and (b) nonbridging oxygen atoms, as used for the analysis of energies of the normal modes described in the text.

peak rising above a background spectrum of just under 300 cm^{-1}. The differences between free-end and fixed-end spectra for vitreous beryllium fluoride are relatively insignificant.

The calculated spectra agree well with what is known of experimental results relating to the vibrational spectra of the glasses considered. One cannot make a direct comparison of vibrational frequency spectra with experimental infrared and Raman spectra, for the experimentally measured results depend not only upon the normal mode density at each frequency but also upon intensity factors depending upon the changing dipole moments or polarizabilities of the various modes. One expects, though, that there should be an agreement in position (rather than in intensities) of bands of the computed spectra with those in experimental infrared and Raman spectra. When comparisons are in fact made, agreement is found to be good. In Fig. 21, the histogram (a) is the computed vibrational frequency spectrum for vitreous silica [as in Fig. 18(b)]. Figures 21(b) and (c) depict, respectively, composite infrared and Raman spectra based upon the results of various experimental studies up to about 1959 (Simon, 1960). There is clearly excellent agreement in the positions of all the main bands of (a) with those in (b) or (c). Similar good agreement exists for comparisons which have been undertaken for vitreous germania and beryllium fluoride. This agreement, for all three glasses, suggests that the models adopted, based upon the ideas of the random network theory with diffuse bond angle distributions at the oxygen (or fluoride) angles, are reasonable representations of the atomic structure of the glasses. The reason for comparing with experiment a spectrum, in Fig. 21, calculated on the basis of the free-end boundary condition will become clear later.

By studying the nature of the atomic displacement eigenvectors, assignments of the modes of vibration in the various regions of the spectrum have been made. In contrast to the cases of crystalline solids and simple molecules one cannot in general specify, in a simple way, the exact nature of a mode of vibration in a glass. It is possible, however, to talk about features of the typical modes within the various bands. One very clear point which must be impressed at the outset is that the modes are not simple waves (except at the very lowest frequencies), nor are they in general intensely localized about particular spatial localities. They are normally quite complex in form, with some evidence of spatial localization particularly at higher frequencies and band edges. Some exceptional types of mode, for example those occurring in the band (already referred to) at about 900 cm^{-1} in the free-end spectrum of vitreous silica, are highly localized.

Figure 22 is an attempt to show in diagrammatic form some details of the nature of the normal mode vibrations for vitreous silica (Bell and Dean, 1970). Diagram (a) is the spectrum of a model under the free-end boundary condition, as depicted earlier. Diagram (b) represents an analysis of contributions to the energy of the normal modes as a function of frequency, and is based upon a sample of 60 modes chosen at roughly equidistant frequencies throughout the spectrum; in (c) information is presented on the spatial extension or localization of the modes.

The energy associated with normal mode vibrations is divided into six classes in Fig. 22(b), each class being represented by an area whose vertical height, at any particular frequency, is a measure of the proportion of the total energy of vibration appropriate to that class. Thus, we see that at the high-frequency end of the spectrum, the total energy is almost exclusively divided into just two classes, those marked S and C, and that the ratio of energy between these classes is about 2:1. The labels S, B, R, C, NB, and NS in the diagram may best be understood by referring to Fig. 23. The motion of each bridging oxygen atom may be decomposed into components along local directions labeled B, S, and R, as shown. The B (or bond-bending) direction is defined as parallel to the bisector of the Si–O–Si angle; the S (bond-stretching) direction is perpendicular to the bisector but still in the Si–O–Si plane, and the bond-rocking R axis is normal to the Si–O–Si plane. For non-

bridging oxygen atoms, *NS* refers to the direction along the Si–O bond, and *NB* to *all* directions perpendicular to this bond. Referring back to Fig. 22(b), each labeled band (with the exception of *C*) refers to the total energy of vibration–at a particular frequency—of all the oxygen atoms moving as indicated in relation to their own local coordinate system. The band marked *C* indicates the energy contribution of all the silicon atoms (cations); this energy is not subdivided further as each silicon is connected to four oxygens and its motion is not easy to categorize in simple terms.

From Fig. 22 it is clear that the spectral band between about 900 cm^{-1} and 1100 cm^{-1} is composed of modes involving primarily Si–O–Si bond stretching vibrations—there is no energy in the bending and rocking types of motion in this spectral region. The band at approximately 800–900 cm^{-1} is composed of modes associated with the vibrations of nonbridging oxygen atoms moving along the line of their Si–O bond, i.e., *NS* vibrations. As we show later, these modes are characterized by intense spatial localization and typically most of the vibrational energy is confined to one or two fairly close such atoms. Perhaps the best way of regarding these excitations is as impurity modes which contribute frequencies of strongly localized vibrations to a region of the unperturbed spectrum (i.e., that associated with no nonbridging oxygen atoms) devoid of frequencies.

The highly localized nature of the Si–O stretching modes associated with the nonbridging oxygen atoms implies that such modes are little altered if they occur at nonbridging oxygen atoms within the bulk of the structure of vitreous silica rather than at the surface. This argument in fact provides confirmation of conjectures of the nature of experimentally observed bands at about 950 cm^{-1} in certain silica samples; these bands were thought to be due to the presence of nonbridging oxygen atoms within the structure generated, for example, in thermal spikes due to fast neutron irradiation (Simon, 1957; Bell and Dean, 1968b; Bell, Dean, and Hibbins-Butler, 1970).

It can be seen from Fig. 22 that modes in the next highest spectral band, one centered at about 750 cm^{-1}, are predominantly angle-bending vibrations, in which each oxygen atom vibrates perpendicularly to the line joining its two adjacent silicons, within the plane of the three atoms. The major peak of the spectrum centered between 400 and 500 cm^{-1} contains modes whose main characteristic is an out-of-plane vibration of each oxygen atom along the line perpendicular to its two neighboring silicons. On the low-frequency side of the peak is a shoulder containing modes associated largely with motion of nonbridging oxygen atoms perpendicular to the Si–O bond.

The spatial localization of vibrational modes in Fig. 22(c) is described by a parameter $N_{\mathrm{EFF}}(\omega)$ which gives some indication of the number of atoms effectively participating in a normal mode of frequency ω. One defines the energy moments

$$M_p(\omega) = \sum_i [\epsilon_i(\omega)]^p, \tag{5.6}$$

where $\epsilon_i(\omega)$ is the mean kinetic energy of atom i in a normal mode of frequency ω. $N_{\mathrm{EFF}}(\omega)$ is then, simply,

$$N_{\mathrm{EFF}}(\omega) = [M_1]^2/M_2. \tag{5.7}$$

It is easy to verify that N_{EFF} always lies between 1 and N. For a monatomic system of N atoms, one can show that for a purely translation mode of the system $N_{\mathrm{EFF}} = N$; if P atoms are in motion with roughly equal amplitudes $N_{\mathrm{EFF}} \simeq P$, and for a mode involving effectively only one atom vibrating $N_{\mathrm{EFF}} \simeq 1$. For the typical wavelike modes of crystals, we have $N_{\mathrm{EFF}} \simeq N/2$.

For a system of more than one type of atom, N_{EFF} tends to be mass dependent, even for translational modes. One can overcome this by restricting summations to just one species of atom, and Fig. 22(c) is based upon the summations being confined to silicon atoms only. The vertical scale in the diagram has a maximum of 101, the total number of silicon atoms in the particular model on which these localization calculations were based. One notices from the figure that the localization is very intense both near band edges and in the band at 800–900 cm^{-1}, as referred to earlier. Elsewhere the localization, although somewhat higher than for a crystalline solid, is by no means intense. Of course, one is limited in understanding the extent of localization of the more extended modes by the finite size of model.

Detailed investigations of vibrational modes of the vitreous germania and beryllium fluoride models have also been carried out (Bell, Bird, and Dean, 1968; Bell, Dean, and Hibbins-Butler, 1971). In a sense the modes in vitreous germania are somewhat simpler than those in vitreous silica for the mass ratio in the former structure is higher and therefore the bands of the spectrum and the types of vibration are more clearly separated and distinct. One notices, for example, the presence of a substantial band gap at about 700 cm^{-1} for the fixed-end model; within this gap there appears for the free-end case a really distinctive band of localized modes due to nonbridging oxygen atoms. Again, the presence of a distinctive peak at about 300 cm^{-1} for the free-end models indicates the presence of low-frequency vibrations associated with the nonbridging boundary oxygen atoms vibrating perpendicular to their Ge–O bond.

In vitreous beryllium fluoride there is the difference that the lighter atom (Be) is at the center of a tetrahedron whose vertices are the heavier fluorine atoms; consequently the vibrational modes are somewhat different in character from those for vitreous silica and germania.

One final point relating to Figs. 18–22 should be noted. In computing the spectra, in each case a ratio of 3:17 for the noncentral to central force constant was chosen, mainly from suggestions in the existing literature. Given this ratio, the frequency scale in the figures

then depends upon arbitrarily assigning an absolute value for either the central or noncentral force constant. For vitreous silica the value of 4.0×10^2 N m^{-1} proposed by Zarzicki and Naudin (1960) was chosen for the central force constant; comparison with experiment however suggests that this value is perhaps 15% too low. The higher force constant value would involve a simple linear rescaling of the figures, the spectra being shifted to somewhat higher values; this point should be borne in mind if detailed comparisons with experimental spectra are made from the data provided.

The problem of deriving infrared and Raman spectra from computed atomic displacement eigenvalues is relatively trivial by comparison with the problems of structure, matrix algebra, and computation already outlined. To calculate infrared activities, one assigns effective positive and negative charges to the cations and anions (the silicon and oxygen atoms of vitreous silica, for example), and computes the total net dipole moment fluctuations from the appropriate eigenvector. Some assumption must be made about the effects of the boundaries but, in general, it is found that these have relatively little influence on the computed infrared activity. One feature noted from such computations is that eigenvectors of adjacently spaced eigenvalues do not in general give similar infrared activities so that, in order to compute an accurate infrared spectrum, one must average over the activities of numbers of fairly closely spaced modes at various selected frequencies. The process is thus somewhat time consuming, but presents no problem of principle. In the calculation of Raman scattering, it is necessary to make an assumption as to the way in which polarizability should be calculated. One can simply assign certain polarizability parameters to nearest-neighbor bonds and sum appropriately for the various vectors considered. As with infrared results, such calculations show no smooth variation of Raman activity with frequency or mode number. One gets meaningful averages for the various spectral bands which are in rough agreement with experiment, but results for individual modes vary considerably, even within the same band.

One disadvantage of the numerical approach we have described, as applied to three-dimensional glasses, is that it is not able to yield information about the nature of low-frequency atomic vibrations below, say, 50 cm^{-1}. This is the consequence of a number of factors. One expects, for example, these low-frequency modes, with their long wavelengths and considerable spatial extension, to be influenced by the boundaries of the models. Again, the number of modes for any given model decreases as ω^2 with decreasing frequency (ω), so that typically a structure of say 1000 degrees of freedom may provide only a few modes below 50 cm^{-1}. Of more significance, though, is the fact that numerous low-frequency modes in the real glass may well depend upon particular features of structure or force field which are not provided in the theoretical model. Thus, while there is little doubt that the bulk of the spectrum is accounted for well by a central and noncentral force field which fairly accurately represents the physical forces in the glass, the very low-frequency spectra may have important features associated with relatively weak forces or local structure anomalies; such features will clearly not appear in the output from models containing only strong forces and no built-in structural anomalies. The low temperature excess specific heat in numerous glasses, in particular vitreous SiO_2, is almost certainly due to low-frequency localized modes associated with particular local force fields or structural features. Such behavior unfortunately cannot be derived from the "first-order" approximations to vibrating amorphous systems considered up to the present time.

6. MIXED-CRYSTAL SYSTEMS

In this section we consider systems of the composition AB_xC_{1-x} (where x has a value between 0 and 1) and which consist of two sub-lattices, with the A atoms lying on the sites of one, and the B and C atoms occupying randomly the sites of the other. These systems present similar theoretical problems to those of the binary disordered lattices discussed in Sec. 4. In recent years there has been much interest in them, and numerous infrared and Raman studies have been carried out.

The experimental work shows that the behavior of infrared or Raman-active lattice modes in mixed crystals can be of two types. In one class of system, the optically active band varies continuously in frequency from that of one end member to that of the other, as x varies throughout its range. This type of behavior is now generally referred to as "one-mode" behavior. In the other class of mixed-crystal system, two bands of frequencies are observed which occur at or close to the optically active frequencies of the end members; the strength of each band varying continuously from its maximum (for the pure end member) to zero as x varies from 0 to 1, or from 1 to 0. Behavior of this type is referred to as "two-mode" behavior. The one- and two-mode types of behavior have also been referred to in the literature as "amalgamation" and "persistence"-type behavior, respectively, or a- and p-type behavior (Matsuda and Miyata, 1968). Examples of mixed crystals showing one-mode behavior are $Na_xK_{1-x}Cl$, $Rb_xK_{1-x}Cl$, $Tl_xK_{1-x}Cl$, $Co_xNi_{1-x}O$, $Ca_xSr_{1-x}F_2$, $Ba_xSr_{1-x}F_2$, and $Zn_xCd_{1-x}S$; among the systems which exhibit two-mode behavior are $GaAs_xP_{1-x}$, CdS_xSe_{1-x}, $InAs_xP_{1-x}$, $Ga_xIn_{1-x}As$, and ZnS_xSe_{1-x}.

A variety of methods have been proposed to study theoretically the vibrations of mixed crystal systems; in particular, there has been much interest in the formulation of criteria for predicting whether particular systems will be of the one-mode or two-mode type of behavior. Lucovsky, Brodsky, and Burstein (1968) have summarized some of these methods, for example the virtual crystal (Poon and Bienenstock, 1966a, b),

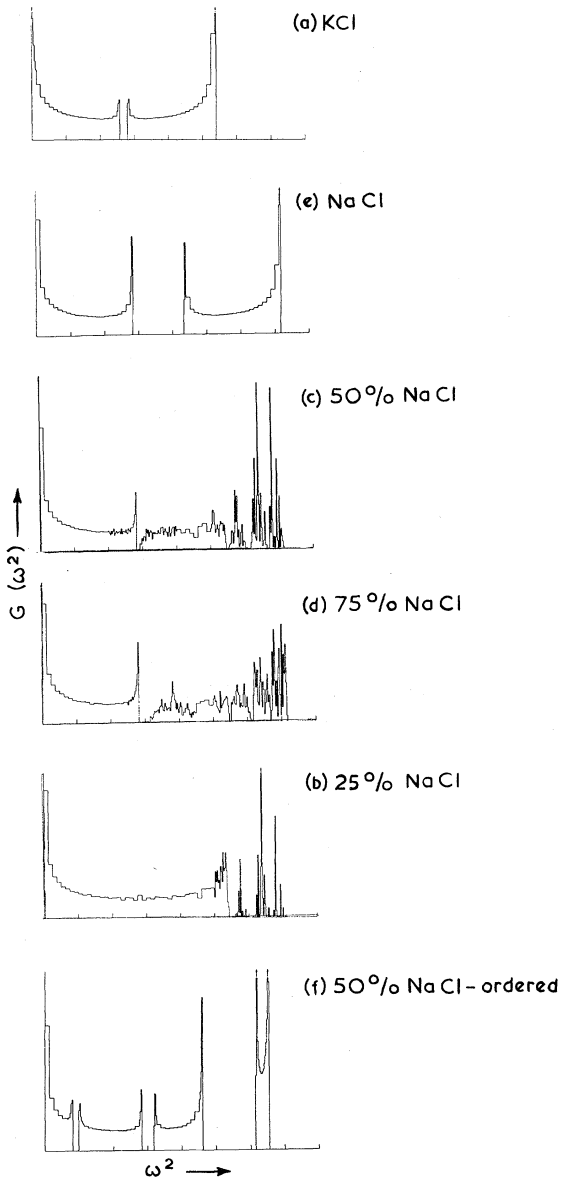

FIG. 24. Results of studies of the mixed-crystal system $Na_xK_{1-x}Cl$ in the form of a linear chain. The squared frequency spectra were computed by the method described in Sec. 3; a nearest-neighbor force field with force constants independent of atomic species was chosen. Diagrams (b), (c), and (d) refer to disordered systems, and (f) to the ordered system ···NaClKClNaClKCl···.

cluster model (Verleur and Barker, 1966; Barker, 1968), and random element isodisplacement models (Chen, Shockley, and Pearson, 1966), each of which suffers from the limitation of being based upon somewhat arbitrary assumptions. They also mention the work of Matossi (1951) in which, by studying periodic chains containing three types of atoms, an attempt was made to determine the properties of random systems of the mixed crystal type AB_xC_{1-x} and to predict the form of the spectrum. We now know the fact that, in general, the vibrational properties of randomly disordered systems are so different from those of their ordered counterparts that one simply cannot accept Matossi's results [or the results of similar work (Aggarwal and Saksena, 1951)] as pertinent to the disordered state. The work on regular structures does not, for example, include the possibility of localized modes of vibration—and we have seen in Sec. 4 how important a role such modes can play in the discussion of the vibrations of disordered systems.

Matsuda and Miyata (1968) have given an interesting and useful approximate criterion for predicting whether a system will be of the one-mode or two-mode type of behavior. They show that the quantity

$$r = | m_B^{-1} - m_C^{-1} | / m_A^{-1} \tag{6.1}$$

where m_A, m_B, and m_C are the masses of the atoms in AB_xC_{1-x}, can normally be used to determine the spectral behavior; a variety of experimental data indicates that if $r<1$, the behavior of a system is normally of one-mode type; if $r>1$, the behavior is of the two-mode type. This criterion has some basis in the Saxon–Hutner theorem which relates to the band gap of a randomly ordered system in terms of the gap positions of the two extreme component systems. Matsuda and Miyata also apply a method known as MEAPS (Matsuda, 1966a; Matsuda and Ogita, 1967; Okada and Matsuda, 1968)—the method of the ensemble average of periodic chains—for investigating the spectra of one-dimensional models of mixed crystal systems. The MEAPS method is that of finding the value of a property for a disordered system by determining the average value for an ensemble of periodic chains of unit cell length p atoms, each chain of the ensemble having in its unit cell one of the various possible arrangements of p atoms. In principle, by taking p large enough, one can compute a quantity—such as spectral density, or infrared absorption—to any desired accuracy; in practice, the method converges rapidly and by taking p up to about only 16, results of good accuracy are obtained.

The direct numerical method, based upon the techniques outlined in Sec. 3, is almost certainly the best method available for studying the basic properties of the vibrations of models of mixed-crystal systems. The method has some disadvantages, along with all the other methods of investigating mixed-crystal models: for example, it becomes somewhat slower and less useful if long-range forces are present, and there is no simple extension to include the effects of anharmonicity. However, it can succeed in yielding detailed and accurate results for the spectrum, eigenvectors, infrared absorption, and Raman scattering of models of disordered mixed-crystal systems—results of an accuracy that no other method seems likely to achieve. The following indicates some of the work that has been carried out using the direct numerical method.

Figure 24 depicts squared frequency spectra for a one-dimensional model of the mixed $Na_xK_{1-x}Cl$ system, using the numerical method of negative factor counting for long sample chains as outlined in Sec. 4. In Fig. 24(a), at the top, is the spectrum for one end system, pure KCl; the histogram represents well the exactly known spectrum for the diatomic chain:

$$G(\omega^2)=\pi^{-1}\,|\,\omega^2-\gamma(m_K^{-1}+m_{Cl}^{-1})\,|$$
$$\times\left[\omega^2\left(\frac{2\gamma}{m_K}-\omega^2\right)\left(\frac{2\gamma}{m_{Cl}}-\omega^2\right)\left(\frac{2\gamma}{m_K}+\frac{2\gamma}{m_{Cl}}-\omega^2\right)\right]^{-1/2},$$
$$0<\omega^2<(2\gamma/m_K);$$
$$2\gamma/m_{Cl}<\omega^2<2\gamma(m_K^{-1}+m_{Cl}^{-1}), \qquad (6.2)$$

in which m_K and m_{Cl} represent the masses of the potassium and chlorine atoms, respectively. With the introduction of sodium atoms into the system, there appear impurity localized modes both in the band gap and above the optical band, as described by Mazur, Montroll, and Potts (1956). At the 25% composition of NaCl, the spectrum is as indicated in Fig. 24(b), the narrow band gap of pure KCl being filled and a number of distinct peaks associated with various localized impurity modes having developed at the high-frequency end of the continuum. At the 50%–50% composition, in (c), the spectrum is still more complex. The high-frequency peaks remain much in evidence, but their intensities have now changed somewhat from those in (b), due to the different probabilities of occurrence of the various local clusters in the chain. In addition, at the 50%–50% composition there appears a certain amount of structure at lower frequencies. With increasing NaCl content, one notices the emergence of a distinct acoustic band, and the movement of more modes towards the highest frequencies in the spectrum. At the 75% NaCl composition, the spectrum is still most complex in form with numerous peaks due to localized modes. Finally, for the pure system NaCl, in Fig. 24(e) we have again the histogram form of the function (6.2), with m_{Na} now replacing m_K.

The comparison between Figs. 24(f) and (c) should be noted. Figure 24(f) depicts the spectrum for the periodic system $\cdots$NaClKClNaClKCl$\cdots$, and it is quite unlike that for the randomly ordered 50%–50% system. The poor agreement suggests that little reliance can be placed on the conclusions of Matossi (1951) and Aggarwal and Saksena (1951) applying to randomly disordered systems.

Results similar to those in Fig. 24 have been obtained by Payton (1966). Payton (1966) and Payton and Visscher (1968) have also used the direct numerical method to study a disordered three-dimensional NaCl–KCl model. Although their models are rather limited in size (up to $5\times5\times40$ atoms), nevertheless the results are probably the most accurate available for the mixed NaCl–KCl system. With really fast computers it would not now be difficult to extend this work further to deal with larger three-dimensional models with more realistic force fields; such work could provide really accurate details of the dynamics of the systems considered and would lead to a thorough understanding of the experimental situation.

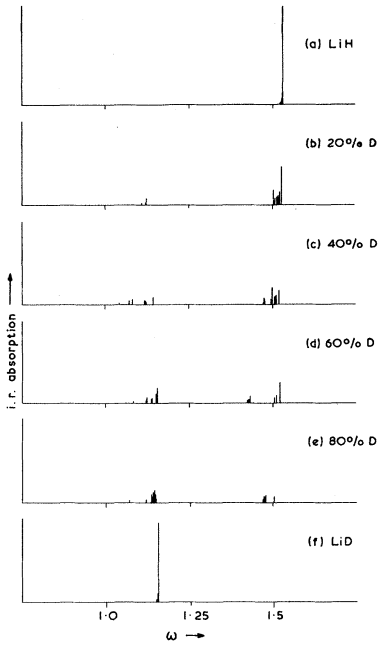

FIG. 25. Infrared absorption plots for the LiH–LiD linear system based upon directly computed eigenvectors on linear chains of 100 atoms (after C. Hall, 1969, unpublished). The two-mode behavior indicated does not represent the experimental situation, indicating that the model is inadequate—possibly due to an unrealistically simple force field.

Calculations on one-dimensional systems, similar to those outlined above, have been extended by Hall (1969, unpublished) to the derivation of eigenvectors (using inverse iteration, as in Sec. 4) and the calculation of infrared absorption. In Fig. 25, we depict some of his results for the infrared spectrum of a linear chain based on the LiH–LiD system. His spectrum may contain spurious effects associated with finite chain lengths—the results depicted are based upon chains of length 100 atoms only—although comparison with shorter chains suggests that these effects are relatively unimportant. One can see that his results indicate that the LiH–LiD system appears to be in the category of a "two-mode" system, although this conflicts somewhat with experiment (Montgomery and Hardy, 1965). It is probable that Hall's model is not realistic enough in its force field.

Models of the systems $CdS_{1-x}Se_x$ and $Cd_{1-x}Zn_xS$ have been considered in a similar way by Hass, Rosenstock, and McGill (1969), the former being an example of a two-mode system, and the latter of a one-mode system. Using the negative factor counting method for the linear chain in a form introduced by Rosenstock and McGill (1962), they computed the frequencies of the modes of chains 40 atoms long for various values of x. Figure 26, in which normal mode frequency is plotted against mode number for each of the systems and compositions studied, summarizes their results. Although

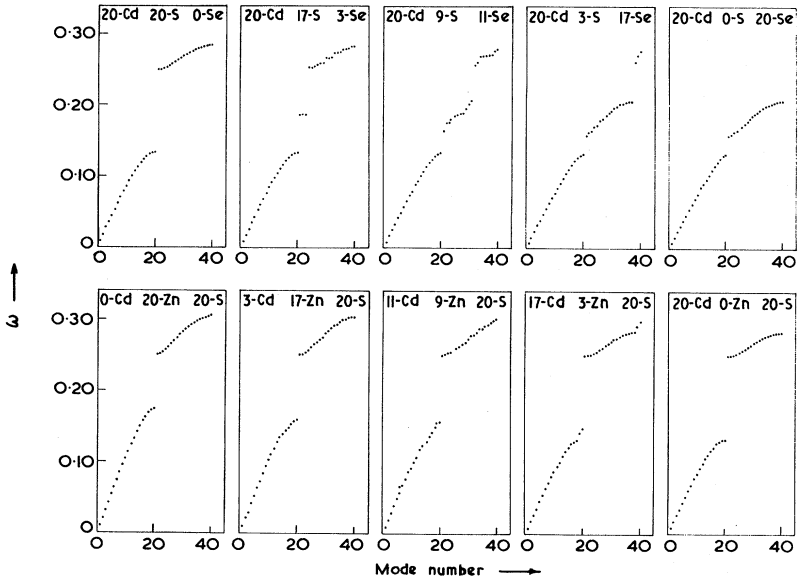

FIG. 26. Frequency-mode number curves for random mixed chains of the type $AB_{1-x}C_x$. The chains are of length 40 atoms, and the force field is limited to nearest neighbors with equal force constants. The top diagram refers to the system $CdS_{1-x}Se_x$; that at the bottom to $Cd_{1-x}Zn_xS$ (after Hass, Rosenstock, and McGill, 1969).

these plots give no direct indication of infrared activity (except for the end compositions) one can see something of a gradual transition between the two overlapping optical bands of the pure members in the case of the $Cd_{1-x}Zn_xS$ one-mode system, and the persistence and distribution throughout the composition range of the remnants of the optical bands of the pure members in the $CdS_{1-x}Se_x$ two-mode system. It is important not to attribute to the intermediate compositions of the two systems properties which do not hold; for example, at intermediate compositions the plots of Fig. 26 must not be regarded as the familiar $\omega-\mathbf{k}$ dispersion curves one encounters in the theory of periodic lattices. For disordered arrangements of atoms, the concept of the wave number is not, in general, a meaningful one, except at very low frequencies.

Hass *et al.* computed infrared absorption from the eigenvectors of their models. Figure 27 summarizes these results. The point is made that the absorption for the pure compounds shows one strong band at the fundamental mode with decreasing intensity associated with odd harmonics, and that there is no absorption associated with even harmonics due to symmetry. The spread of the lines in the spectrum of the end members is associated with the shortness of the chains. In the case of the mixed chains, the absorption lines for a particular array contains effects due both to the finite size of the chains and to the localized modes of the disordered system. The authors interpret the absorption lines of Fig. 27 in terms of localized and gap modes, developing the kind of ideas introduced by Mazur, Montroll, and Potts (1956).

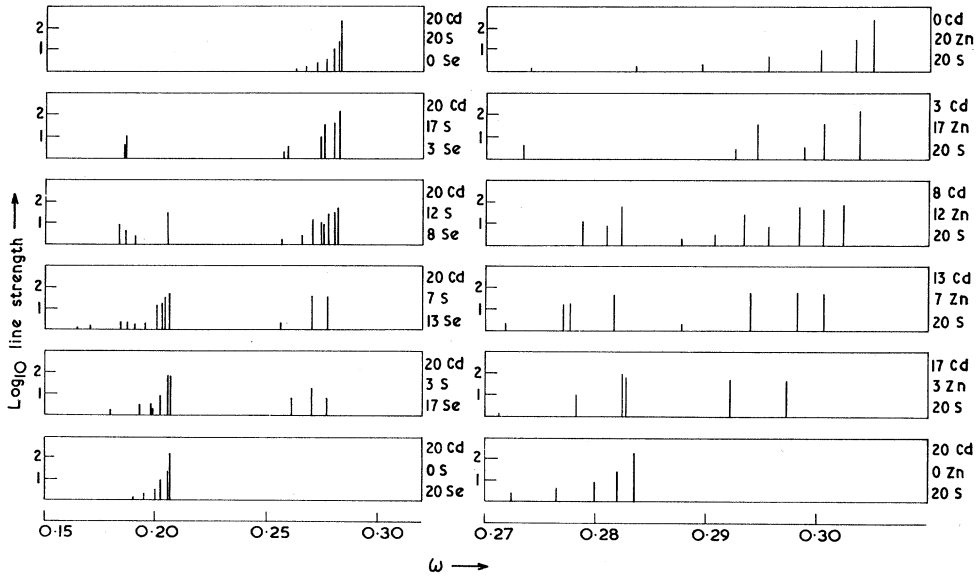

FIG. 27. Calculated $\log_{10}$ line strengths for various forty-atom random linear chains representing the systems $CdS_{1-x}Se_x$ (on the left), and $Cd_{1-x}Zn_xS$ (on the right). (Hass, Rosenstock, and McGill, 1969.)

Although absorption plots such as those in Fig. 27 are informative and, of course, fully accurate as descriptions of the models they apply to, yet it is not always easy to use such data to deduce how the real mixed-crystal system will behave. The results, for example, are in general agreement with experiment for the systems $CdS_{1-x}Se_x$ and $Cd_{1-x}Zn_xS$ but appear inadequate for the LiH_xD_{1-x} system. The place of such work in the development of an understanding of mixed-crystal systems must not, however, be underrated. These calculations are direct calculations, and are based upon no assumptions as to the dynamical motion of the atoms of the models. The development of these direct numerical methods to realistic three-dimensional mixed-crystal systems—and without doubt this can be done at the present time—should lead to a full understanding of the systems.

7. ORIENTATIONALLY DISORDERED CRYSTALS

A class of solids which has received relatively little attention is that of orientationally disordered solids. In these solids, the basic molecular units, although forming a regular lattice array, are orientated randomly with respect to one another. The common form of ice, hexagonal ice I, typifies materials of this class; other examples include the ammonium halides and carbon tetrachloride; there are numerous complicated organic systems exhibiting this type of disorder.

Hexagonal ice I is the only orientationally disordered solid on which detailed lattice dynamical calculations, taking into full account the randomness of the system, have been carried out. In this phase of ice, the oxygen atoms form a regular space lattice whose positions correspond to the lattice sites of the wurtzite lattice. Hydrogen atoms lie along nearest-neighbor oxygen-oxygen lines, being strongly bonded to one of the oxygens and only weakly bonded to the other. Each oxygen atom has associated with it two closely bound and two weakly bound hydrogen atoms. Within these restrictions, the structure is random: thus, for a given oxygen atom any two of the four lines to nearest-neighbor oxygens may contain strongly bonded hydrogens. Each H_2O molecular unit thus takes one of six possible orientations subject to compatibility with neighboring units.

The random orientation of molecular units prevents the use of a conventional lattice dynamical approach. To some extent Whalley and Bertie (1967) have overcome the difficulty for the translation molecular vibrations (i.e., low-frequency modes) by assuming that the mechanical vibrations are those of the corresponding regular crystal, but that disorder leads to a breakdown of selection rules for the interaction of radiation with the crystal. They find that, to a first approximation, the intensity of infrared or Raman scattering for the low-frequency lattice modes varies as $\omega^2 g(\omega)$, where (as before) $g(\omega)$ is the frequency distribution function. The usefulness of the numerical approach, in which we are primarily interested in this review, is not restricted to the low-frequency region, and it has yielded useful information on both intra- and intermolecular modes. Two models have been used, a two-dimensional system which has been most valuable in providing qualitative data on the vibrational effects of orientational disorder (Dean, 1969; Shawyer and Dean, 1972a), and a realistic three-dimensional model of hexagonal ice I (Shawyer and Dean, 1969, 1972b).

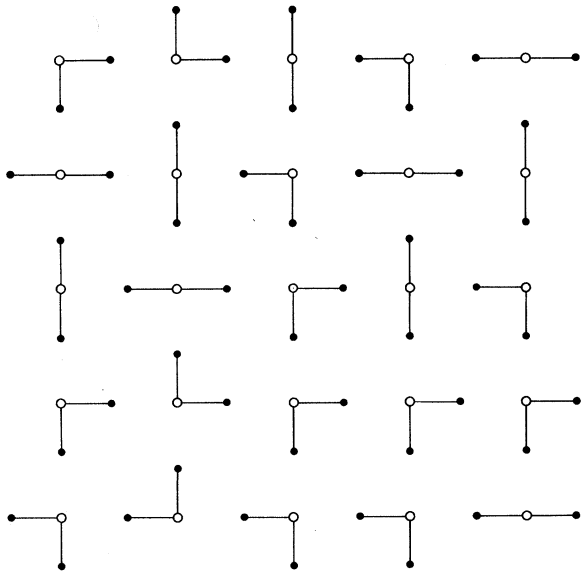

FIG. 28. Indicating the nature of the two-dimensional model of ice. Each three-atom molecular unit can take six possible orientations, subject to the fact that only one atom represented by a closed circle lies between two neighboring atoms represented by open circles. The 180° molecular configuration is needed in two dimensions to ensure a properly random structure; such a configuration does not occur in real ice.

The nature of the two-dimensional model is indicated in Fig. 28. The force field imposed consisted of strong central and noncentral interactions between neighboring atoms in the same molecular unit, and weak central and noncentral interactions between neighboring atoms on adjacent molecular units. The ratio of central to noncentral force constants for both strong and weak forces was fixed at 4:1 throughout the calculations, various values being taken for the ratio of strong to weak forces. The mass ratio of atomic species was taken as 16:1 and 8:1, corresponding to H_2O and D_2O. Fixed-end boundary conditions were used on lattice sections of various sizes up to 40×40 molecular units.

Figure 29 indicates roughly the kind of result obtained in the computation of spectra for the two-dimensional model, using the direct numerical methods described in Sec. 3 on sample structures. The top spectrum in the figure refers to an ordered lattice in which each molecular unit (in the 90° configuration) is orientated in the same direction. The low-frequency band contains modes associated with movements of the molecular unit as a whole; these are long wave vibrations for which local geometry can be disregarded. The middle-frequency band contains molecular angle bend-

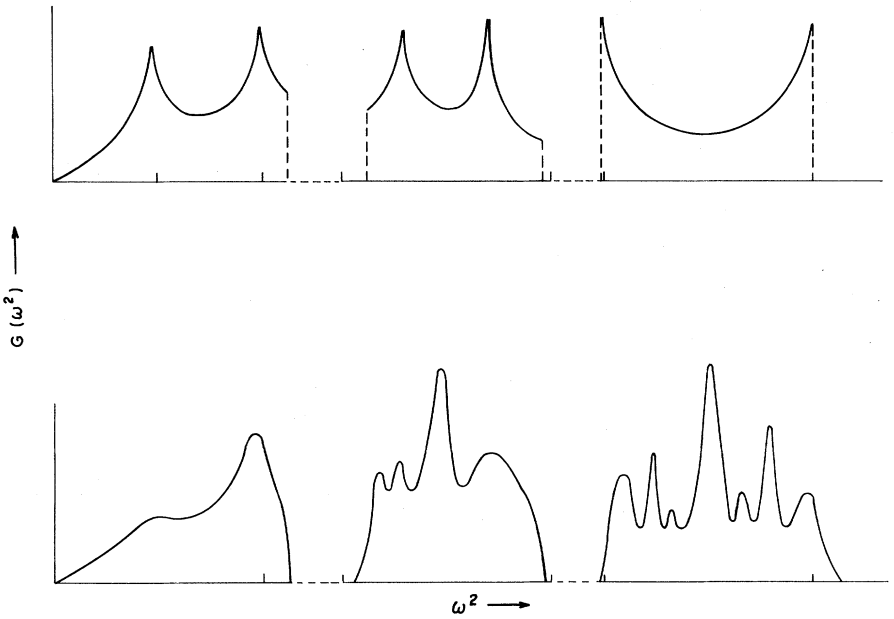

FIG. 29. Approximate representation of frequency spectra for two-dimensional models of ice. The top spectrum refers to the ordered structure in which all the molecular units are right angle units and point in the same direction; the lower spectrum refers to the disordered structure. Note that the frequency scale is broken between the bands which, in fact, lie in quite separate frequency regions.

ing modes, and the high-frequency band is associated with bond-stretching modes. The lower spectrum in the figure refers to the orientationally disordered model. One notices here that the upper two bands—in particular the high-frequency band—have a detailed structure with a number of well-defined peaks. A study of eigenvectors (computed by the method of inverse iteration described in Sec. 3) shows that one has much the same situation as that noticed for the two-component disordered system reviewed in Sec. 4. The high-frequency modes are spatially localized, in many cases intensely so, and linked to particular types of local lattice structure. Each peak in the high-frequency band contains modes of one or just a few major "types" associated with fairly common local molecular configurations. In the middle-frequency band, the spatial localization is not intense; typically as many as 20 molecular units will vibrate with amplitudes greater than, say, 20% of the maximum amplitude. Although one cannot easily assign normal mode "types" to the peaks in the middle-frequency band, it is quite clear from the calculations that the spectral peaks are not spurious but are associated with geometric features of the model. Modes in the low-frequency band are extended and, in the lower-frequency region of this band, almost identical to those for the ordered lattice.

Calculations on the three-dimensional model of hexagonal ice I used the realistic eight-parameter force field indicated in Fig. 30. The sample structures (generated by computer) to which this force field applied contained as many as about 1500 degrees of freedom, although preliminary calculations on much smaller sections were carried out in order to quickly determine (by comparing results with experiment) an approximate set of values for the force constants. The spectrum in Fig. 31 is based upon the following set of force constants, each in units of 10^2 N m^{-1}: $k_1=5.44$, $k_2=-0.19$, $k_3=0.10$, $k_4=0.02$, $k_5=0.04$, $h_1=0.74$, $h_2=0.024$, $h_3=0.024$. The atomic masses were taken as those of hydrogen and oxygen, and a fixed-end boundary condition was imposed on an approximately cubic system of about 1500 degrees of freedom.

For comparison, the vibrational frequencies obtained from experimental Raman (Taylor and Whalley, 1964), infrared (Bertie and Whalley, 1964, 1967), neutron

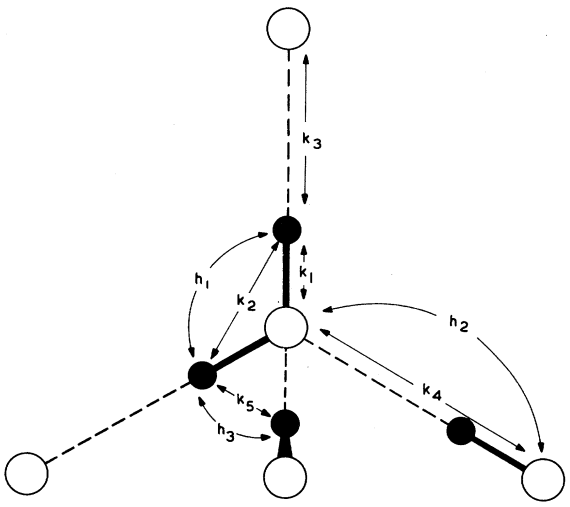

FIG. 30. The harmonic force field used in the computations for hexagonal ice I. Oxygen atoms are shown as open circles, hydrogen atoms as closed circles. The full lines represent strong covalent bonds and the dashed lines weak hydrogen bonds.

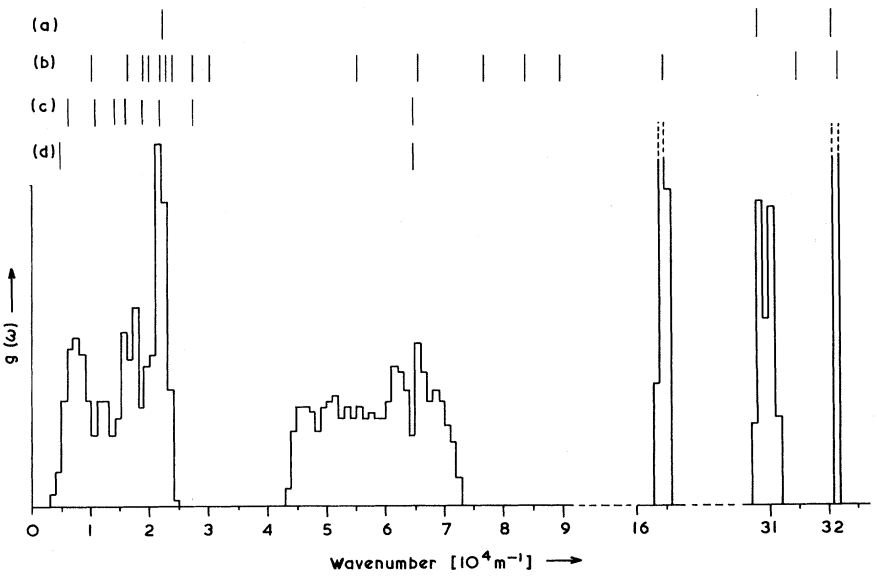

FIG. 31. The histogram is the computed frequency spectrum for hexagonal ice I. In the upper half of the figure, the lines indicate the positions of features (peaks and shoulders) in the bands of the experimentally observed spectra from (a) Raman experiments at 77 K; (b) infrared experiments at 100 K; (c) inelastic neutron scattering experiments at 150 K; and (d) thermodynamic studies reduced to 0 K.

(Prask, Boutin, and Yip, 1968), and thermodynamic (Leadbetter, 1965) studies are also indicated in Fig. 31 in (a), (b), (c), and (d), respectively. We noted in Sec. 5.2 that direct intensity comparisons between vibrational frequency spectra and experimentally observed spectra are not normally meaningful, but that, for disordered systems, a comparison of positions of bands can provide useful data. On this basis, the general agreement with experiment is seen to be good. The only major feature of the experimental spectrum that does not accurately agree with the corresponding feature in the calculated spectrum is the broad band of frequencies (from 5×10^4 to 9×10^4 m^{-1}) in the infrared spectrum of ice (Bertie and Whalley, 1964, 1967) which has its maximum intensity at about 8×10^4 m^{-1}. The corresponding region of the neutron spectrum (Prask, Boutin, and Yip, 1968) consists of a peak with a maximum at about 6.5×10^4 m^{-1}, in good agreement with the calculations. The computed band also agrees with an analysis of thermodynamic data (Leadbetter, 1965). These results suggest that the vibrations in a high-frequency tail of the band are mainly responsible for infrared activity in this region of the spectrum; that this tail does not occur in the computed spectrum is probably a consequence of the particular model used—it is clear that all band edges in the model have sharp cutoffs.

A study of sample eigenvectors, computed by the method of inverse iteration, led to broad assignments of the various spectral bands. The low-frequency band, below 2.5×10^4 m^{-1}, contains translational lattice modes, while the region from 4.3×10^4 to 7.3×10^4 m^{-1} contains hindered rotational (or librational) modes. The band at 16.4×10^4 m^{-1} is associated with the bending vibration of the H_2O molecule and the bands at 31×10^4 and 32×10^4 m^{-1} with the symmetric and antisymmetric stretching vibrations. The order of the assignment of the two highest frequency bands ω(antisymmetric)$>$ ω(symmetric) is a consequence of the initial choice of the force constants. There is an alternative set of intramolecular force constants consistent with observed frequencies: $k_1=5.05\times10^2$ N m^{-1}; $k_2=0.48\times10^2$ N m^{-1}; $h_1=0.52\times10^2$ N m^{-1}. This choice reverses the assignments, making ω(symmetric)$>\omega$(antisymmetric), but has little effect on the rest of the spectrum.

Similar computations were carried out for heavy ice (Shawyer and Dean, 1969), again with good general agreement with experiment.

8. RANDOM POLYMERS

Random polymer systems, particularly the long unbranched chain variety, represent ideal subjects for study by the direct numerical techniques outlined in this paper. If one takes the interatomic forces of an unbranched polymer chain to be short range in character, then by numbering the atoms of the system in an obvious way, one derives a dynamical matrix of narrow-band form. The bandwidth is related to the number of atoms in each unit of the chain, and also to the effective range of the interatomic forces. For a polymer containing several atoms in each monomeric unit, and with short-range forces, the half-bandwidth of the dynamical matrix would be of the order of 10^1 or 10^2. Bandwidths as narrow as this ensure that the numerical procedure for deriving the vibrational spectrum of the polymer can be made very fast indeed, and chain lengths of hundreds or even thousands of units can be dealt with. At the present time, the potential of the negative factor counting method for disordered polymer systems has not yet been fully exploited, and little work has been done. A good deal of new information on the structure and chemistry of a wide range of polymeric systems is

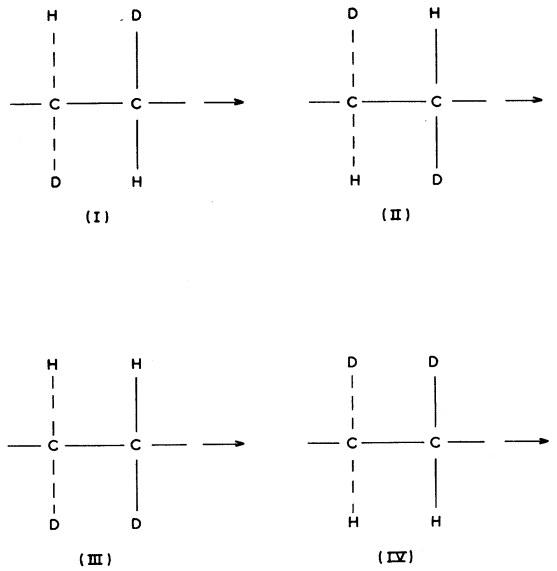

FIG. 32. Configurations of monomeric units, as used in the polymer systems of Tasumi and Zerbi (1968). The arrows indicate the direction of chain growth.

potentially available by using the numerical techniques outlined, and comparing the computed results with observed experimental data, mainly from infrared absorption experiments. Tasumi and Zerbi (1968) point out that most of the actual polymers presently available have various kinds of randomness or disorder within their structure. We know it to be quite clear, from work such as that on two-component disordered systems as described in Sec. 4, that the spectra and modes of vibration of these disordered polymers can prove to be drastically different from their periodic counterparts.

Tasumi and Zerbi (1968) considered a number of models of polymers isotopically disordered due to the presence of both hydrogen and deuterium atoms. They studied first a simple model, a zigzag chain representing a polyethylene type structure with the methylene groups reduced to point masses. From this they calculated, by the negative factor counting method, frequency distributions for (a) a regular chain corresponding to normal polyethylene (with the point mass of 14 amu), (b) a regular chain corresponding to perdeuterated polyethylene (with a point mass of 16 amu), and (c) a chain corresponding to a random copolymer of ethylene and perdeuterated ethylene. These structures exhibited clearly the effects of disorder in the high-frequency region (at about 1000 cm^{-1}) of the spectrum in spite of the small mass difference between the units of the chains. The more realistic models studied take into account in a proper manner the hydrogen atoms of polymers of *cis*-CHD=CHD and *trans*-CHD=CHD. The molecular structure assumed in this work had the planar zigzag conformation, with tetrahedral angles at each carbon atom. A force field, which included interactions between neighboring methylene groups but with no interaction between units further apart, was used. The frequency spectra of two regular polymers, referred to as polymer A and polymer B, were computed by the negative factor counting method. Polymer A is a random sequence composed of equal numbers of the two units I and II shown in Fig. 32. Similarly, polymer B consists of III and IV. The sequence of units was generated by means of a random number computer program, the condition being imposed that every successive sequence of twenty units was made up of ten units of each type. The total chain lengths used were limited to 100 units (200 methylene groups). Some care was taken to ensure that what are referred to as "good" random sequences were used in the calculations, for it was found that for the (moderately short) chain lengths used the randomness had decisive effects on the results of calculations.

In Fig. 33 we depict computed vibrational frequency spectra for polymers A and B of lengths 100 monomeric units, as given by Tasumi and Zerbi. Some caution must be exercised in comparing these with the infrared absorption spectra of poly-(*cis*-CHD=CHD) and poly-(*trans*-CHD=CHD), as in Fig. 34 (again taken from the paper by Tasumi and Zerbi), as the intensity factors appropriate to infrared absorption are not included in the computed spectra. However, Tasumi and Zerbi

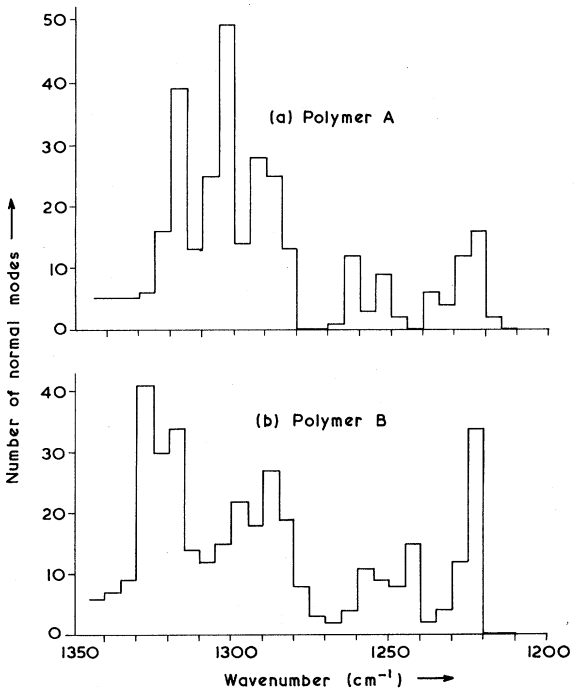

FIG. 33. Calculated frequency spectra of polymers A and B, as referred to in the text, each with 100 monomeric units (after Tasumi and Zerbi, 1968).

showed that it is reasonably clear that the spectrum of polymers A and B correspond, respectively, to the infrared spectra of poly-(*cis*-CHD=CHD) and poly-(*trans*-CHD=CHD), and they interpret various features in the high-frequency spectra of these polymers.

Another class of system for which comparison was made between results computed by the direct numerical approach and experimentally determined infrared spectra are copolymers of CH_2=CH_2, CHD=CD_2, and CD_2=CD_2. Various sequences of polymer units, giving a range of monomer ratios, were used as a basis for calculations; on the experimental side a number of copolymers of various compositions were synthesized and their infrared spectra observed. The agreement between the computed results and experiment, although reasonable, is not entirely satisfactory. However, this could be anticipated. For one thing, the comparison is not between like quantities, for the infrared intensity factors are not implicit in the calculated data; for another, there is evidence that the chain lengths used in the computations are too short to get good "ensemble-averaged" spectra. Both these deficiencies could be made good by (a) computing typical eigenvectors for polymers of about the size (100 monomeric units) considered by Tasumi and Zerbi in order to estimate infrared activity in the various spectral bands, and (b) computing spectra for copolymers of appreciably longer lengths.

Jannink and Summerfield (1966) considered the dependence of the frequency spectrum on the conformation of a simple carbon skeleton chain. They set up various randomly produced chain sequences of *trans* and *gauche* angles, and used the negative factor counting method to compute frequency spectra. Although their model was rather too simple to afford a detailed description of the spectra and atomic dynamics of the real polymer systems on which they are based, their results do at least show clearly the difference between the spectra of periodic and disordered polymer chains. The results also indicate clearly the progressive changes which occur in a spectrum as the concentration of randomly distributed *gauche* confirmations is increased. One interesting, although rather academic, point is that all the squared frequency spectra produced by Jannink and Summerfield in their work are symmetric about their mean squared frequency; this result can be explained in terms of their model satisfying certain simple criteria for such spectral symmetry (Bell and Dean, 1968a).

Similar work on the dependence of spectra on the chain conformations of a simplified model of polyethylene, again with the methylene groups represented by point masses, was carried out by Piseri and Zerbi (1968). Chains of 200 particles representing random sequences of *trans* (T) and *gauche* (G and G′) conformations were generated by computer program; their vibrational frequency spectra were then calculated using the technique outlined in Sec. 3. Characteristic

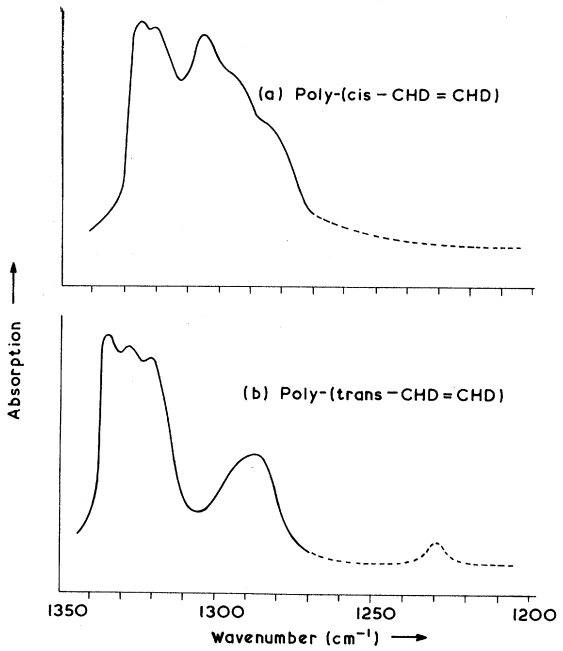

FIG. 34. Observed infrared spectra of poly-(*cis*-CHD=CHD) and poly(*trans*-CHD=CHD). (Tasumi and Zerbi, 1968.)

changes dependent upon the proportion of *trans* conformation present were observed.

A substantially more realistic model of randomly conformated polyethylene was used in later work by Zerbi, Piseri, and Cabassi (1971). In this model, full account was taken of all atoms in the methylene groups and the chains of 200 monomeric units, on which calculations were based, entailed computations on matrices of size 1800×1800; a 28 parameter valence force field of Snyder (1967) was used in this work. *Trans* (T) and *gauche* (G and G′) sequences of internal rotational angles were generated for various temperatures of an Ising model and computed spectra compared with infrared, Raman and neutron inelastic data. Figure 35 shows a comparison between the calculated spectrum and the infrared absorption spectrum at room temperature (ordered structure of a *trans* sequence), and at 160 °C (a fairly highly disordered structure). One cannot compare directly computed intensities with experiment, but the positions of bands are comparable and agreement is quite good. By studying in detail those spectral features which change with temperature and thus disorder, these authors made a number of conclusions on the changing configurations of polyethylene with temperature and on the structure of solid polyethylene.

9. CONCLUDING REMARKS

It is clear from the foregoing sections that the direct numerical method has been of much use in leading

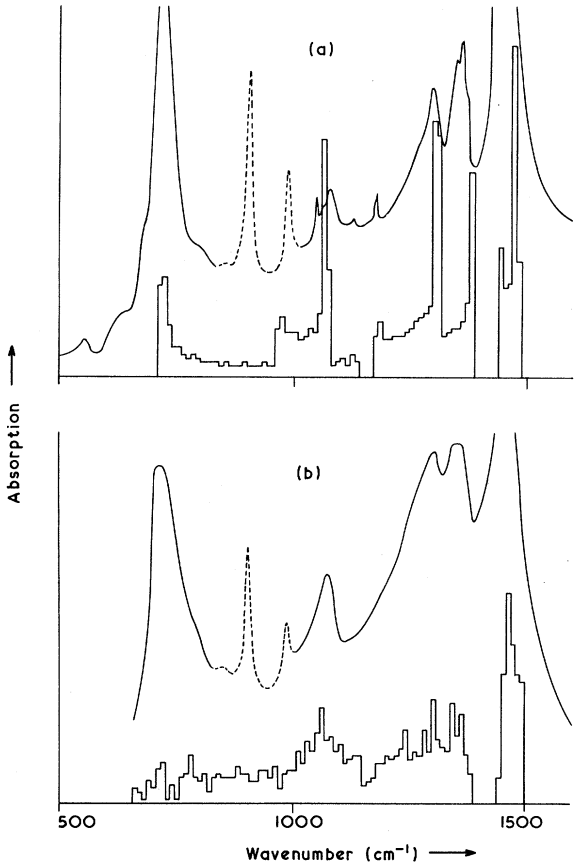

FIG. 35. Comparison of computed spectra with experimental infrared data for polyethylene (a) at room temperature, (b) at 160 °C. At room temperature, the polymer is largely ordered and computation is based on a model of 200 *trans* conformations in sequence; at 160 °C, polyethylene is fairly highly disordered, and the model contains a computer generated random sequence of *trans* and *gauche* conformations (Zerbi, Piseri, and Cabassi, 1971).

to an understanding of the atomic vibrational properties of several classes of disordered system. The method has been applied mainly to two-component disordered lattices, as described in Sec. 4. It has shown clearly the detailed changes which occur in the spectrum as the various system parameters—ratio of atomic species, mass ratio, etc.—are changed. More important, it has led to an understanding of why those changes occur, and to a knowledge of the characteristics of typical normal modes. We have indicated that only one other method has so far yielded an accurate and detailed spectrum, that of Agacy (1964) for an ensemble-averaged spectrum of the linear chain. On the analytical side, some progress has been achieved in deriving the exact results at special frequencies (Borland, 1964; Hori, 1964a, b; Matsuda, 1964; Matsuda and Okada, 1965) mentioned in the text; these exact data confirm well the accuracy of the direct numerical method and Agacy's approach. Other methods, on the whole, have proved less accurate in predicting spectra and eigenvector characteristics, although much useful descriptive and explanatory work related to the nature of vibrations in two-component disordered systems has been made possible by the detailed development of the phase theory by Hori (1968a) and others. The Green's function method has so far proved unsuccessful as a method for investigating vibrational properties of disordered two-component chains, except at the extremes of composition when the analysis becomes simpler and exact. It is true that it has succeeded in producing results in three-dimensional systems in good agreement with spectra obtained by the direct numerical method; however a real difficulty exists in assessing the accuracy of results of the Green's function method for any given system. On the whole it appears to reproduce spectra which are known to be reasonably smooth fairly accurately (Taylor, 1967), but fails in deriving any detailed structure which is known to exist. For this reason it cannot be regarded as holding promise as a predictive method. A starting point for an assessment of the Green's function method is provided by Hori (1968a) in which this approach and others, notably that of phase theory, are described and compared. Of interest is Hori's classification of the Green's function method for disordered systems as an "approximate theory". Indeed only in the limiting case of dilute crystalline impurity systems can it be regarded as an exact method.

The numerical approach is the only method which has so far been applied to realistic three-dimensional models of glass structure, and it has succeeded in providing a detailed understanding (except at far infrared frequencies) of the spectra of the three glasses (SiO_2, GeO_2, and BeF_2) considered. It is not clear that any other method can be applied in a practical way to a realistic model of a glass. One difficulty in attempting to use a Green's function approach is the lack of a reasonable "unperturbed" system such as always exists in a lattice structure. In one dimension, a Green's function method has been applied to glasslike chains (cf. Sec. 5.1) and the agreement with the results of the numerical approach is quite good, but this again is a case in which the spectrum is smooth.

The vibrational properties of disordered mixed-crystal systems are of much current interest. In this area only a little work has been undertaken by the direct numerical method, and this has been confined to near-neighbor interacting systems (mainly one-dimensional)—i.e., models which are almost certainly too simplified to give other than a qualitative description of the effects of disorder. With increasing computer speeds and capacity, it is just now becoming feasible to use longer-range more realistic force fields in calculations based directly on the form of the dynamical matrix for large sample systems. Such an approach, relying upon no empirical approximation based on experimental results, should prove most fruitful in providing a detailed understanding of vibrational behavior in mix-crystal systems. A system of just a thousand or so atoms would prove

sufficient, providing care is taken over the nature of the boundary conditions.

Again, only a little work has been carried out on orientationally disordered crystals and disordered polymers. In these areas it is not easy to see how any approach other than the direct numerical method could be successfully used in dealing with the complex atomic geometries which occur. The direct numerical method is particularly well suited to the investigation of vibrations of polymers. The dual features of a reasonably short-range force field and a simple sequential enumeration of monomeric units lead to a banded form of dynamical matrix ideally suited for efficient computation. Tasumi and Zerbi (1968), Piseri and Zerb (1968), and Zerbi, Piseri, and Cabassi (1971) have shown the potential of the method in applications to perdeuterated and randomly conformated polyethylene and we can expect similar calculations for more complex polymer systems in the future.

ACKNOWLEDGMENT

The author is grateful to Drs. R. J. Bell and R. E. Shawyer for many helpful comments.

APPENDIX

Proof of the Negative Eigenvalue Theorem

We write the matrix $\mathbf{M}-x\mathbf{I}$, where $\mathbf{M}$ has the block tridiagonal form (3.1), as the product of lower and upper block triangular matrices, thus:

$$\mathbf{M}-x\mathbf{I}=\mathbf{L}(x)\cdot\mathbf{U}(x) \tag{A1}$$

where

$$\mathbf{L}(x)=\begin{bmatrix} \mathbf{I}_{l_1} & 0 & & & & 0 \\ \mathbf{L}_2 & \mathbf{I}_{l_2} & 0 & & & \\ & \mathbf{L}_3 & \mathbf{I}_{l_3} & 0 & & \\ & & \cdot & \cdot & \cdot & \\ & & & \cdot & \cdot & \cdot \\ & & & & \cdot & \cdot \\ 0 & & & & \mathbf{L}_n & \mathbf{I}_{l_m} \end{bmatrix} \tag{A2}$$

and

$$\mathbf{U}(x)=\begin{bmatrix} \mathbf{U}_1 & \mathbf{V}_1 & & & & 0 \\ 0 & \mathbf{U}_2 & \mathbf{V}_2 & & & \\ & 0 & \mathbf{V}_3 & \mathbf{V}_3 & & \\ & & \cdot & \cdot & \cdot & \\ & & & \cdot & \cdot & \cdot \\ & & & & \cdot & \cdot \\ 0 & & & & 0 & \mathbf{U}_m \end{bmatrix}. \tag{A3}$$

The partitioning in each case corresponds to that of $\mathbf{M}$, $\mathbf{I}_{l_j}$ being the unit matrix of order l_j (i.e., of the order of $\mathbf{A}_j$). The blocks $\mathbf{I}_{l_j}$, $\mathbf{L}_j$, $\mathbf{U}_j$, and $\mathbf{V}_j$ ($j=1, 2, \cdots, m$) contain all the nonzero elements of $\mathbf{L}(x)$ and $\mathbf{U}(x)$.

Block matrix multiplication applied to the right-hand side of (A1) leads to the following relations

$$\begin{aligned} \mathbf{A}_1-x\mathbf{I}_{l_1}&=\mathbf{U}_1 \\ \mathbf{A}_j-x\mathbf{I}_{l_j}&=\mathbf{L}_j\mathbf{V}_j+\mathbf{U}_j \\ \mathbf{B}_j&=\mathbf{V}_j \\ \mathbf{B}_j{}^T&=\mathbf{L}_j\mathbf{V}_{j-1} \qquad (j=2, 3, \cdots). \end{aligned} \tag{A4}$$

Therefore, if $\mathbf{U}_{j-1}$ is not singular

$$\begin{aligned} \mathbf{U}_j&=\mathbf{A}_j-x\mathbf{I}_{l_j}-\mathbf{B}_j{}^T\mathbf{U}_{j-1}{}^{-1}\mathbf{B}_j, \\ \mathbf{U}_1&=\mathbf{A}_1-x\mathbf{I}_{l_1}. \end{aligned} \tag{A5}$$

From (A1) and the structure of $\mathbf{L}(x)$, we note that the leading principal minors of $\mathbf{U}(x)$ are identical to those of $\mathbf{M}-x\mathbf{I}$. Let p_i ($i=0, 1, 2, \cdots, n$; $p_0\equiv 1$) be the ith leading principal minor of $\mathbf{U}(x)$, and q_{jk} ($j=1, 2, \cdots, m$; $k=0, 1, 2, \cdots, l_j$; $q_{j0}\equiv 1$) the kth leading principal minor of $\mathbf{U}_j$. Then, as $\mathbf{U}(x)$ is of block triangular form, we have

$$p(j-1; k)\equiv p_{l_1+l_2+\cdots+l_{j-1}+k}=q_{1l_1}q_{2l_2}\cdots q_{j-1l_{j-1}}q_{jk}. \tag{A6}$$

Consequently, the number of changes in sign between the consecutive minors

$$p(j-1; 0),\ p(j-1; 1),\ p(j-1; 2),\ \cdots,\ p(j-1; l_j) \equiv p(j; 0)$$

is equal to the number of changes in sign between consecutive members of the sequence

$$q_{j0}\equiv 1,\ q_{j1},\ q_{j2},\ \cdots,\ q_{jl_j}.$$

But this latter number is $\eta(\mathbf{U}_j)$, according to the well-known theorem (Jeffreys and Jeffreys, 1950) that the number of negative eigenvalues of a symmetric matrix is equal to the number of changes in sign between consecutive leading principal minors, starting with the zeroth-order minor as positive. It follows that the total number of changes in sign in the sequence of all p_i ($i=0, 1, 2, \cdots, n$) is equal to

$$\sum_{j=1}^{m}\eta(\mathbf{U}_j).$$

Therefore, by a further application of the theorem just stated, we have

$$\eta(\mathbf{M}-x\mathbf{I})=\sum_{j=1}^{m}\eta(\mathbf{U}_j). \tag{A7}$$

REFERENCES

Agacy, R. L., 1964, Proc. Phys. Soc. **83,** 591.
Aggarwal, R. R., and B. D. Saksena, 1951, J. Chem. Phys. **19,** 1480.
Aiyer, R. N., R. J. Elliott, J. A. Krumhausl, and P. L. Leath, 1969, Phys. Rev. **181,** 1006.
Alway, G. G., and D. W. Martin, 1965, Computer J. **8,** 264.
Anderson, O. L., 1965, *Physics of Non-Crystalline Solids*, (North-Holland Publ. Co., Amsterdam), pp. 179–88.
Anderson, P. W., 1958, Phys. Rev. **109,** 1492.
——, 1970, Solid State Phys. **2,** 193.
Barker, A. S., 1968, *Localized Excitations in Solids*, (Plenum Press, New York), pp. 581–91.
Bell, R. J., N. F. Bird, and P. Dean, 1968, J. Phys. C **1,** 299.
——, and P. Dean, 1966, Nature **212,** (5068), 1354.
——, and P. Dean, 1967, National Physical Laboratory Math. Rept., NPL No. 62.
——, and P. Dean, 1968a, J. Inst. Maths. Its Appl. **4,** 375.
——, and P. Dean, 1968b, *Localized Excitations in Solids* 1967 (Plenum Press, New York), pp. 124–31.
——, and P. Dean, 1970, Discussions Faraday Soc. **50,** 55.
——, P. Dean, and D. C. Hibbins-Butler, 1970, J. Phys. C **3,** 2111.
——, P. Dean, and D. C. Hibbins-Butler, 1971, J. Phys. C **4,** 1214.
Bertie, J. E., and E. Whalley, 1964, J. Chem. Phys. **40,** 1637.
——, and E. Whalley, 1967, J. Chem. Phys. **46,** 1271.
Borland, R. E., 1964, Proc. Phys. Soc. **83,** 1027.
Born, M., and J. von Karman, 1912, Zeit. Phys. **13,** 297.
Borrelli, N. F., and G. J. Su, 1968, Mater. Res. Bull. **3,** 181.
Bradley, J. C., 1961, Ann. Phys. **15,** 411.
Chen, Y. S., W. Shockley, and G. L. Pearson, 1966, Phys. Rev. **151,** 648.
Davies, R. W., and J. S. Langer, 1963, Phys. Rev. **131,** 163.
Dean, P., 1960, Proc. Roy. Soc. **A254,** 507.
——, 1961, Proc. Roy. Soc. **A260,** 263.
——, 1964, Proc. Phys. Soc. **84,** 727.
——, 1967, J. Inst. Maths. Its Appl. **3,** 98.
——, 1969, J. Phys. Soc. Japan Suppl. **26,** 20.
——, and M. D. Bacon, 1963, Proc. Phys. Soc. **81,** 642.
——, and M. D. Bacon, 1965, Proc. Roy. Soc. **A283,** 64.
——, and N. F. Bird, 1967, Proc. Cambridge Phil. Soc. **63,** 477.
——, and J. L. Martin, 1960a, Proc. Roy. Soc. **A259,** 409.
——, and J. L. Martin, 1960b, Proc. Phys. Soc. **65,** 452.
Debye, P., 1912, Ann. Phys. **39,** 689.
Domb, C., 1963, Proc. Roy. Soc. **A276,** 418.
——, A. A. Maradudin, E. W. Montroll, and G. H. Weiss, 1959, Phys. Rev. **115,** 18, 24.
Dyson, F. J., 1953, Phys. Rev. **92,** 1331.
Economou, E. N., 1971, Solid State Commun. **9,** 1317.
——, and M. H. Cohen, 1971, Phys. Rev. B **4,** 396.
Faulkner, J. S., and J. Korringa, 1961, Phys. Rev. **122,** 390.
Flinn, P. A., A. A. Maradudin, and G. Weiss, 1961, Westinghouse Research Lab. Scientific Paper 029–G000–P10.
Givens, W., 1953, Nat. Bur. Stand. (U.S.), Appl. Math. Ser. **29,** 111, 1954; Oak Ridge National Laboratory Report No. 1574.
Hass, M., H. B. Rosenstock, and R. E. McGill, 1969, Solid State Commun. **7,** 1.
Hindley, N. K., 1967, Phys. Rev. **153,** 952.
Hori, J., 1964a, Prog. Theor. Phys. **31,** 940.
——, 1964b, Prog. Theor. Phys. **32,** 471.
——, 1968a, *Spectral Properties of Disordered Chains and Lattices* (Pergamon Press, Oxford).
——, 1968b, J. Phys. C **1,** 304.
——, and J. Asahi, 1957, Prog. Theor. Phys. **17,** 523.
——, and K. Wada, 1970, Prog. Theor. Phys. Suppl. No. 45, 36.
Householder, A. S., and F. L. Bauer, 1959, Numerische Mathematik **1,** 29.
Jannink, G., and G. C. Summerfield, 1966, J. Appl. Phys. **37,** 3953.
Jeffreys, H., and B. S. Jeffreys, 1950, *Methods of Mathematical Physics* (Cambridge U. P., Cambridge), p. 140.
Langer, J. S., 1961, J. Math. Phys. **2,** 584.
Leadbetter, A. J., 1965, Proc. Roy. Soc. **A287,** 403.
Leath, P. L., and B. Goodman, 1969, Phys. Rev. **181,** 1062.
Lucovsky, G., M. Brodsky, and E. Burstein, 1968, *Localized Excitations in Solids*, 1967 (Plenum Press, New York), pp. 592–601.
Maris, H. J., 1966, Phil. Mag. **13,** 465.
Martin, J. L., 1961, Proc. Roy. Soc. **A260,** 139.
Matossi, F., 1951, J. Chem. Phys. **19,** 161.
Matsuda, H., 1964, Prog. Theor. Phys. **31,** 161.
——, 1966a, Prog. Theor. Phys. Suppl. No. 36, 97.
——, 1966b, Prog. Theor. Phys. **36,** 1070.
——, and T. Miyata, 1968, *Persistence and Amalgamation Types in Optical Spectra of Mixed Crystals*, Research Institute for Fundamental Physics Report. No. 79.
——, and N. Ogita, 1967, Prog. Theor. Phys. **38,** 81.
——, and K. Okada, 1965, Prog. Theor. Phys. **34,** 539.
——, and E. Teramoto, 1965, Prog. Theor. Phys. **34,** 314.
Mazur, P., E. W. Montroll, and R. B. Potts, 1956, J. Wash. Acad. Sci. **46,** 2.
Montgomery, D. J., and J. R. Hardy, 1965, *Lattice Dynamics*, edited by R. F. Wallis (Pergamon Press, Oxford), pp. 491–5.
Okada, K., and H. Matsuda, 1968, Prog. Theor. Phys. **39,** 1153.
Ortega, J. M., 1964, NASA Report No. TR–64-12 NSG–398.
Payton, III, D. N., 1966, Los Alamos Scientific Laboratory Rept No. LA-3510.
——, and W. M. Visscher, 1967a, Phys. Rev. **154,** 802.
——, and W. M. Visscher, 1967b, Phys. Rev. **156,** 1032.
——, and W. M. Visscher, 1968, Phys. Rev. **175,** 1201.
Piseri, L., and G. Zerbi, 1968, Chem. Phys. Letters **2,** 127.
Poon, H., and A. Bienenstock, 1966a, Phys. Rev. **142,** 466.
——, and A. Bienenstock, 1966b, Phys. Rev. **147,** 710.
Prask, H., H. Boutin, and S. Yip, 1968, J. Chem. Phys. **48,** 3367.
Rosenstock, H. B., and R. E. McGill, 1962, J. Math. Phys. **3,** 200.
——, and R. E. McGill, 1968, Phys. Rev. **176,** 1004.
Sah, P., and K. P. Srivasta, 1970, Physica **45,** 537.
Schmidt, H., 1957, Phys. Rev. **105,** 425.
Shawyer, R. E., and P. Dean, 1969, Discussions Faraday Soc. **48,** 102.
——, and P. Dean, 1972a, J. Phys. C **5,** (to be published).
——, and P. Dean, 1972b, J. Phys. C **5,** (to be published).
Simon, I., 1957, J. Amer. Ceramic Soc. **40,** 150.
——, 1960, *Modern Aspects of the Vitreous State*, edited by J. D. Mackenzie (Butterworths, London), Chapt. 6.
Snyder, R. G., 1967, J. Chem. Phys. **47,** 1316.
Takeno, S., 1962, Prog. Theor. Phys. Suppl. No. 23, 94.
——, 1968, Prog. Theor. Phys. **40,** 942.
Tasumi, M., and G. Zerbi, 1968, J. Chem. Phys. **48,** 3813.
Taylor, D. W., 1967, Phys. Rev. **156,** 1017.
Taylor, M. J., and E. Whalley, 1964, J. Chem. Phys. **40,** 1660.
Thouless, D. J., 1970, J. Phys. C **3,** 1559.
Verleur, H. W., and A. S. Barker, Jr., 1966, Phys. Rev. **149,** 715.
Whalley, E., and J. E. Bertie, 1967, J. Chem. Phys. **46,** 1264.
Wilkinson, J. H., 1965, *The Algebraic Eigenvalue Problem* (Clarendon Press, Oxford).
Wu, S., and P. L. Taylor, 1969, Phys. Rev. **181,** 1136.
Yonezawa, F., 1968, Prog. Theor. Phys. **40,** 734.
Zarzycki, J., and F. Naudin, 1960, Verres Réfract. **14,** 113.
Zerbi, G., L. Piseri, and F. Cabassi, 1971, Molec. Phys. **22,** 241.